Advanced Ceramic Materials Series Volume 5

edited by Aleksander Gurlo

Hiba Bensalah

# Natural and synthetic apatites as adsorbents for the removal of azo dyes from aqueous solutions

Technische Universität Berlin

# Natural and Synthetic Apatites as Adsorbents for the Removal of Azo Dyes from Aqueous Solutions

vorgelegt von

Hiba Bensalah

von der Fakultät III – Prozesswissenschaften
der Technischen Universität Berlin

und der

Hassan II Universität in Casablanca, Marokko

(im Rahmen des Doppel-Promotionsabkommens)

zur Erlangung des akademischen Grades

Doktor der Ingenieurwissenschaften

- Dr.-Ing. –

genehmigte Dissertation

Promotionsausschuss:

Vorsitzende: Prof. Mama El Rhazi (Hassan II Universität Casablanca, Marokko)
Gutachterin: Prof. Murielle Rabiller Baudry (Rennes 1 Universität, Frankreich)
Gutachter: Prof. Dr. Aleksander Gurlo (Technische Universität Berlin, Deutschland)
Gutachter: Prof. Jason A. Cody (Lake Forest College Chicago, USA)

Tag der wissenschaftlichen Aussprache: 13. Dezember 2019 an der Hassan II Universität, Casablanca

Berlin 2020

**Technische Universität Berlin**
Fakultät III – Prozesswissenschaften –

**Université Hassan II de Casablanca**
CEDoc: Sciences, Techniques, Ingénierie et Développement durable
Laboratoire des Matériaux, Membranes et Environnement

# Natural and Synthetic Apatites as Adsorbents for the Removal of Azo Dyes from Aqueous Solutions

by

**Hiba Bensalah**

*Doctoral dissertation submitted in fulfillment of the requirements for the degree of:*

**Doktor der Ingenieurwissenschaften**
**-Dr.-Ing.-**

Publicly defended at FSTM on the 13th of December 2019

**Board of examiners:**

| | | | |
|---|---|---|---|
| **Pr. Mama El Rhazi** | PES | FST Mohammedia<br>Université Hassan II de Casablanca | Chair |
| **Pr. Jason A. Cody** | PES | Lake Forest College Chicago – USA | Reporter |
| **Pr. Murielle Rabiller Baudry** | PES | Université de Rennes 1 – France | Reporter |
| **Pr. Dr. Aleksander Gurlo** | PES | Technische Universität Berlin – Germany | Supervisor |
| **Pr. Saad Alami Younssi** | PES | FST Mohammedia<br>Université Hassan II de Casablanca | Supervisor |
| **Pr. Mohamed Ouammou** | PES | FST Mohammedia<br>Université Hassan II de Casablanca | Co-supervisor |

*"النَجاحُ هو الحَظ الجيّد الذِي يَأتي مِنَ الطّمُوح وَ اليَأس وَ التّعَب وَ الإلهَام*

*,,Success is the good fortune that comes from aspiration, desperation, perspiration and inspiration.*

# Summary

With the rapid growth of society, demand for water has increased tremendously with agricultural, industrial and domestic sectors consuming a big volume of available fresh water, which has resulted in the generation of large amounts of wastewater containing various pollutants. One of the important class of these pollutants is dyes. Unfortunately, most of those produced dyes are discharged directly in aqueous effluents, which poses a serious hazard to aquatic living organisms and humans. Azo dyes are found to be toxic, mutagenic and even carcinogenic. Therefore, it is necessary to eliminate dyes from wastewater before it is discharged. However, it is not an easy task since dyes are highly insoluble, resistant to aerobic digestion, and are stable to light, heat and oxidizing agents. Accordingly, the main goal of this work is to propose an efficient process for the removal of dyes from aqueous solutions using low-cost materials as adsorbents. Adsorption process has been chosen in this work due to its simple design, ease of operation and low investment.

In the first part of this work, Moroccan natural phosphate, as a natural fluorapatite (FAp), was tested as an effective low-cost adsorbent for the removal of cationic dye rhodamine 6G (Rh6G) as well as anionic dye congo red (CR) from wastewater. Moroccan natural phosphate has been chosen as adsorbent in this study due to its abundance, since Morocco is the largest phosphate producer in the world and holds about 75% of the world's estimated reserves. The X-ray diffraction (XRD), Fourier-transform infrared spectroscopy (FTIR) and Energy-dispersive X-ray spectroscopy (EDX) characterizations reveal that the sample contains 98 wt% FAp ($Ca_5(PO_4)_3F$) with 1 wt% quartz ($SiO_2$) and 1 wt% calcium carbonate ($CaCO_3$). Nitrogen sorption analysis shows that the BET specific surface area and BJH pore volumes of the sample are 18.8 m²/g and 0.10 cm3/g, respectively. Batch adsorption experiments of the dyes from aqueous solution were conducted, taking into account the influence of initial dye concentration, adsorbent dosage, contact time and solution pH. The Langmuir isotherm model best represents the equilibrium adsorption process of the two dyes. The calculated maximum adsorbed quantity $q_{max}$ of CR and Rh6G at dosage 20 g/L and pH value of 5.2 were found 19.81 and 6.84 mg/g, respectively. The adsorption of Rh6G and CR on natural phosphate was found to follow the pseudo-second-order model. Natural phosphate was also tested as an effective adsorbent for a simulated dye effluent under industrial conditions of temperature and pH. Desorption studies were conducted using HCl as an eluent and the highest elution efficiency for both dyes was

obtained with a 0.1 M solution. Accordingly, it is demonstrated in this work that natural phosphate is a very efficient adsorbent for both cationic and anionic dyes from contaminated water, and represents a great low-cost alternative to commercial adsorbents due to its abundance as a natural resource in Morocco.

In the second part, hydroxyapatite (HAp) nanorods are synthesized from PG waste and potassium dihydrogen phosphate ($KH_2PO_4$) under hydrothermal conditions. PG has been selected for this synthesis because 85% of its worldwide production remains at present stored into piles near the factory that occupy considerable land resources, or completely discharged into water, which lead to serious contamination. In consequence, within the framework of this thesis, minimizing the negative effects of this waste consists one of our greatest goal. The influence of several synthesis parameters such as temperature, synthesis time, and solution pH on product structure and purity is addressed by XRD and FT-IR spectroscopy. Phase pure HAp nanorods with diameter and length of 18 and 63 nm, respectively, are obtained after 10 h at 200 °C and pH∼11. The influence of Brij-93 surfactant on the morphology of prepared HAp is investigated by TEM and SEM. The aspect ratio and the mean size of HAp crystals increase to 1013 and 205×20 nm, respectively, with increasing the concentration of Brij-93 surfactant to 0.01 mol. Hence, the PG recycling could be accomplished using an easy synthesis route with relatively cheap reactants for the production of nanocrytalline HAp.

Finally, the synthesized nano-sized HAp with high surface area was tested as an effective adsorbent for anionic dye Congo Red from aqueous solution. The influence of Brij-93 surfactant on the adsorptive properties of HAp was studied using XRD, TEM, nitrogen sorption analysis, FT-IR, XPS, and zeta potential analysis. The BET specific area of the prepared Hap was 85.88 $m^2/g$, while, the surfactant modified B93- HAp had SBET of 135.25 $m^2/g$. The B93-HAp adsorbent showed higher adsorption capacity compared to the HAp adsorbent at the same conditions. Effects of pH solution, contact time, initial dye concentrations and adsorbent dosage on the adsorptive properties of B93-HAp adsorbent were also studied. The CR adsorption onto B93-HAp adsorbent was favourable at acidic condition with pH 5.5. Kinetics study showed that the adsorption of CR on HAp follows pseudo first order reaction model. Freundlich non-linear isotherm model - used to fit the adsorption data – gives a maximum adsorption capacity of 139 mg/g. FTIR and XPS studies on the adsorbent before and after dye adsorption experiment suggest that chemical adsorption might be involved in the adsorption process. Desorption studies indicate that 0.1 M HCl is the best eluent and exhibits higher elution efficiency (64 %) with a great quantitative CR recovery after 6 cycles.

# Zusammenfassung

Mit dem rasanten gesellschaftlichen Wachstum stieg der Bedarf an Wasser in den landwirtschaftlichen, industriellen und häuslichen Bereichen enorm an und verbraucht ein hohes Volumen an verfügbarem frischem Wasser. In Folge dessen werden große Mengen an Abwasser produziert, welche unterschiedlichste Verunreinigungen enthalten. Eine wichtige Art dieser Schadstoffe sind Farbstoffe. Der Großteil dieser Farbstoffe werden aktuell leider direkt in die Abwässer geleitet, was zu einer ernstzunehmenden Gefährdung von Wasserorganismen und Menschen führt. Azofarbstoffe werden toxische, erbgutverändernde und sogar krebserregende Eigenschaften nachgewiesen. Es ist daher dringend notwendig, Farbstoffe aus den Abwässern zu beseitigen, bevor diese entsorgt werden. Dies ist jedoch keine einfache Aufgabe, da Farbstoffe hochgradig unlöslich und widerstandsfähig gegen aeroben Abbau sind sowie beständig gegen Licht, Hitze und Oxidationsmittel. Die Zielsetzung dieser Arbeit ist daher, einen effizienten Prozess für den Abbau von Farbstoffen in Wasserlösungen unter Nutzung von kostengünstigen Werkstoffen als Adsorptionsmittel vorzuschlagen. Der Adsorptionsprozess wurde in dieser Arbeit aufgrund seines einfachen Aufbaus, seiner einfachen Umsetzung und geringen Kosten ausgewählt.

Im ersten Teil dieser Arbeit wurde natürliches Phosphat aus Marokko als natürliches Flour-Apatit (FAp) in seiner Verwendung als kostengünstiges Adsorptionsmittel für die Beseitigung des katatonischen Farbstoffes Rhodamin 6G (Rh6G) sowie des anionischen Farbstoffes Congo Red (CR) aus Abwässern getestet. Natürliches Phosphat aus Marokko wurde für diese Studie als Adsorptionsmittel aufgrund seines häufigen Vorkommens ausgewählt. Marokko ist weltweit der größte Produzent von Phosphat und besitzt etwa 75 % des weltweit angenommenen Vorkommens. Die Charakteristika aus Röntgenbeugung (XRD), Fourier-Transformations-Infrarotspektroskopie (FTIR-Spektroskopie) und energiedispersive Röntgenspektroskopie (EDX) zeigen, dass Stichproben 98 wt% FAp ($Ca_5(PO_4)_3F$) mit 1 wt% quartz ($SiO_2$) und 1 wt% calcium carbonate ($CaCO_3$) enthalten. Die Nitrogen Adsorptions-Analyse zeigt, dass der BET-spezifischen Oberflächenbereich und die BJH Porenvolumina der Stichproben jeweils 18.8 m²/g und 0.10 cm3/g betragen.

Batch-Adsorptions-Experimente mit Farbstoffen aus Wasserlösungen wurden unter Berücksichtigung des Einflusses von anfänglicher Farbstoffkonzentration, Adsorptionsmitteldosierung, Kontaktdauer und pH-Wert der Lösung durchgeführt. Das Langmuir-Isotherm-Modell veranschaulicht den Prozess des Adsorbtionsgleichgewichtes

zweier Farbstoffe am besten. Die berechnete Maximaladsorbtionsmenge $q_{max}$ von CR und Rh6G bei einer Dosierung von 20g/L und einem pH-Wert von 5.2 wurde jeweils mit 19.81 und 6.84 mg/g ermittelt. Es wurde herausgefunden, dass die Adsorption von Rh6G und CR auf natürliches Phosphat dem Pseudo-Erste-Ordnungsmodell folgt. Außerdem wurde natürliches Phosphat als effektives Adsorptionsmittel für simulierte Farbstoffabwässer unter industriellen Temperatur- und pH-Wert-Bedingungen getestet. Desorptionsstudien unter Nutzung von HCl als Eluent wurden durchgeführt, in denen eine 0.1 M Lösung als höchste Elutions-Wirksamkeit für beide Farbstoffe erreicht werden konnte. Dementsprechend wird in dieser Arbeit erwiesen, dass natürliches Phosphat ein sehr wirksames Adsorptionsmittel für sowohl kationische als auch anionische Farbstoffe aus verunreinigtem Wasser darstellt und durch sein Vorkommen als natürliche Ressource in Marokko eine sehr gute, kostengünstige Alternative zu gewerblichen Adsorptionsmitteln bietet.

Im zweiten Teil werden Hydroxyapatit (HAp) Nanostäbchen aus Phosphogibs (PG) Abfällen und Kalium-Dihydrogen-Phosphat unter hydrothermalen Bedingungen synthetisiert. PG wurde für diese Synthese ausgewählt, da 85% der weltweiten Produktion im Moment noch in Stapeln in der Nähe der Fabriken gelagert werden und damit erhebliche Landflächen belegen oder im Gesamten im Wasser entsorgt werden, was zu ernstzunehmenden Kontaminierungen führt. In Folge dessen, ist es im Rahmen dieser Arbeit unser größtes Ziel, diese Abfälle nutzbar zu machen und deren negativen Effekte zu minimieren. Der Einfluss zahlreicher Parameter der Synthese wie Temperatur, Synthese-Dauer und pH-Wert der Lösung auf die Struktur und Reinheit des Produktes wurden mit XRD und FT-IR-Spektroskopie untersucht. Nach 10 Stunden bei 200 ° C und pH∼11 wurden phasenreine HAp Nanostäbchen mit Durchmesser und Länge von 18 bzw. 63 nm gewonnen. Durch TEM und SEM wurde der Einfluss von Brij-93 Tensid auf die Morphologie von behandeltem HAp untersucht. Das Seitenverhältnis und die durchschnittliche Größe der HAp Kristalle vergrößerte sich auf 1013 und 205x20 nm durch die Erhöhung der Konzentration von Brij-93 Tensid auf 0.01 mol. Die PG Wiederverwertung für die Produktion von nanokristallinem HAp konnte somit unter Nutzung eines einfachen Synthese-Verfahrens mit relativ günstigen Reaktionsmitteln erreicht werden.

Zuletzt wurde das synthetisierte nanoskalige HAp mit hoher Oberfläche als effektives Adsorbtionsmittel für den anionischen Farbstoff Congo Red aus einer Wasserlösung getestet. Der Einfluss von Brij-93 Tensid auf die adsorptiven Eigenschaften von HAp wurde unter Einsatz von XRD, TEM, Nitrogen-Sorptions-Analyse, FT-IR, XPS und Zeta-Potentials-Analyse gemessen. Der BET-spezifische Oberfläche des behandelten HAp lag bei 85.88 m²/g,

während das oberflächen-modifizierten B93-HAp ein S-BET von 135.25 m²/g besaß. Unter den gleichen Bedingungen zeigte das B93-HAp-Adsorptionsmittel eine höhere Adsorptions-Kapazität im Vergleich mit dem HAp-Adsorptionsmittel. Auswirkungen der pH Lösung, Kontaktdauer, anfänglicher Farbmittel-Konzentration und Adsorptionsmittel-Dosierung auf die adsorptiven Eigenschaften des B93-HAp-Adsorbtionsmittel wurden ebenfalls untersucht. Die CR-Adsorption auf das B93-HAp-Adsorptionsmittel war günstiger bei einer sauren Bedingung von pH 5.5. Kinetische Untersuchungen zeigten, dass die Adsorption von CR auf HAp dem Pseudo-Erste-Ordnungsmodell folgt. Freundlichs non-lineares Iostherm-Modell - welches für die Berechnung der Adsorptions-Daten benutzt wurde - zeigt eine maximale Adsorptions-Kapazität von 139 mg/g. FTIR und XPS-Untersuchungen auf das Adsorptionsmittel vor und nach dem Farbstoff-Adsorptions-Experiment weisen darauf hin, dass chemische Adsorption im Adsorptions-Prozess enthalten ist. Desorptions-Untersuchungen zeigen, dass 0.1 M HC1 das beste Eluent ist und höhere Elutionseffizienz (64 %) mit einer hohen quantitativen CR-Rückgewinnung nach 6 Zyklen aufweist.

# Table of Contents

# 1. Introduction

## 1.1. Structure of the thesis

The present dissertation is a compilation of three peer-reviewed publications, that cover results obtained within this thesis:

1. H. Bensalah, M.F. Bekheet, S. Alami Younssi, M. Ouammou, A. Gurlo, Hydrothermal synthesis of nanocrystalline hydroxyapatite from phosphogypsum waste, *Journal of Environmental Chemical Engineering*, 6 (**2018**) 1347-1352.
   DOI: https://doi.org/10.1016/j.jece.2018.01.052
   This publication is the chapter 4.1 of the dissertation.

2. H. Bensalah, M.F. Bekheet, S.A. Younssi, M. Ouammou, A. Gurlo, Removal of cationic and anionic textile dyes with Moroccan natural phosphate, *Journal of Environmental Chemical Engineering*, 5 (**2017**) 2189-2199.
   DOI: https://doi.org/10.1016/j.jece.2017.04.021
   This publication is the chapter 4.2 of the dissertation.

3. H. Bensalah, S. Alami Younssi, M. Ouammou, A. Gurlo, M.F. Bekheet, Azo dye adsorption on an industrial waste-transformed hydroxyapatite adsorbent: Kinetics, isotherms, mechanism and regeneration studies, *Journal of Environmental Chemical Engineering,* 8 (**2020**) 103807.
   DOI: https://doi.org/10.1016/j.jece.2020.103807
   This publication is the chapter 4.3 of the dissertation.

This dissertation is structured in 5 chapters, as follows:

***Chapter 1*** exhibits the problem statements of the PhD thesis and the mains goals followed to address them.

***Chapter 2*** consists of a literature survey that introduces the reader to the concerned challenges regarding wastewater effluents, and especially azo dyes, which is one of the very serious environmental issues nowadays. It also reviews the advantages and the drawbacks of

the most important wastewater treatment techniques, hence explains the reason behind choosing adsorption. In addition, it presents a wide variety of adsorbents used for the removal of various azo dyes, reported recently in the literature.

***Chapter 3*** describes extensively the structures and the properties of the materials used in this work; (fluorapatite, hydroxyapatite) and their eventual applications in different fields and especially environmental ones. It also reports the environmental impacts of another hazardous material, which is an industrial waste: phosphogypsum. This chapter extends the two main techniques used during this work: surfactant-assisted hydrothermal synthesis and adsorption. And briefly describes the other used characterization techniques, that are well defined in the respective manuscripts in Chapter 4.

***Chapter 4*** encloses the three peer-reviewed publications that answers the problems statements addressed in chapter 1.

***Chapter 5*** summarizes the main findings of this work and provides guidelines and suggestions for further investigations.

The references used along this thesis are listed at the end of every chapter.

## 1.2. Motivation and goal

Colour has always been an important factor in human history. The use of natural dyes to create colours is common to all civilizations, hence it is a very important part of our cultural heritage. Throughout history, natural colorants have played a major part in economic and cultural exchanges between nations. Almost all colours were extracted from existing elements in nature such as roots of plants, certain insects, vegetables, fruits, flowers and fish. Unfortunately, natural dyes gave a limited and a dull range of colours. Besides, they showed low colour fastness when exposed to washing and sunlight. The major industrial break that occurred during the 19th century, with the growth of the textile production industry, has necessitated the development of more efficient and reliable dyes. These chemical compounds are easily synthesized, have excellent fixative and permanency properties, in addition they offer a large variety of colours, when compared to natural dyes. Those synthetic dyes are produced to be extremely soluble in water and very stable to light, heat and oxidizing agents, which makes the separation of dyes from aqueous solutions very difficult. Accordingly, we focus in this study only on azo dyes. During the dyeing processes, enormous quantities of those pollutants are discharged into water, which represents a huge hazard on the environment and can lead to a

serious public health issue. Considering that by reductive cleavage, of one or more azo groups, can release one or more aromatic amines in detectable concentrations considered as toxic, mutagenic and carcinogenic. As a result, coloured effluents can affect photosynthetic process of aquatic plants, reducing oxygen levels in water, which leads to the suffocation of aquatic flora and fauna. Therefore, finding a suitable way to treat this problem is of prime importance.

Morocco is currently facing the same types of environmental problems experienced by the industrialized countries but does not have the same technological capabilities as these countries in order to cope with water pollution. Nonetheless, Morocco holds a variety of natural resources that may be good candidates for precursors in wastewater treatment techniques. In fact, it is the largest phosphate producer in the world and it holds about 75% of the world's estimated reserves. Fluoroapatite $Ca_{10}(PO_4)_6F_2$ is the major phase that constitutes the Moroccan natural phosphate. Apatite's most interesting property is its ability to accept ionic substituents and vacancies. Therefore, this material that has a sedimentary origin, has been used in water treatment and has shown great effectiveness as a catalyst as well as ceramic support of a microfiltration membrane. Only two studies were found using natural phosphate as an adsorbent for cationic and anionic dyes. However, the natural phosphate showed good adsorption capacities of only cationic dyes, whereas in the case of anionic dyes, it showed a low adsorption affinity. Furthermore, some factors that could affect the adsorption capability, such as the surface charges of the phosphate adsorbents at different pH values and the amount of impurity phases, have not been sufficiently investigated thus far.

Another hazard that threatens Moroccan coasts is called phosphogypsum (PG), which is the principal waste of phosphoric acid manufacture. It is produced, in a large quantity, in the basic reaction of the sulphuric acid on phosphate ore. This reaction leads to the elimination, by filtration, of PG ($CaSO_4$, 2 $H_2O$) as a cake. About 5 tons of PG are produced for every ton of $P_2O_5$ manufactured. Worldwide PG production is huge, and it is estimated that 280 million tons are produced annually in phosphoric acid plants. For Morocco, this production can exceed annually more than thirteen million tons. Only about 15% of world PG production is recycled, mostly in building materials, agricultural fertilizers or soil stabilization amendments and as setting regulator instead of natural gypsum in the Portland cement industry. Therefore, 85% of the worldwide production remains at present stored into piles near the factory that occupy considerable land resources, or completely discharged into water, which lead to serious contamination. Hence, transforming this industrial waste into nano-crystalline HAp, using an

environmentally friendly method, can be a suitable way for recycling and minimizing the negative effects of this waste.

Nano-HAp can be synthesized by various methods such as solid-state reaction, co-precipitation, sol-gel process, hydrothermal methods, and microwave synthesis route. Some of these synthesis techniques have some drawbacks such as long reaction times, agglomeration, uncontrolled particle size and non-stoichiometric products. Among all these synthesis methods, the hydrothermal method is an attractive solution process to serve the objective of this experiment and is advantageous in terms of its single-step, low-energy-consuming, producing high purity and time-saving process. In addition, it can be useful to control grain size, particle morphology, crystalline phase and surface chemistry through regulation of the solution composition, reaction temperature, pressure, solvent properties, additives and aging time. Consequently, HAp recently gained attention as efficient adsorbents, owing to its physical and chemical nature as it can substitute both cationic and anionic complexes present in an aqueous solution in its atomic arrangement. Its chemical characteristics such as crystallinity, stability, ion adsorption capability and highly specific catalytic activity make it suitable for a variety of applications especially in water treatment. Nanostructured HAp can exhibit multi-adsorbing sites and a quiet large surface area, that can be controlled and improved using surfactant assisted synthesis. In fact, surfactants have proven to be the best shape directing agents in the synthesis of nanomaterials, which is primarily related to the surface adsorption of surface-active molecules on different crystal planes of nucleating centres, thus controlling their overall shape. Different kinds of surfactants have been used for shape-controlled synthesis of nanomaterials, while ionic surfactants demonstrate clear shape directing effects.

Accordingly, these thesis deals with two main topics:

- ***(i)*** Recycling of an industrial waste PG by converting it into a useful material (HAp) via hydrothermal synthesis.
- ***(ii)*** Enhance of the adsorption capacities of natural FAp and synthetic HAp for the removal of azo dyes from aqueous solutions.

The ***first goal*** of the present thesis is to investigate the ability of natural phosphate to adsorb organic cationic and anionic dyes as well as a simulated dye effluent. To simulate the wastewater produced by real textile industries, a synthetic dye effluent was prepared. The cationic dye used in this study is rhodamine 6G (Rh6G), an azo dye with an amino group and the anionic dye is congo red (CR), a diazo sulfonated dye. The simulated dye effluent was

prepared from a CR solution and NaCl. The adsorption capacity and operation parameters including adsorbent dosage, solution pH, adsorption time and initial dye concentration were studied. The results are analysed regarding four adsorption isotherms and kinetic models to understand the mechanism of adsorption on the dye molecules onto the natural phosphate. In order to have a better understanding of the adsorption mechanisms and to make this method more environmentally friendly, desorption studies were also carried out by testing different eluents.

The ***second goal*** of this work is to convert industrial waste PG into nanocrystalline HAp and to achieve control over the size and morphology of the HAp crystals by applying surfactant-assisted hydrothermal technique. A non-ionic Brij-93 surfactant, containing polar polyoxyethylene groups separated by hydrophobic polyethylene chain, is applied in this study. The influence of pH, temperature, time and surfactant concentrations on the structure and composition of HAp formed in a hydrothermal process are investigated by X-ray diffraction (XRD), Fourier Transformed-Infrared Spectroscopy (FTIR), scanning (SEM) and transmission electron microscopy (TEM).

The ***third goal*** of the present study is to demonstrate that waste-transformed HAp can be applied as an adsorbent for the removal of azo dyes. Hence, HAp and surfactant-modified B93-HAp have been thoroughly characterized by XRD, FT-IR spectroscopy, $N_2$ adsorption, TEM, zeta potential and XPS. In addition, they were tested as potential adsorbents of the anionic azo dye Congo Red (CR), evaluating parameters such as dye concentration, pH solution and adsorbent dosage. Only two studies were found using waste transformed adsorbent from PG for the removal of lead ions and fluoride from aqueous solution, but it has not been approached for azo dyes nor its adsorptive mechanism with azo dyes has been evaluated from a thermodynamic and kinetic view. Finally, various eluents were investigated in order to determine their effectiveness in desorbing CR, in order to regenerate the waste-transformed adsorbent.

# 2. Dyes and their removal from aqueous solutions

## 2.1. Dyes

### 2.1.1. Classification of dyes

Nature offers beautiful colours that attract human attention. Back to ancient times, natural dyes have been used by humans to colour his body, food, walls of caves, leather and clothes using a limited range of natural colorants extracted from both animal and vegetable origin. The use of black, white and yellow pigments made from ochre in cave painting were traced back to 15.000 BC. However, the earliest written record of the use of dyestuffs in China, existed since year 2600 BC [1]. It was also found that the process of dyeing was used by Egyptians, 4000 years ago, because of the evidence of dyed fabrics found in Egyptian tombs [2]. The most valued colours are classified in Figure 1. **Indigo** for the blues, is derived from a plant called Indigofera. **Alizarin** for reds was extracted from Madder plant, and other shades of red were found in fungi and some insects such us cochineal. And finally, **Tyrian Purple** for purples, a secretion produced by specific species of sea snails, has been used since the Roman era.

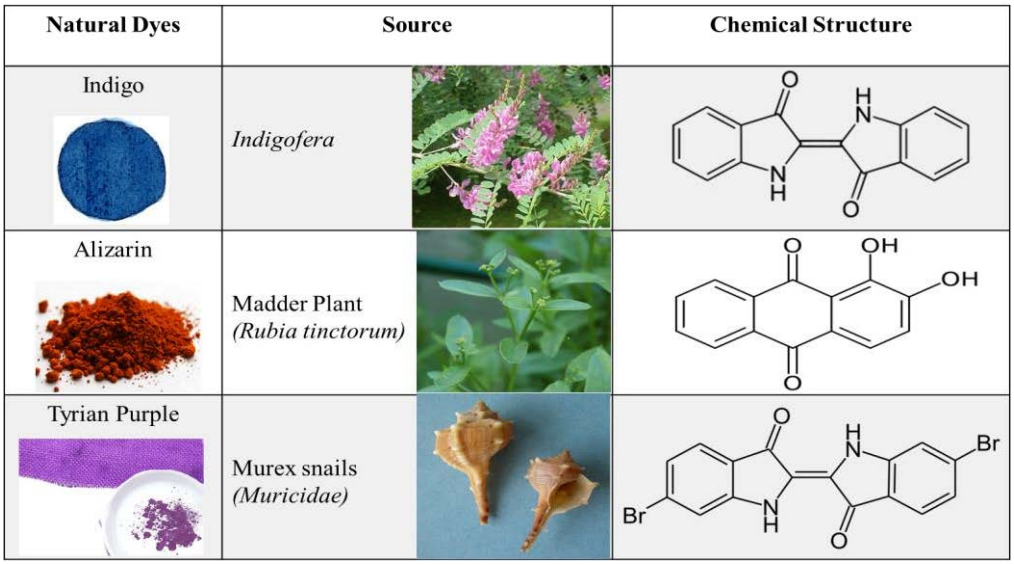


Figure 1. Classification of the first palette of colours Indigo [3]. Alizarin [4] and Tyrian Purple [5] by source and chemical structure. Copyright Kurt Stüber, Carstor and Benjah-bmm27 licensed under Creative Commons Attribution License.

The industrial revolution that occurred in the 19th century, led to the decline of the use of natural dyes and the rise of synthetic dyes. In fact, the growth of the textile industry aroused the increase in demand for dyes. While natural dyes, originated from animal, vegetable or mineral resources, had to be shipped over considerable distances, thus were subject to severe damage. Besides, knowing that 1.4 g of Tyrian Purple dye was generated from 12.000 snails, natural dyes showed an economic limitation with a low reliability of supply. Therefore, compared with natural dyestuffs, synthetic colorants are better able to meet the increasingly rigorous technical demands of the present day in terms of stability and fastness. The discovery of the first human-made synthetic dye, *mauveine*, by William Henry Perkin in 1856 [6], represented one of the great technical triumphs of the 19th century, as they played a major role in the birth of organic chemistry and subsequently led to a various of other synthetic substances

Early synthetic organic dyestuffs belong to the group of organic colorants consisting of carbon compounds. They are sometimes referred to as 'coal tar dyes', since they are manufactured from substances which, until recently, were only obtained from coal tar. All these compounds are derivatives of the hydrocarbon benzene ($C_6H_6$). The development of the early synthetic dyes can be divided into three time periods [7]:

**1856–1876**: basic and acid dyes,

**1876–1893**: azo dyes and direct dyes,

**1893–1902**: sulphur dyes.

Dyes are generally divided into different groups and classes depending on their source, general dye structure and the fiber type with which they are most compatible. On the basis of their origin, natural dyes can be grouped into three distinct classes: from vegetable sources; from insect or animal sources and those derived from mineral sources. The major types of natural dyes and their origin have been classified by Hill [8].

- **Vegetable dyes** are extracted from different parts of plants and herbs including the stem, wood, roots, bark, leaves, flowers, fruits and skin of plants. These dyes give distinct pale to dark shades on both natural as well as synthetic fibres. The most known dyes derived from plants or vegetables are, i.e., logwood, turmeric, pine wood, catechu and madder.
- **Insect sources dyes** are mainly red colour, based on the anthraquinone structure. They combine with metal salts to form metal-complex dyes, to give a good wash fastness. Examples of this type of dye are, i.e., lac, kermes, cochineal and lichen.

- **Mineral sources dyes** include chrome yellow, chrome orange, chrome green, manganese brown, mineral khaki, etc. They are inorganic compounds, insoluble in water and precipitated onto the fibre by double decomposition. Certain important minerals widely used as natural dyes are, i.e., cinebor, red lead, laminated red earth, ultramarine and zinc white.

Based on their general structure, dyes can also be classified as anionic, non-ionic and cationic dyes. The anionic dyes mainly include direct acidic and reactive dyes, that form covalent bonds with the hydroxyl groups in the cellulose [9]. Major non-ionic dyes include; disperse dyes which are water insoluble and are used for most synthetic fibers [10], and cationic dyes include mainly basic and disperse dyes [11].

Acid dyes contain sulfonic groups. They are named so, as they are commonly used on nitrogenous fibers under acidic conditions. Direct dyes are often used in cotton dyeing. They are applied to the fabric under neutral conditions. Mordant dyes are acid dyes which are reacted with a metal salt prior to dyeing. The second class of dyes needs chemical reaction before application. Vat dyes are soluble in their reduced form. They are made insoluble by oxidation after they are applied to organic fibers. Sulfur dyes are also made insoluble through oxidation. The third dye class are special dyes such as disperse, solvent, and natural dyes and pigments. Disperse dyes are water insoluble and are used for most synthetic fibers. They contain anthraquinone or azo groups. Solvent dyes have an improved solubility in solvents. Pigments are set to the fabric by an adhesive [12]. Dyes most commonly applied to cotton are reactive and direct dyes. Cotton/polyester goods are dyed using reactive or direct dyes for the cotton portion of the fabric and disperse dyes for the polyester. Several auxiliary chemicals are added to the bath during the dyeing processes. These chemicals can be divided into two groups: commodity chemicals and specialty chemicals. Specialty chemicals are mixtures which have an unknown composition due to proprietary information. The mixtures are often developed to solve problems specific to the process.

### 2.1.2. Azo dyes

Among major dye categories, azo dyes constitute by far the largest group of colourants and the most important class of commercial inorganic colorant. In fact, over 50% of all the dyes used in traditional textile industries are azo dyes. As the name implies, azo dyes contains a double bond of nitrogen (-N=N-), where at least one of the nitrogen atom is attached to an aromatic group. Moreover, they acquire amphoteric properties due to the presence of additional

carboxyl, hydroxyl, amino or sulfoxyl functional groups. In other words, azo dyes can behave anionic (deprotonation at the acidic group), cationic (protonated at the amino group) or non-ionic depending upon the pH of the medium. Thus, they are excellent pH indicators. The most notable azo dyes are: acid dyes, basic dyes (cationic dyes), direct dyes (substantive dyes), disperse dyes (non-ionic dyes), reactive dyes, vat dyes and sulfur dyes [13]. Methyl yellow, methyl orange, methyl red, congo red and alizarine yellow are the most known commercial ones.

The motivation behind the commercial importance of azo dyes relies in their cost-effectiveness compared to other chemical classes of organic dyes and pigments. As a matter of fact, it may be due to the nature of the processes used in their manufacture. Almost all azo dyes are prepared on an industrial scale following two-stage reaction; the first being the synthesis of an aromatic diazonium ion from an aniline derivative (diazotisation) and the next step is coupling of the diazonium salt with an aromatic compound (azo coupling), as shown in the equation below:

$$\mathrm{Ar - NH_2} \xrightarrow[\text{Diazotisation}]{\mathrm{HNO_2}} \mathrm{Ar - N{=}N^+} \xrightarrow[\text{Azo coupling}]{\mathrm{Ar' - H}} \mathrm{Ar - N{=}N - Ar'} \qquad (1)$$

On an industrial scale, they are straightforward to synthesize, which involves low cost organic starting materials such as aromatic amines and phenols. Besides, they are capable of producing high yields; the processes are carried out at or below ambient temperatures, hence showing low energy demand. Furthermore, the synthesis reaction is carried out in water as solvent, which offers obvious economic and environmental advantages over all other solvents.

### 2.1.3. Toxicity and environmental hazard of azo dyes

The global consumption of dyes is estimated at $7x10^5$ tons/year, where textile industry consumes about two-thirds of all the world production [14]. For instance, In India, which is the second largest exporter of dyestuffs, after China, accounts for the largest consumption of dyestuffs at 80 000 tonnes. According to Guaratini et al. [15], annually in Brazil, 26.500 tons of dyes are consumed. During the textile process, it has been estimated that about 10% of the dyestuff in the dyeing process of textiles do not bind to fibres and are, therefore, released to the environment. Accordingly, enormous quantities of pollutants are discharged directly into water bodies. Among the residues of dyes that pollute environment, there are azo dyes that are discharged in large quantities, reaching until 50% of the total dye used by the industries [16]. It is true that, in one hand, azo dyes meet our needs thanks to their affordable cost, the

straightforward synthesis and great fixative properties. In the other hand, the uncontrolled disposal of azo dyes in water bodies is considered as a huge threat to the environment, especially that they showed carcinogenic and mutagenic activity, to humans, animals and plants.

Colour is the first wastewater contaminant to be recognized; in fact, a very small concentration of azo dye in water (<1ppm) is highly visible. This affects aesthetic aspect, transparency and water-gas solubility. Decreasing light penetration through water decreases photosynthetic activity, generating oxygen deficiency and de-regulating the biological cycles in lakes, rivers, and other bodies of water. Many azo dyes are also highly toxic to the ecosystem. Therefore, they can be connected to growth reduction, neurosensory damage, metabolic stress and can lead to death of fish, which impacts the growth and productivity in plants. Contamination therefore limits downstream human water use such as recreation, drinking, fishing and irrigation.

More than a century ago, the history of azo dyes effects on human health began, while numerous cases of bladder cancer in workers involved in their manufacture were observed [17]. Generally, carcinogenicity of azo dyes appears after reductive cleavage of the azo linkage to the free component amines. The example of Congo Red reduction cleavage of the –N=N- azo bond to form 1-Naphthylamine as shown in Figure 2, was suggested by Chandanshive et al. [18]. Hence, the toxicity of azo dyes would therefore be based on the toxicity of the corresponding component aromatic amine. The carcinogenicity of many azo dyes is due to the existence of benzene rings in their structure. In fact, as recently reviewed by Platzek et al.[19], aromatic amines exposures from consumer products bear risks for human health, especially associated to mutagenic and carcinogenic properties of certain aromatic amines. Benzidine, for instance, and its congeners, such as *3,3'-dimethylbenzidine*, *3,3'-dimethooxy-benzidine*, and *3,3'-dichlorobenzidine* are structural components of many azo dyes, also known as carcinogen for humans and animals. Amin et al. investigated toxic effects of two azo dyes (tartrazine and carmoisine) widely used in food products, drugs and cosmetics, on male albino rats. The dyes were administrated orally one low and the other high dose for 30 days [20]. It was concluded that those azo dyes affect adversely and alter biochemical markers in vital organs, such as liver and kidney not only at higher doses but also at low doses. Rowe et al. investigated the use of another azo dye Ponceau 4R [21]. The study results connected this dye to behaviour issues in children. It was concluded that this azo dye may increase hyperactivity in affected children. It is important to emphasize that azo dyes are toxic only after reduction and cleavage of the azo linkage to give aromatic amines. The aromatic amines are metabolically oxidized to reactive

electrophilic species that covalently bind DNA. In fact, Ali et al. studied the genotoxic effects of the azo dye Sunset yellow [22]. This dye was assessed in vivo in female rats for 12 weeks. Different dosages of the Sunset Yellow induced a DNA damage in liver cells.

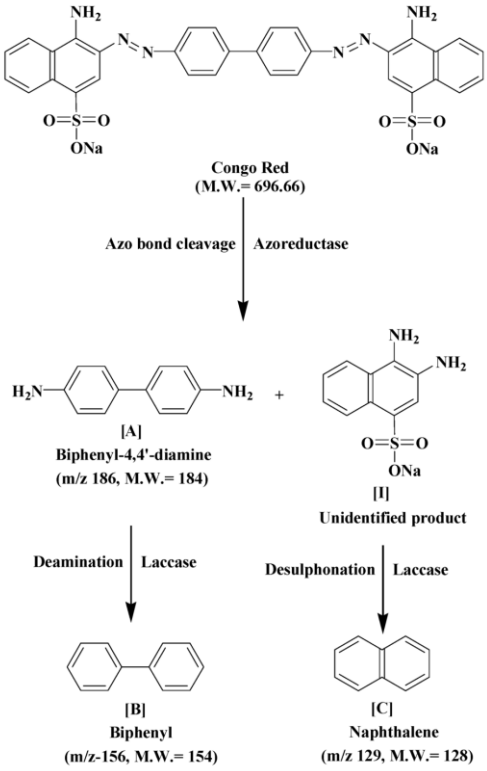


*Figure 2. Reduction cleavage mechanism of the anionic azo dye Congo Red [23].* Reprinted by permission from *International Journal of Environmental Research and Public Health,* 12, H. Lade et al., Mineralization and Detoxification of the Carcinogenic Azo Dye Congo Red and Real Textile Effluent by a Polyurethane Foam Immobilized Microbial Consortium in an Upflow Column Bioreactor, 6894-6918. Copyright (2015), with permission from MDPI.

In addition to the carcinogenic and genotoxic effects, it was shown that azo dyes cause dysfunction in the reproductive organs of some rodents. For instance, a pre-natal exposure to Congo Red affects the reproductive organs of young female rats with a reduction of the fertility [24]. This study was confirmed by Suryavathi et al. [25]. They showed that toxic effects of textile effluents containing azo dyes caused the decrease of the body weight and length of the reproductive organ of the animals treated.

Luckily, several countries have adopted environmental legislation and requirements to restrict the use of hazardous dyes. One of the most known laws is called "*The German Azo Ban*". According to the German legislation, effective from 1st April 1996, requires that articles regularly in contact with the human body must not be treated with azo dyestuffs, which release harmful amines on reductive cleavage of the groups [26]. It was also established that the referred textile articles cannot contain the 22 amines listed in the banned list [27], in a

concentration higher than 30 ppm and, if the articles are made of recycled fibres, they cannot contain more than 70 ppm. Few other countries, such as Netherlands, Turkey, France and India, followed the same restrictions imposed by Germany, and therefore, prohibited the import and marketing of textiles containing azo dyes, that on reductive cleavage release any of the cited below named amines.

Accordingly, the legislation covering liquid industrial effluent is becoming stricter, especially in the more developed countries, and imposes the treatment of any wastewater before it is released into the environment. Since the end of the 1970s, in Europe, the directives are increasingly severe and zero rejection is being sought by 2020.

## 2.2. Wastewater treatment techniques

During the last 30 years, several physical, chemical and biological technologies have been reported such as flotation [28], precipitation [29], oxidation [30], adsorption [31], ion exchange [32], membrane filtration [33], electrochemistry [34], biodegradation [35] and phytoremediation [36]. What is the most efficient technique? It is almost impossible to give a direct answer, since every treatment presents its own advantages, and constraints not only in terms of cost but also in terms of efficiency, feasibility and environmental impact. Usually in practice, conventional wastewater treatment consists of a combination of physical, chemical and/or biological processes and operations to remove solids including colloids, organic matter, nutrients, soluble contaminants (metals, organics, etc.) from effluents. Table 1 summarizes the advantages and disadvantages of the most used conventional water treatment processes:

Table 1. Overview of the main techniques for the treatment of polluted industrial wastewater.

| Process | Advantages | Drawbacks |
|---|---|---|
| **Chemical precipitation** | Technologically simple<br>Economically feasible<br>Adapted to high pollutant loads<br>Not metal selective | Chemical consumption<br>Low removal efficiency of metal ions at low concentration<br>High sludge production and disposal problems |
| **Coagulation/Flocculation** | Simple, economically attractive<br>Commercial availability of a wide range of chemicals<br>Good sludge settling<br>Efficiency for insoluble contaminants (dyes…) | High sludge volume generation, handling and disposal problems<br>Low removal efficiency of arsenic<br>Use of non-reusable chemicals (coagulants, flocculants, aid chemicals) |
| **Oxidation**<br>**Chemical oxidation** | Simple, rapid and efficient process<br>No sludge production<br>Good elimination of colour and odour<br>Initiation and acceleration of azo bond cleavage<br>Possibility of water recycle | High energy cost<br>Chemicals required<br>Efficiency influenced by the type of oxidant<br>Formation of by-products<br>Generate sludge |
| **Membrane filtration** | Availability of a wide range of commercial membranes<br>Simple, rapid and efficient at high concentrations<br>Production of high-quality treated effluent<br>Almost no chemicals required<br>Low solid waste generation<br>Elimination of all types of dyes<br>Possible to be metal selective | High investment costs for small and medium industries<br>High energy requirements<br>High maintenance and operation costs<br>Rapid membrane fouling at high concentrations<br>Not interesting at low solute feed concentrations<br>Elimination of the concentrate |
| **Biological methods** | Large number of species used in mixed cultures<br>Efficiently elimination of biodegradable organic matter<br>High removal of biochemical oxygen demand and suspended solids | Requires maintenance of the microorganisms<br>Change of mixed cultures during the decomposition process<br>Complexity of the microbiological mechanisms |
| **Flotation** | Efficient for removal of small particles<br>Useful for primary clarification<br>Metal selective<br>Low retention time | High initial capital cost<br>Energy costs<br>Maintenance costs no negligible<br>Chemical required |
| **Ion exchange** | Wide range of commercial products available from several manufacturers<br>Technologically simple<br>Rapid and efficient process<br>Produce a high-quality treated effluent<br>Relatively inexpensive and efficient for metal removal | Large volume requires large columns<br>Rapid saturation and clogging of the reactors<br>Elimination of the resin<br>Very sensitive to pH of effluent |

Conventional treatment methods such as chemical oxidation, distillation, ion exchange, biological degradation, oxidation, chemical precipitation, adsorption and membrane filtration are frequently used to treat textile effluents, and some of them are generally efficient but present some limitations. For example, distillation is probably the oldest method of water purification. However, organics with boiling points lower than 100 °C cannot be removed efficiently and can actually become concentrated in the product water. Besides, distillation requires large amounts of energy and water, therefore it is an expensive technique. Biological treatment processes are also frequently used to treat textile effluents. However, they have not been very successful for the removal of dyes, due to the essential non-biodegradable nature of most of the dyes These processes are generally efficient for biochemical oxygen demand and suspended solids removal but they are ineffective for removing colour from the waste. The physical/chemical methods that have been proven to be successful are adsorption, coagulation/flocculation, membrane filtration, chemical oxidation and electrochemical treatment. On the other hand, ion exchange and reverse osmosis are more attractive processes because the pollutant values can be recovered along with their removal from the effluents. However, reverse osmosis, ion exchange and advanced oxidation processes do not seem to be economically feasible because of their relatively high investment and operational cost. Among these processes, we chose to use adsorption as a technique for cationic and anionic azo dyes removal from aqueous solutions. Adsorption process shows potential as one of the most efficient methods for the treatment and removal of organic contaminants in wastewater treatment. Adsorption offers the advantage of its simple design, ease of operation and low investment in term of both initial cost and land required [37]. Moreover, adsorption technology is widely considered to be the most promising and robust method to remove contaminants with exceedingly low concentrations, a regime where most other separation techniques are challenged due to the small concentration gradients involved. In addition, adsorption is a versatile method that can remove or minimize a wide variety of organic and inorganic compounds, hence producing highly pure effluents for point-of-use water applications.

### 2.2.1. Adsorption

Adsorption can be defined as the process of accumulation of any substance giving higher concentration of molecular species on the surface of another substance as compared to that in the bulk. The substance that concentrates at the surface is called adsorbate, and the material upon whose surface the adsorption takes place is called an adsorbent. Adsorption is strictly an

interfacial phenomenon, unlike "absorption" wherein the absorptive species penetrates the absorbent. The nature of the interface may be solid-liquid, gas-liquid, liquid-liquid or solid-gas. Of these types of adsorption, only liquid–solid adsorption is widely used in water and wastewater treatment. Although adsorption may be classified based on different parameters such as localized, non-localized or static dynamic, the most common one is based on the strength of the binding forces i.e., *physisorption* and *chemisorption*. In *physisorption*, the target molecules are attracted to the surface of pore walls within a high surface-area sorbent by van der Waals forces and have a low heat of adsorption that is only slightly greater than heat of sublimation of the adsorbate. In *chemisorption*, the target molecule undergoes a covalent chemical reaction to bind to certain sites on the sorbent with a much greater heat of adsorption, roughly equal to the heat of reaction [38]. The adsorption can occur in two modes of operation; *(i) in a batch process,* where the adsorbent is dumped into a constant volume of contaminated fluid and adsorption then ensues, the adsorbent is ultimately in equilibrium with the residual concentration in the bulk. Material balances on the solution dictate that this latter concentration is significantly lower than that of the feed, and by contrast *(ii) in a fixed bed process*, contaminated fluid is fed continuously through a packed column of adsorbent, which ultimately becomes fully loaded with contaminants (i.e., adsorbate) when the adsorbent achieves equilibrium with the feed concentration. Mass transfer limitations and axial dispersion in actuality limit the degree of adsorbent utilization, but a large fraction of the column is in fact in equilibrium with the feed. Accordingly, in this work we chose to use the batch process for the adsorption of different azo dyes onto FAp and HAp. Although continuous flow adsorption in fixed bed columns has wide application in different areas of the petroleum refining and chemical industry, cyclic-batch processes may be preferred in some cases because of the complexity of design and difficulties in controlling the continuous processes [39]. Kausar et al. compared the adsorption of radioactive metals onto rice husk waste using batch and column modes. Results revealed that the adsorbent has potential to remove U(VI) ions and batch adsorption was found to be efficient versus column mode.[40]

In order to carry out the adsorption experiments and to prevent common mistakes in interpreting adsorption processes and mechanisms, it is important to study the properties of the adsorbent using various techniques to characterize it, as detailed in Figure 3.

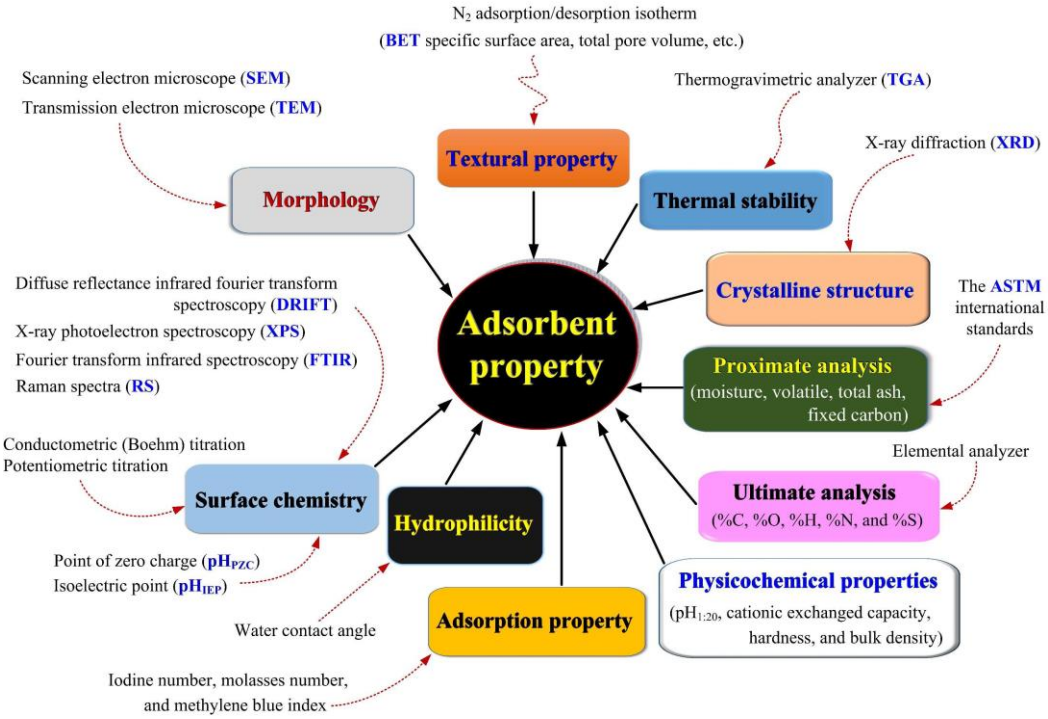


Figure 3. Numerous properties of the adsorbent determined by different techniques [41]. Reprinted from Water Research, 120, H. N. Tran et al., Mistakes and inconsistencies regarding adsorption of contaminants from aqueous solutions: A critical review, 88-116, Copyright (2017), with permission from Elsevier.

The behaviour of an adsorbing substance onto surfaces has been interpreted by different models. In fact, more than forty theories have been developed so far to describe adsorption. Thus, the first requirement is that the proposed model should fit the experimental isotherm. A proper understanding and interpretation of adsorption isotherms is critical for the overall improvement of adsorption mechanism pathways and effective design of adsorption system [42]. In the following, we will describe different isotherm and kinetic models than the most common ones, *i.e* Langmuir, Freundlich, Tempkin, and Dubinin-Radushkevich for isotherms and pseudo-first-order, pseudo-second-order, intra-particle diffusion model and Elovich kinetic models. Those models were extensively investigated in our published work, and for more details we refer you to section 4.2.

- **Henry Isotherm model** is the simplest adsorption isotherm in which the amount of surface adsorbate is proportional to the partial pressure of the adsorptive gas. This isotherm model describes an appropriate fit to the adsorption of adsorbate at relatively low concentrations such that all adsorbate molecules are secluded from their nearest neighbours [43]. Thus, the equilibrium adsorbate concentrations in the liquid and adsorbed phases are related to the linear expression:

$$q_e = K_{HE} C_e \quad (2)$$

where $q_e$ is amount of the adsorbate at equilibrium (mg/g), $K_{HE}$ is Henry's adsorption constant, and $C_e$ is equilibrium concentration of the adsorbate on the adsorbent.

- **Hill Isotherm model** describes the binding of different species onto homogeneous substrates. This model assumes that adsorption is a cooperative phenomenon with adsorbates at one site of the adsorbent influencing different binding sites on the same adsorbent [44]. The linear form of this isotherm is expressed as follows, where $K_D$, $n_H$, and $q_H$ are constants:

$$\log \frac{qe}{q_H - qe} = n_H \log(Ce) - \log(K_D) \quad (3)$$

- **Kahn Isotherm model** is a general model for adsorption of biadsorbate from pure dilute equations solutions [45]. This isotherm model is expressed as follows:

$$Q_e = \frac{Q_{max}\, b_k\, C_e}{(1 + b_k\, C_e)\, a_k} \quad (4)$$

where $a_k$ is Kahn isotherm model exponent, $b_k$ is Khan isotherm model constant, and $Q_{max}$ is Khan isotherm maximum adsorption capacity (mg $g^{-1}$).

- **Jovanovic Isotherm model** is predicated on the assumptions contained in the Langmuir model, but in addition the possibility of some mechanical contacts between the adsorbate and adsorbent. The linear form of the Jovanovic isotherm is expressed as follows [46]:

$$\ln q_e = \ln q_{max} - K_j C_e \quad (5)$$

where $qe$ is amount of adsorbate in the adsorbent at equilibrium (mg $g^{-1}$), $q_{max}$ is maximum uptake of adsorbate obtained from the plot of ln $q_e$ versus $C_e$, and $K_J$ is Jovanovic constant.

Adsorption kinetics can be represented by a plot of uptake vs. time; this plot is known as a kinetic isotherm. This plot forms the basis of all kinetics studies because its shape represents the under- lying kinetics of the process. The kinetics are dependent on material factors, such as adsorbent and adsorbate types, and experimental factors, such as temperature and pH [47]. Typically, a batch experiment is conducted to collect kinetic data. Ensuring constant experimental conditions during batch adsorption is important.

- **Avrami kinetic model**: The adsorption rate coefficient might have a temporal dependency during the adsorption process [48]. A kinetic system with a time-dependent rate

coefficient is said to exhibit "fractal-like kinetics". The Avrami rate equation is one model that describes such kinetic behaviour. The equation is:

$$\frac{dq}{dt} = k\, n\, t^{n-1}\, (q_e - q) \quad (6)$$

where k is the Avrami kinetic constant, and n is a model constant related to the adsorption mechanism. $k\, n\, t^{n-1}$ can be construed as the effective rate coefficient.

- **Linear film diffusion kinetic model**: When the accumulation of adsorptive on the sorbent surface is equal to the adsorptive diffusion rate across the liquid film (boundary layer), as in a film diffusion-dominated system, the bulk liquid phase concentration of adsorptive can be expressed as [49]:

$$\frac{dC}{dt} = -\, k_f\, (C - C_s) \quad (7)$$

where $k_f$ is a film diffusion coefficient ($min^{-1}$), and Cs is the concentration at the liquid–solid interface (mg/l).

The list of models covered here is by no means comprehensive. Other models that are useful for adsorption or adsorption–diffusion modelling but are not discussed here are parabolic diffusion [50], hyperbolic model [51], branched pore diffusion model [52], second-order reversible reaction model [53] and mixed-order rate equation [54], among others.

Generally, linear regression analysis is one of the most applied tools for defining the best fitting adsorption models due to its simplicity to be implemented and its applicability to a broad array of isotherm and kinetic adsorption systems [55]. Malpractices are common to the point of gaining ground in liquid systems modelling. Therefore, a large experimental error can make the right model fit poorly and the wrong model fit adequately, thereby providing misleading isotherm and kinetic information. Fortunately, the nonlinear forms of kinetic models are more robust toward experimental errors and are hence preferred, especially when experimental errors are not controlled [56]. In addition, with the arrival of the evolution of computer technology, the use of nonlinear isotherm modelling has been extensively used, since nonlinear regression has become less of a hassle and should therefore be prioritized over the linear method. In our both adsorption studies, we chose to work with both fittings, linear fitting for the adsorption of MB, CR and Rh6G onto the FAp, in section 4.2. While, the nonlinear regression for the adsorption of CR onto HAp, detailed in section 4.3.

### 2.2.2. Adsorbents for removal of azo dyes

One of most known and widely used adsorbent is activated carbon (AC). In fact, it has been proven to be an effective adsorbent for the removal of a wide variety of organic and inorganic pollutants dissolved in aqueous media, or from gaseous environment [57]. The efficiency of AC as an adsorbent, is due to its unique properties that are usually related to its internal pore structure, surface characteristics, and especially the presence of functional group on pore surface and the activation process. In fact, surface structures of these functional groups are by far the most important structures influencing surface characteristics of activated carbon. Despite its prolific use in water and wastewater treatment, the biggest barrier of its application by industries is its initial cost and the need for a constant regeneration system make it less economically viable as an adsorbent [58]. Besides, alumina and silica gel were often used for dye wastewater treatment [59, 60]. In fact, they show high surface area ranging from 200 to 300 $m^2g^{-1}$ for alumina [61] and from 250 to 900 $m^2g^{-1}$ for silica gel [62]. Although the adsorption capacities were high but the drawbacks were that those adsorbents are costly. Thus, the challenge for lot of scientists is to find and design a suitable adsorbent which possess both high adsorption capacity and at the same time meet the standards of low cost and minimal environmental impact.

Low-cost adsorbents (LCAs) involve generally natural materials or wastes of industries or synthetically prepared materials, that are less expensive and can be used without or after some minor treatment as adsorbents. These LCAs can be classified (i) depending on their origins; natural such as wood, peat, phosphate, coal, etc, industrial/agricultural wastes such as slag, fly ash, phosphogypsum, etc, or (ii) on basis of their nature, either organic or inorganic. In search for alternatives to AC and other expensive adsorbents, the first use of natural coal as an adsorbent was studied by Mittal et al.[63] for the removal of two cationic dyes (Rhodamine B and methylene blue), and one anionic dye (Sandola rhodine). The coal was pre-treated and was sulfonated then heated in a water batch. Coal is not a pure material; hence it possesses a variety of surface and sorption properties. The results showed that the nature of adsorption depended on the nature of the dye: In fact, the adsorption was found to be physisorption only in the case of the anionic dye. It has been also suggested that the physical and chemical change after pre-treatment usually determines the sorption properties. Mohan et al. [64] studied coal based sorbents for colour removal of the dye direct brown, and compared the results with commercial activated carbon. The coal-based adsorbents were found to achieve equilibrium in a short time 60 min compared to AC 400 min. It can be explained by the presence of acidic

groups (carboxyl and hydroxyl) on the coal-based adsorbents. The sorption interaction of the direct dye on to the coal-based sorbents obeyed a first-order irreversible rate equation suggesting a chemisorption mechanism, while on activated carbon the data fitted a first-order reversible rate equation indicating physisorption. Besides, peat is also one of the natural adsorbents widely available and often studied for the removal of dyes. It was studied for the first time in 1976 by Poots et al [65], for the removal of telon blue. It was found that peat showed better performance than wood, and achieved an equilibrium adsorption capacity of 16.3 $mg.g^{-1}$ with a contact time of 2h. Regarding the recycling of the adsorbent afterword, and just like wood, the exhausted peat adsorbent may be disposed by burning and use the heat for steam generation. More recently, Sun et al. [66] used modified peat with polyvinylalcohol and formaldehyde. It was used for the removal of a variety of anionic dyes, such as basic violet 14 and basic green 4. It showed better adsorption capacities, 400 and 350 $mg.g^{-1}$ respectively.

Natural clay minerals are well known as strong candidates as a LCA. In fact, clay materials possess a layered structure and are considered as host materials. Their sorption properties also come from their high surface area and high porosity [67]. It is considered to be 20 times cheaper than that of activated carbon [68]. Recently, clay was extensively studied as an adsorbent not only for inorganic but also organic molecules, especially interactions between dyes and clays. Clay minerals exhibit a strong affinity for both cationic and anionic dyes. However, the sorption capacity for cationic dye is much higher than for anionic dye because of the ionic charges on the dyes and character of the clay. The adsorption of dyes on clay minerals is mainly dominated by ion-exchange processes. This means that the sorption capacity can vary strongly with pH. This was proved by Al-Ghouti et al. [69] by showing that the mechanism of adsorption of dye onto diatomite is due to physical adsorption (depending on the particle size) and the presence of electrostatic interactions (depending on the pH used). One of the best removal capability of clay materials to take up dye has been reported by Espantaleon et al [70]. The adsorption capacity of 360.5 $mg.g^{-1}$ by the bentonite was achieved. Due to its high surface area, it was suggested that bentonite is a good adsorbent for cationic dye removal. Similar results have been published by Bagane et al [71]. The adsorption of dyes on kaolinite was also studied. The adsorption to kaolinite was about 20 times greater than to alumina Hence, *Table 2* is a summary of some relevant published data in the adsorption properties of some alternative LCAs used for azo dyes removal.

Table 2: Adsorption capacities and other parameters for the removal of azo dyes by a commercial activated carbon and other alternative low-cost adsorbents.

| Adsorbent | Azo dye | Concentration mg $L^{-1}$ | Contact time | pH | Adsorption capacity ($mg.g^{-1}$) | Ref |
|---|---|---|---|---|---|---|
| **Commercial AC (E.Merck India)** | Basic blue 9 | 100 - 400 | 90 min | 7.4 | 980.3 | [72] |
| **Wood** | Basic blue 69 | - | 2 h | - | 100.1 | [73] |
| **Rice Husk** | Basic Red 2 | 10 - 1000 | 6 h | - | 838 | [74] |
| **Neem Sawdust** | Rhodamine B | 12 | 30 min | 7.2 | 2.355 | [75] |
| **Activated sewage sludge** | Crystal Violet | 100 - 1000 | 20 min | - | 270.88 | [76] |
| **Orange Peel** | Congo Red | 10 - 90 | 90 min | | 7.08 | [77] |
| **Chitosan** | Congo Red | - | 12 h | 7 | 81.23 | [78] |
| **Modified zeolite** | Reactive red 239 | - | - | - | 111.1 | [79] |
| **Treated cotton** | Reactive yellow 23 | - | - | - | 302 | [80] |
| **Mixture almond shells** | Direct red 80 | 50 - 150 | - | 6 | 22.422 | [81] |
| **Palm oil ash** | Disperse blue<br>Disperse Red | -<br>- | 60 min | 2 | 49.5<br>61.4 | [82] |
| **Pinewood** | Acid blue 264 | | 5 days | 6.4 | 1176 | [83] |
| **Fly ash** | Basic Blue 9 | | | | 75.52 | [84] |
| **Clay** | Basic Blue 9 | | 60 min | | 6.3 | [85] |
| **Metal hydroxide sludge** | Reactive red 141 | 10 - 200 | - | 7 | 56.18 | [86] |
| **Red mud** | Direct red 28 | 10 - 90 | 90 min | | 7.08 | [87] |
| **Calcined alunite** | Acid blue 40 | 25 - 200 | 90 min | 2 | 212.8 | [88] |
| **Modified silica** | Acid blue 25 | - | - | - | 45.8 | [89] |
| **Kaolnite** | Metomega chrome- Orange | 10 | 150 min | 3h | 0.6506 | [90] |

## 2.3. References

[1] A. Kramell, X. Li, R. Csuk, M. Wagner, T. Goslar, P.E. Tarasov, N. Kreusel, R. Kluge, C.-H. Wunderlich, Dyes of late Bronze Age textile clothes and accessories from the Yanghai archaeological site, Turfan, China: Determination of the fibers, color analysis and dating, *Quaternary International*, 348 (**2014**) 214-223.
[2] M.C. Burkitt, Ancient Egyptian Materials and Industries, *Nature*, 162 (**1948**) 429-429.
[3] C.J. Cooksey, Indigo: an annotated bibliography, *Biotechnic & Histochemistry*, 82 (**2007**) 105-125.
[4] H. Puchtler, S.N. Meloan, M.S. Terry, On the history and mechanism of alizarin and alizarin red stains for calcium *Journal of Histochemistry & Cytochemistry*, 17 (**1969**) 110-124.
[5] R.R. Stieglitz, The Minoan Origin of Tyrian Purple, *The Biblical Archaeologist*, 57 (**1994**) 46-54.
[6] T.F.G.G. Cova, A.A.C.C. Pais, J.S. Seixas de Melo, Reconstructing the historical synthesis of mauveine from Perkin and Caro: procedure and details, *Scientific Reports*, 7 (**2017**) 6806.
[7] F.J. Baker, R.E. Silverton, Biological Staining, *Introduction to Medical Laboratory Technology*, 5 (**1976**), 384-392.
[8] D.J. Hill, Is there a future for natural dyes?, *Review of Progress in Coloration and Related Topics*, 27 (**1997**) 18-25.
[9] T. Robinson, G. McMullan, R. Marchant, P. Nigam, Remediation of dyes in textile effluent: a critical review on current treatment technologies with a proposed alternative, *Bioresour Technol*, 77 (**2001**) 247-255.
[10] K. Blus, J. Bemska, Effect of nonionic surfactants on the dyeing process of cellulose fibres with C.I. Reactive Blue 217, *Autex Research Journal*, 10 (**2010**) 64-68.
[11] Y. Zhou, M. Zhang, X. Hu, X. Wang, J. Niu, T. Ma, Adsorption of Cationic Dyes on a Cellulose-Based Multicarboxyl Adsorbent, *Journal of Chemical & Engineering Data*, 58 (**2013**) 413-421.
[12] G.M. Ziarani, R. Moradi, N. Lashgari, H.G. Kruger, Introduction and Importance of Synthetic Organic Dyes, *Metal-Free Synthetic Organic Dyes*, 1 (**2018**), 1-7.
[13] A. Price, A.C. Cohen, I. Johnson, J.J. Pizzuto, Fabric science swatch kit, *Fairchild Publications-New York*, (**2005)**.
[14] M. Scholz, Dye Wastewater Treatment by Vertical-Flow Constructed Wetlands, *Sustainable Water Treatment*, 8 (**2019**), 191-213.
[15] C.C.I. Guaratini, M.V.B. Zanoni, Corantes têxteis, *Quim Nova*, 23 (**2000**) 71-78.
[16] R.B. Chavan, Environmentally friendly dyes, H*andbook of Textile and Industrial Dyeing*, 7 (**2011**), 515-561.
[17] L. Rehn, Blasengeschwülste bei Fuchsin-Arbeitern, *Aktuel Urol*, 22 (**1991**) 387-388.
[18] V.V. Chandanshive, N.R. Rane, A.S. Tamboli, A.R. Gholave, R.V. Khandare, S.P. Govindwar, Co-plantation of aquatic macrophytes Typha angustifolia and Paspalum scrobiculatum for effective treatment of textile industry effluent, *J Hazard Mater*, 338 (**2017**) 47-56.
[19] T. Platzek, Risk from exposure to arylamines from consumer products and hair dyes, *Front Biosci (Elite Ed)*, 2 (**2010**) 1169-1183.
[20] K.A. Amin, H. Abdel Hameid, A.H. Abd Elsttar, Effect of food azo dyes tartrazine and carmoisine on biochemical parameters related to renal, hepatic function and oxidative stress biomarkers in young male rats, *Food Chem Toxicol*, 48 (**2010**) 2994-2999.
[21] M. Šuleková, M. Smrčová, A. Hudák, M. Heželová, M. Fedorová, Organic Colouring Agents in the Pharmaceutical Industry, *Folia Veterinaria*, 61 (**2017**) 32-46.
[22] M.Y. Ali, G.M. Hassan, A.M.S. Hassan, Z.A. Mohamed, M.F. Ramadan, In vivo genotoxicity assessment of sunset yellow and sodium benzoate in female rats, *Drug Chem Toxicol*, (**2018**) 1-10.

[23] H. Lade, S. Govindwar, D. Paul, Mineralization and Detoxification of the Carcinogenic Azo Dye Congo Red and Real Textile Effluent by a Polyurethane Foam Immobilized Microbial Consortium in an Upflow Column Bioreactor, *International Journal of Environmental Research and Public Health*, 12 (**2015**) 6894-6918.
[24] L.E. Gray, Jr., J.S. Ostby, R.J. Kavlock, R. Marshall, Gonadal effects of fetal exposure to the azo dye congo red in mice: infertility in female but not male offspring, *Fundam Appl Toxicol*, 19 (**1992**) 411-422.
[25] V. Suryavathi, S. Sharma, S. Sharma, P. Saxena, S. Pandey, R. Grover, S. Kumar, K.P. Sharma, Acute toxicity of textile dye wastewaters (untreated and treated) of Sanganer on male reproductive systems of albino rats and mice, *Reproductive Toxicology*, 19 (**2005**) 547-556.
[26] M.S. Narvekar, A.K. Srivastava, Separation of banned amine isomers in relation to german ban on azo dyes by derivatization on GC-MS, *Chromatographia*, 55 (**2002**) 729-735.
[27] EC, Commission Regulation (EC) No 552/2009 of 22 June 2009 Amending Regulation (EC) No 1907/2006 of the European Parliament and of the Council on the Registration, Evaluation, Authorisation and Restriction of Chemicals (REACH) as Regards Annex XVII, *http://eur-lexeuropaeu/LexUriServ/LexUriServdo?uri=OJ:L:2009:164:0007:0031:EN:PDF*, (**2009**).
[28] J. Rubio, M.L. Souza, R.W. Smith, Overview of flotation as a wastewater treatment technique, *Miner Eng*, 15 (**2002**) 139-155.
[29] L.K. Wang, D.A. Vaccari, Y. Li, N.K. Shammas, Chemical Precipitation, *Physicochemical Treatment Processes*, (**2005**), 141-197.
[30] B. Legube, N. Karpel Vel Leitner, Catalytic ozonation: a promising advanced oxidation technology for water treatment, *Catal Today*, 53 (**1999**) 61-72.
[31] I. Ali, V.K. Gupta, Advances in water treatment by adsorption technology, *Nature Protocols*, 1 (**2006**) 2661-2667.
[32] I. Dobrevsky, M. Dimova-Todorova, T. Panayotova, Electroplating rinse waste water treatment by ion exchange, *Desalination*, 108 (**1997**) 277-280.
[33] G. Pearce, Introduction to membranes: Filtration for water and wastewater treatment, *Filtration & Separation*, 44 (**2007**) 24-27.
[34] Y. Feng, L. Yang, J. Liu, B.E. Logan, Electrochemical technologies for wastewater treatment and resource reclamation, *Environmental Science: Water Research & Technology*, 2 (**2016**) 800-831.
[35] P. Dhall, R. Kumar, A. Kumar, Biodegradation of Sewage Wastewater Using Autochthonous Bacteria, *The Scientific World Journal*, 2012 (**2012**) 8.
[36] X.-b. Zhang, P. Liu, Y.-s. Yang, W.-r. Chen, Phytoremediation of urban wastewater by model wetlands with ornamental hydrophytes, *Journal of Environmental Sciences*, 19 (**2007**) 902-909.
[37] Z. Al-Qodah, Adsorption of dyes using shale oil ash, *Water Res*, 34 (**2000**) 4295-4303.
[38] A.H. Berger, A.S. Bhown, Comparing physisorption and chemisorption solid sorbents for use separating $CO_2$ from flue gas using temperature swing adsorption, *Energy Procedia*, 4 (**2011**) 562-567.
[39] M.B. Park, E.D. Park, W.-S. Ahn, Recent Progress in Direct Conversion of Methane to Methanol Over Copper-Exchanged Zeolites, *Frontiers in chemistry*, 7 (**2019**) 514-514.
[40] A. Kausar, H.N. Bhatti, M. Iqbal, A. Ashraf, Batch versus column modes for the adsorption of radioactive metal onto rice husk waste: conditions optimization through response surface methodology, *Water Sci Technol*, 76 (**2017**) 1035-1043.
[41] H.N. Tran, S.-J. You, A. Hosseini-Bandegharaei, H.-P. Chao, Mistakes and inconsistencies regarding adsorption of contaminants from aqueous solutions: A critical review, *Water Res*, 120 (**2017**) 88-116.
[42] M.I. El-Khaiary, Least-squares regression of adsorption equilibrium data: Comparing the options, *J Hazard Mater*, 158 (**2008**) 73-87.

[43] F.G. Helfferich, Principles of adsorption & adsorption processes, by D. M. Ruthven, John Wiley & Sons, 1984, xxiv + 433 pp, *AlChE J*, 31 (**1985**) 523-524.
[44] N. Ayawei, A.N. Ebelegi, D. Wankasi, Modelling and Interpretation of Adsorption Isotherms, *Journal of Chemistry*, 2017 (**2017**) 11.
[45] M. Rahbari, A.S. Goharrizi, Adsorption of Lead(ll) from Water by Carbon Nanotubes: Equilibrium, Kinetics, and Thermodynamics, *Water Environ Res*, 81 (**2009**) 598-607.
[46] D.N. Misra, Jovanovich adsorption isotherm for heterogeneous surfaces, *J Colloid Interface Sci*, 43 (**1973**) 85-88.
[47] A. Regti, M.R. Laamari, S.-E. Stiriba, M. El Haddad, Use of response factorial design for process optimization of basic dye adsorption onto activated carbon derived from Persea species, *Microchem J*, 130 (**2017**) 129-136.
[48] M. Haerifar, S. Azizian, Fractal-Like Adsorption Kinetics at the Solid/Solution Interface, *The Journal of Physical Chemistry C*, 116 (**2012**) 13111-13119.
[49] F.E. Ahmed, B.D. Young, A.W. Bryson, Comparison and modelling of the adsorption kinetics of gold cyanide onto activated carbon and resin in a silica slurry, *Hydrometallurgy*, 30 (**1992**) 257-275.
[50] X.-E. Shen, X.-Q. Shan, D.-M. Dong, X.-Y. Hua, G. Owens, Kinetics and thermodynamics of sorption of nitroaromatic compounds to as-grown and oxidized multiwalled carbon nanotubes, *J Colloid Interface Sci*, 330 (**2009**) 1-8.
[51] L. Cáceres, M. Escudey, E. Fuentes, M.E. Báez, Modeling the sorption kinetic of metsulfuron-methyl on Andisols and Ultisols volcanic ash-derived soils: Kinetics parameters and solute transport mechanisms, *J Hazard Mater*, 179 (**2010**) 795-803.
[52] X.-Y. Yang, B. Al-Duri, Application of branched pore diffusion model in the adsorption of reactive dyes on activated carbon, *Chem Eng J*, 83 (**2001**) 15-23.
[53] D.C. Koopman, H.H. Lee, Second-order reversible reactions and diffusion in a slab-like medium: an application of the weierstrass elliptic pe-function, *Chem Eng Sci*, 46 (**1991**) 1165-1177.
[54] A.W. Marczewski, Application of mixed order rate equations to adsorption of methylene blue on mesoporous carbons, *Appl Surf Sci*, 256 (**2010**) 5145-5152.
[55] Y.-S. Ho, Review of second-order models for adsorption systems, *J Hazard Mater*, 136 (**2006**) 681-689.
[56] K.L. Tan, B.H. Hameed, Insight into the adsorption kinetics models for the removal of contaminants from aqueous solutions, *Journal of the Taiwan Institute of Chemical Engineers*, 74 (**2017**) 25-48.
[57] R. Malik, D.S. Ramteke, S.R. Wate, Adsorption of malachite green on groundnut shell waste based powdered activated carbon, *Waste Manage (Oxford)*, 27 (**2007**) 1129-1138.
[58] F.K. Yuen, B.H. Hameed, Recent developments in the preparation and regeneration of activated carbons by microwaves, *Adv Colloid Interface Sci*, 149 (**2009**) 19-27.
[59] S. Banerjee, S. Dubey, R.K. Gautam, M.C. Chattopadhyaya, Y.C. Sharma, Adsorption characteristics of alumina nanoparticles for the removal of hazardous dye, Orange G from aqueous solutions, *Arabian Journal of Chemistry*, (**2017**).
[60] R.S.d. Farias, H.L.d.B. Buarque, M.R.d. Cruz, L.M.F. Cardoso, T.d.A. Gondim, V.R.d. Paulo, Adsorption of congo red dye from aqueous solution onto amino-functionalized silica gel, *Engenharia Sanitaria e Ambiental*, 23 (**2018**) 1053-1060.
[61] C.L. Mantell, Adsorption, *McGraw-Hill-New York*, (**1951**).
[62] D.D. Duong, Adsorption analysis : equilibria and kinetics, in, Imperial College Press, London, **1998**.
[63] A.K. Mittal, C. Venkobachar, Sorption and Desorption of Dyes by Sulfonated Coal, *Journal of Environmental Engineering*, 119 (**1993**) 366-368.
[64] D. Mohan, C.U. Pittman, Activated carbons and low cost adsorbents for remediation of tri- and hexavalent chromium from water, *J Hazard Mater*, 137 (**2006**) 762-811.

[65] V.J.P. Poots, G. McKay, J.J. Healy, The removal of acid dye from effluent using natural adsorbents—I peat, *Water Res*, 10 (**1976**) 1061-1066.
[66] Q. Sun, L. Yang, The adsorption of basic dyes from aqueous solution on modified peat–resin particle, *Water Res*, 37 (**2003**) 1535-1544.
[67] M. Alkan, S. Çelikçapa, Ö. Demirbaş, M. Doğan, Removal of reactive blue 221 and acid blue 62 anionic dyes from aqueous solutions by sepiolite, *Dyes and Pigments*, 65 (**2005**) 251-259.
[68] S. Babel, T.A. Kurniawan, Low-cost adsorbents for heavy metals uptake from contaminated water: a review, *J Hazard Mater*, 97 (**2003**) 219-243.
[69] M.A. Al-Ghouti, M.A.M. Khraisheh, S.J. Allen, M.N. Ahmad, The removal of dyes from textile wastewater: a study of the physical characteristics and adsorption mechanisms of diatomaceous earth, *Journal of Environmental Management*, 69 (**2003**) 229-238.
[70] A.G. Espantaleón, J.A. Nieto, M. Fernández, A. Marsal, Use of activated clays in the removal of dyes and surfactants from tannery waste waters, *Applied Clay Science*, 24 (**2003**) 105-110.
[71] M. Bagane, S. Guiza, Elimination d'un colorant des effluents de l'industrie textile par adsorption, *Annales de Chimie Science des Matériaux*, 25 (**2000**) 615-625.
[72] N. Kannan, M.M. Sundaram, Kinetics and mechanism of removal of methylene blue by adsorption on various carbons—a comparative study, *Dyes and Pigments*, 51 (**2001**) 25-40.
[73] V.J.P. Poots, G. McKay, J.J. Healy, Removal of Basic Dye from Effluent Using Wood as an Adsorbent, *Journal (Water Pollution Control Federation)*, 50 (**1978**) 926-935.
[74] G. McKay, J.F. Porter, G.R. Prasad, The Removal of Dye Colours from Aqueous Solutions by Adsorption on Low-cost Materials, *Water, Air, Soil Pollut*, 114 (**1999**) 423-438.
[75] S.D. Khattri, M.K. Singh, Colour Removal from Synthetic Dye Wastewater Using a Bioadsorbent, *Water, Air, Soil Pollut*, 120 (**2000**) 283-294.
[76] M. Otero, F. Rozada, L.F. Calvo, A.I. Garcı□a, A. Morán, Elimination of organic water pollutants using adsorbents obtained from sewage sludge, *Dyes and Pigments*, 57 (**2003**) 55-65.
[77] M. Arami, N.Y. Limaee, N.M. Mahmoodi, N.S. Tabrizi, Removal of dyes from colored textile wastewater by orange peel adsorbent: Equilibrium and kinetic studies, *J Colloid Interface Sci*, 288 (**2005**) 371-376.
[78] L. Wang, A. Wang, Adsorption characteristics of Congo Red onto the chitosan/montmorillonite nanocomposite, *J Hazard Mater*, 147 (**2007**) 979-985.
[79] O. Ozdemir, B. Armagan, M. Turan, M.S. Çelik, Comparison of the adsorption characteristics of azo-reactive dyes on mezoporous minerals, *Dyes and Pigments*, 62 (**2004**) 49-60.
[80] I. Bouzaida, M.B. Rammah, Adsorption of acid dyes on treated cotton in a continuous system, *Materials Science and Engineering: C*, 21 (**2002**) 151-155.
[81] F. Doulati Ardejani, K. Badii, N.Y. Limaee, S.Z. Shafaei, A.R. Mirhabibi, Adsorption of Direct Red 80 dye from aqueous solution onto almond shells: Effect of pH, initial concentration and shell type, *J Hazard Mater*, 151 (**2008**) 730-737.
[82] M. Hasnain Isa, L. Siew Lang, F.A.H. Asaari, H.A. Aziz, N. Azam Ramli, J.P.A. Dhas, Low cost removal of disperse dyes from aqueous solution using palm ash, *Dyes and Pigments*, 74 (**2007**) 446-453.
[83] R.-L. Tseng, F.-C. Wu, R.-S. Juang, Liquid-phase adsorption of dyes and phenols using pinewood-based activated carbons, *Carbon*, 41 (**2003**) 487-495.
[84] Z. Eren, F.N. Acar, Equilibrium and kinetic mechanism for Reactive Black 5 sorption onto high lime Soma fly ash, *J Hazard Mater*, 143 (**2007**) 226-232.
[85] A. Gürses, Ç. Doğar, S. Karaca, M. Açikyildiz, R. Bayrak, Production of granular activated carbon from waste Rosa canina sp. seeds and its adsorption characteristics for dye, *J Hazard Mater*, 131 (**2006**) 254-259.

[86] S. Netpradit, P. Thiravetyan, S. Towprayoon, Application of 'waste' metal hydroxide sludge for adsorption of azo reactive dyes, *Water Res*, 37 (**2003**) 763-772.
[87] A. Tor, Y. Cengeloglu, Removal of congo red from aqueous solution by adsorption onto acid activated red mud, *J Hazard Mater*, 138 (**2006**) 409-415.
[88] M. Özacar, İ.A. Şengil, Adsorption of reactive dyes on calcined alunite from aqueous solutions, *J Hazard Mater*, 98 (**2003**) 211-224.
[89] T.N.T. Phan, M. Bacquet, M. Morcellet, Synthesis and Characterization of Silica Gels Functionalized with Monochlorotriazinyl β-Cyclodextrin and their Sorption Capacities towards Organic Compounds, *Journal of inclusion phenomena and macrocyclic chemistry*, 38 (**2000**) 345-359.
[90] V.K. Gupta, I. Ali, Suhas, D. Mohan, Equilibrium uptake and sorption dynamics for the removal of a basic dye (basic red) using low-cost adsorbents, *J Colloid Interface Sci*, 265 (**2003**) 257-264.

# 3.Phosphate rock, phosphogypsum and apatites

In this work, natural fluorapatite (FAp) as the main component of phosphate rock (PR) and synthetic hydroxyapatite (HAp) prepared from a by-product phosphogypsum (PG) of phosphoric acid production by hydrothermal method, are used as efficient adsorbents for the removal of azo dyes from contaminated effluents (Figure 4).

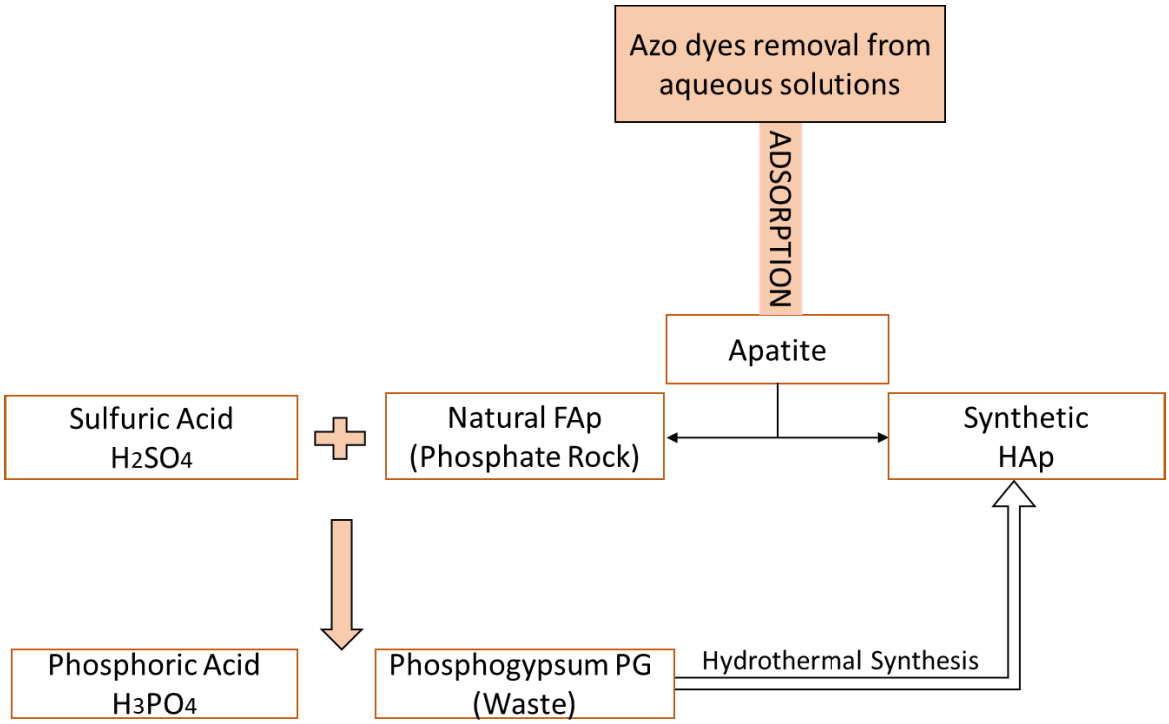


Figure 4. Materials used in this work for the removal of azo dyes from aqueous solutions

## 3.1. Production of phosphoric acid from phosphate rock

Global distribution of phosphate reserves and production is limited, highly concentrated and unequally distributed. China's phosphate mining production decreased in 2018 to 140 million metric tons (MT) from 144 million MT in 2017, while Morocco produced 30 million MT of phosphate in 2018. Despite producing significantly less than China, Morocco has the largest phosphate reserves. With 50 billion MT stockpiled, the region's phosphate reserves account for over 70 percent of the global number [1], as shown in Figure 5.

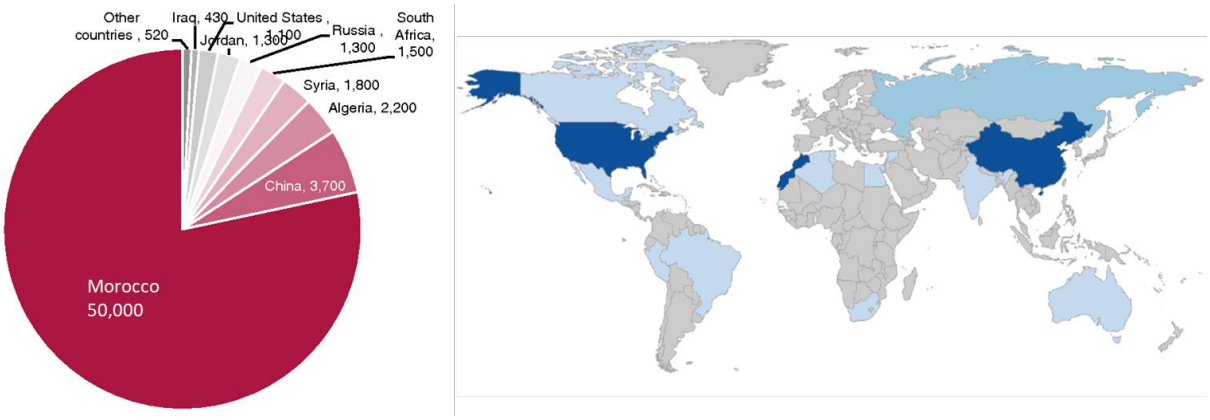


Figure 5. Breakdown of phosphate rock reserves by country, and map of countries by phosphate production in 2018 (Morocco, China, USA). Units are in 1000 MT of phosphate rock [1]. Reprinted by permission from Springer Nature, *Food Security*, Tracking phosphorus security: indicators of phosphorus vulnerability in the global food system, D. Cordell et al., Copyright 2015.

In Morocco, phosphate exploration and extraction are exclusively managed by a state-owned company named OCP Group, whereas the main activity (i.e., production of Phosphoric Acid and Fertilizers) is managed mostly by OCP along with some others foreign producers in the form of joint ventures [2]. Few facts about the OCP group are presented as follow:

- Established as a state-owned company in 1920 and privatized in 2008.
- Started its activity of extracting phosphate and the shipment processing of phosphate in 1921, when the first mine in Boujniba in the Khouribga area, the richest phosphate deposits in the world, was opened.
- Has long been the world's largest phosphate rock and phosphoric acid exporter, as well as one of the world's largest producers of fertilizer [3].

At national level, both extraction and transformation activities significantly contribute to the Moroccan economy. For instance, the value of phosphates and their derivatives represented nearly a quarter of the country's exports and approximately 3.5% of the GDP in 2010.

Morocco's currently known reserves are sufficient to meet several centuries of demand. Large quantities of the phosphate reserves are sedimentary type rock containing appreciable amounts of carbonate minerals. Phosphate deposits in Morocco occur in three areas the Khouribga area (Oulad Abdoun Plateau), the Gantour area (Youssoufia area) and Laayoune-Boucraa. Processing activities of phosphate into phosphoric acid and phosphate fertilizers are essentially concentrated in Jorf Lasfar and Safi sites [4]. Samples of phosphate used as raw material in this work were collected at the mining site of Khouribga.

Phosphoric acid is considered as the most important mineral acid produced in the world, after the sulphuric acid. The major part of phosphoric acid production (80%) is dedicated to chemical fertilizers [5]. It can also be used as precursor for the production of detergents, additives in toothpastes, non-alcoholic drink (soda) and in the surface treatment of stainless metals [6]. There are two main basic processes to produce phosphoric acid: the dry process and the wet process [7]. The first is called pyrometallurgical process, although the acid produced with this process is pure, it was abandoned due to its high production cost, while the second called wet process is more profitable than the first one. The wet process is detailed in Figure 6. It consists of digesting the FAp in mineral acids such as nitric, hydrochloric and most conventionally sulfuric acid ($H_2SO_4$) to produce phosphoric acid and precipitated calcium sulfate, called "phosphogypsum" (PG), as a by-product [8].

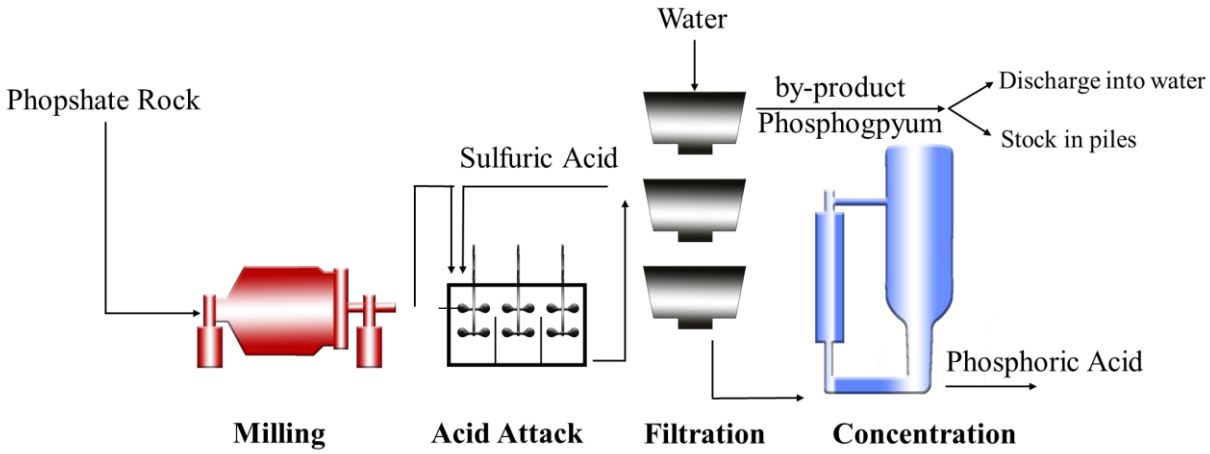


Figure 6. Wet process of phosphoric acid production.

### 3.1.1. Phosphogypsum

As mentioned above, phosphogypsum (PG) is a waste by-product from the processing of phosphate rock by the ‘‘wet acid method’’ of fertiliser production following this reaction:

$$Ca_5F(PO_4)_3 + 5H_2SO_4 + 10H_2O \rightarrow 3H_3PO_4 + 5\,(CaSO_4.2H_2O) + HF \quad (1)$$

The wet process is economic but generates a large amount of PG (5 tonnes of PG per tonne of phosphoric acid produced). The produced PG appears as dihydrate (DH), hemihydrate (HM) or anhydrite (AH), depending on the temperature, $P_2O_5$ and $SO_4$ content of the solution, as shown in Figure 7. In conventional operating conditions (T = 80 °C, 26% $P_2O_5$), the solid formed is the calcium sulfate dihydrated [9].

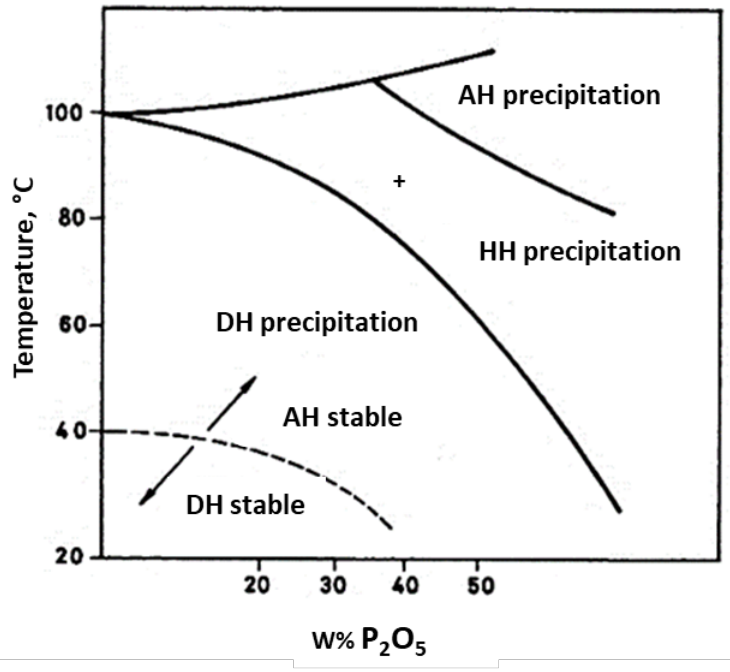


Figure 7. Regions indicating dihydrate DH, hemihydrate HH and anhydrite AH gypsum. Regions are defined by temperature and $\%P_2O_5$ content in the phosphoric acid solution [10]. Reprinted from *Journal of Plant Nutrition and Soil Science*, 124, H.-W. Döring et al., Phosphoric Acid (Fertilizer Science and Technology Series), 174-175, Copyright (2007), with permission from John Wiley and Sons.

The nature and characteristics of PG are strongly influenced by the phosphate ore composition and origin. Table 3 shows the chemical composition (% weight) of the main species and major impurities in PG used in this study compared with other gypsums from different countries. The composition of PG is dominated by calcium, sulphur and water, accompanied with some major impurities like $SiO_2$, $P_2O_5$ and in lesser amount $Al_2O_3$, $Na_2O$ and $K_2O$. The presence of $SiO_2$ in Moroccan PG, although in a small amount (0.49 – 0.61%) is due to the fact that the origin of Moroccan PG is sedimentary rocks. In addition, $SiO_2$ is sometimes added in the production of phosphoric acid to facilitate the crystallization process, and to neutralize F, Na or K in order to form the compounds $H_2SiF_6$, $Na_2SiF_6$ and $K_2SiF_6$ [11]. The presence of soluble phosphorus ($P_2O_5$) in PG can be explained by the remaining phosphoric acid $H_3PO_3$ after filtration, or it can be attributed to the residual non-attacked phosphate rock.

Table 3. Major elements in PG sample determined by X-ray fluorescence spectroscopy.

| Major Elements (%) | This work | Morocco | Tunisia | Egypt | China |
|---|---|---|---|---|---|
| **$Na_2O$** | 0.16 | 0.22 | 0.05 | 0.29 | - |
| **$H_2O$** | 20.22 | 21.58 | - | 19.71 | 18.89 |
| **$Al_2O_3$** | 0.15 | 0.18 | 0.06 | 0.17 | 0.68 |
| **$P_2O_5$** | 0.79 | 1.23 | 1.11 | 1.98 | 1.58 |
| **$K_2O$** | 0.03 | 0.01 | 0.03 | 0.02 | 0.15 |
| **$SiO_2$** | 0.49 | 0.61 | 1.03 | 8.29 | 13.94 |
| **$SO_3$** | 42.25 | 43.93 | 37.50 | 40.45 | 36.96 |
| **CaO** | 34.42 | 30.92 | 37.18 | 28.31 | 26.77 |
| **Others** | 1.49 | 1.32 | 23.04 | 0.78 | 1.03 |
| **References** | | [12] | [13] | [14] | [15] |

From a morphological point of view, and depending on phosphate rock origin and the reactor conditions, PG shows a predominant particle size of 0.250 – 0.045 mm in diameter [16]. PG has a well-defined tabular crystalline form with a majority of rhombic and orthorhombic shaped crystals. This morphology can be explained by the presence of $HPO_4^{2-}$ syncrystallized ions. Similar PG structure can be observed in a morphological study of PG samples from Morocco and Tunisia, as shown in Figure 8. In PG, two types of impurities can be found: *(i)* soluble impurities; salts or acids non eliminated during the washing process. Those acids confer to PG a low pH (generally between 2 and 4). *(ii)* insoluble impurities; non transformed mineral during the phosphoric attack or syncrystallized $P_2O_5$ and trace elements (mainly heavy metals).

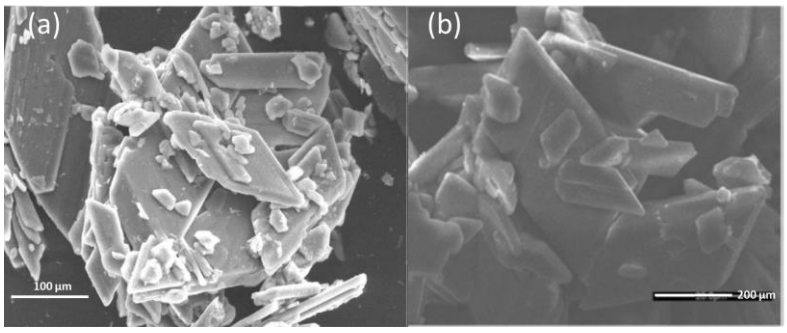


Figure 8. SEM micrographs of PG from (a) Tunisia [17] and (b) Morocco [18], showing similar plate-like morphology. Reprinted by permission from *Construction and Building Materials*, 23, L. Ajam et al., Characterization of the Tunisian phosphogypsum and its valorization in clay bricks, 3240-3247, Copyright (2017), with permission from Elsevier. Reprinted permission *from Journal of Environmental Radioactivity*, 54, M. Azouazi et al., Natural radioactivity in phosphates, phosphogypsum and natural waters in Morocco, 231-242, Copyright (2017), with permission from Elsevier.

PG can be considered as a mixture of waste components impregnated with chemical reactants used during the industrial process. In fact, it contains high concentrations of certain components, mainly phosphate, but also sulfate, fluoride, and often ammonium [19]. Moreover, phosphate rocks also contain, as impurities, metal and radionuclides that are released during the industrial process and finally concentrated in the reaction products. The earth contains numerous radioactive elements, for part of them dates back to the formation of our world, and for other part is continuously produced through nuclear reactions in the universe. In fact, sedimentary phosphate rock naturally holds some Uranium and its decay product [20]. Therefore, PG is considered to be radioactive, as a by-product of the production of phosphoric acid. Their radioactivity is due to the radium content coming from the natural decomposition of Uranium (present in the phosphate ore). The heavy metal content and radionuclide content in PG can vary depending on the phosphate rock source, and to a minor level on other factors such as differences in process plant operation and the age of phosphogypsum [21]. Table 4 shows the values of $^{238}U$, $^{226}Ra$ and $^{232}Th$ present in PG for different regions in the world.

Table 4. Concentrations of radionuclides: $^{238}U$, $^{226}Ra$ and $^{232}Th$ present in PG from different regions

| **PG rock origin** | **Radionuclide concentration (Bq/kg)** | | | **References** |
|---|---|---|---|---|
| | **$^{238}U$** | **$^{226}Ra$** | **$^{232}Th$** | |
| **Morocco** | 140 | 620 | 280 | [20] |
| **Tunisia** | 47 | 215 | 15 | [22] |
| **Florida (USA)** | 130 | 1140 | 3.7 | [23] |
| **Egypt** | 134 | 411 | 19 | [23] |
| **Spain** | 202 | 587 | 4 | [24] |
| **Guidance level in drinking water (Bq/L)** | 10 | 1 | 1 | [25] |

Nowadays, PG represents one of the most serious problems faced by the phosphate industry. Knowing that, the world's total amount of accumulated PG is estimated to be around 100–280 Mt per year [26]. Besides, 85% of the worldwide generation of PG is discharged directly without proper treatment, generally by dumping into the sea and rivers through plastic pipelines, or stocked in large piles exposed to weathering processes, occupying considerable land areas and causing serious environmental contamination of soils, water and the atmosphere, particularly in coastal regions. Several studies have investigated the impact of PG radionuclides. It was concluded that 90% of Ra originally present in phosphate rock remains in PG, whereas the remaining U percentage is below 20%. Thus the potential problem of PG piles is the emanation of $^{222}Rn$ from the alpha-decay of $^{226}Ra$, a radionuclide classified as human carcinogen. Lysandrou et al. measured the $^{222}Rn$ emanation rate of PG samples dumped in a coastal area of Cyprus. After 80h, the emanation rate increased from 0.35 to 1.1 Bq/h, which is higher than the geological background radon emanation rate in Cyprus [27]. Since PG waste is usually disposed as an aqueous slurry, PG piles can be affected by leaching of the elements naturally present in the PG. Those dissolved elements may be deposited in nearby soils or transferred to waters and finally to living beings, which presents a great environmental hazard. Azouazi et al. studied the $^{226}Ra$ solubility from Moroccan PG in aqueous solution by mixing PG with distilled water for 20 h at various pH values. It showed an average $^{226}Ra$ leaching of 26.4%. However, when the PG was calcined at 800°C and leached with acidified aqueous solution such as HCl and $H_3PO_4$, no trace of $^{226}Ra$ was detected. Moreover, the analysis of a water sample from an area close to the Moroccan phosphate mine revealed the presence of 0.2

Bq/l of $^{226}Ra$, which is below the radium chemical safety limit for water (1 Bq/l) [18]. Rabaoui et al. studied the existence of heavy metals along the coastline of the main Tunisian industrial zone for phosphate ore processing. Four heavy metals (Hg, Pb, Cd and Cr) were found and assessed in four mollusc species with high heavy metal concentrations in some species, besides important amounts of $Ca^{2+}$, $SO_4^{2-}$ and $F^-$ were observed along the coastline [28]. Industrial fluoride exists in both gaseous and particulate forms in industrial zones, leading to serious health problems after inhalation or ingestion. Moreover, sulphate can have negative effects on aquatic organisms by inhibiting photosynthesis, causing oxidative stress and increasing toxin production [29].

Considering the characteristics of PG (mainly 95% of $CaSO_4.2H_2O$), its attractive economic potential and especially, the great concerns about environmental pollution; nowadays PG is considered as an alternative raw material for many applications. In fact, PG commercial uses are mostly in manufacturing gypsum board, cement industry and in agricultural fertilisers or soil stabilisation amendments. These applications consume less than 15% of the worldwide generation of PG [30].

Several studies reported the effect of PG as a mineralizer on the burning temperature of clinker, as a substitute for natural gypsum in the production of Portland cement, as a set controller and on cement properties such as mechanical properties. Taher investigated the effect of calcined PG on the properties of Portland cement.[31] The process consists of the calcination of PG, then crushing and sieving through a 90 μm sieve before being mixed with Portland cement clinker. The results showed that increasing the temperature of the PG reduced the $P_2O_5$ and fluorides content. Therefore, the initial and final setting times of the pastes were decreased while their mechanical strength was improved. The properties of Portland cement can be effectively improved with the incorporation of 6% of thermally calcined PG at 800°C. This results were confirmed by Smadi et al. [32], who manufactured concrete using normal and calcined PG at different temperatures. The amount of $P_2O_5$ in the calcined samples at 170°C was 0.41% and decreased to 0.32% at 950°C. In addition, increasing calcining temperature caused the fluoride content to decrease from 0.89% at 170°C to 0.27% at 950°C. It has also been found that the setting times increased when using the calcined PG samples, while improving the flexural strength. Several studies reported that the addition of PG in cement clinker (5-10% addition), after treatment by washing and subsequent calcination, gives interesting and promising results in improving Portland cement properties [33-35]. PG was also used for the production of non-fired bricks as reported by Zhou et al. [36], using a novel process

"the Hydration-Recrystallization". Results showed that the optimal mix composes of 75% PG, 4.0% Portland cement and 1.5% hydrated lime, with a compressive strength of 21.8 MPa. This high value is due to the recrystallized PG crystals, that present regular, dense and interlock crystalline microstructure. Folek et al. [37] confirmed the suitability of PG-ash-binder mixes for its use in the construction of upper layers of road embankments and parking lot pavements, both in terms of geotechnical and physicochemical parameters.

Environmentally friendly applications for PG are already being investigated. The most interesting one is based on the use of PG as a calcium source for $CO_2$ mineral sequestration in the framework of the mitigation of greenhouse gases emission. Recent alternative mineral feedstock for carbon sequestration has been found in the PG stockpiles [38]. PG is first transformed into a carbon sequestration agent (calcium hydroxide) and sodium sulfate by alkaline dissolution with soda and then, this agent reacts rapidly and completely with $CO_2$ giving mineral carbonates. Other experimental studies propose to convert PG into ammonium sulfate via PG carbonation with ammonia [39]. In summary, in the cited studies, the reuse of PG and the valorization of the by-products obtained are achieved since calcite and sodium sulfate or ammonium sulfate are obtained. All these by-products have different industrial applications (fertilizers, filler material, and building materials). Thereby, besides PG valorization, large amounts of $CO_2$ are also fixed into carbonates contributing to carbon emissions control strategies.

Only few studies investigated the use of bare PG in the removal of heavy metals. Raii et al. [40] studied the use of PG as a reactive sorbent material for the removal of $Pb^{2+}$ and $Cd^{2+}$. The obtained results showed that PG had a higher reactivity for the removal of both heavy metals than the commercial gypsum. In other studies, PG had to be lime-preconditioned in order to be used as an adsorbent for the removal of $Zn^{2+}$ and $Cd^{2+}$ from aqueous solution [41, 42]. It was concluded that preconditioned PG can be used effectively as a low-cost alternative approach for treatments of aqueous solutions polluted by heavy metals.

## 3.2. Apatites

With the discovery of petroleum in 1859, and the invention of the internal combustion engine in the late 19$^{th}$ century, important changes occurred as a result of the extraction of large quantities of minerals. Perhaps, the ultimate example, proving how the use of a single mineral had impacted, considerably, the evolution of society in the last 150 years ago, is the mineral of apatite. In fact, the massive growth of population was enabled by the extraction and processing

of sufficient quantities of apatite, extensively used as agricultural fertilizers, necessary to feed that rapidly growing population.

Apatite is named after the Greek word απατείν (apatein), which means to deceive, referring to its widely varying forms, colours, and chemistry that clearly mimic other important minerals. Therefore, apatite was often mistaken by older mineralogists for *aquamarine*, *chrysolite* or amethyst (Figure 9).

It was first introduced in the mineralogical literature by Werner (1786) [43]. According to Slansky, geologically the apatite occurs from igneous (18% $P_2O_5$ content), guanos-types (4% $P_2O_5$) or sedimentary deposits, which are the most abundant in quantity and with $P_2O_5$ contents exceeding 28% [44]. We cite the Moroccan phosphate deposits, as the most important one, and on which this study focuses.

Figure 9. Apatite minerals with various colours and shapes [45]. Copyright Didier Descouens, licensed under Creative Commons Attribution License.

More than 80 years ago, it was stated that "*The structure of apatite seems to be remarkably stable, permitting a number of rather unusual types of substitution and involving a considerable number of ions*" [46]. The impressive use of apatite in geologic and societal applications is due to the properties that derive from its atomic arrangement. The apatite supergroup includes minerals with a generic chemical formula $M1_2M2_3(TO_4)_3X$; chemically they can be phosphates, arsenates, vanadates, silicates, and sulphates. In fact, the structure of apatite is very robust, and can host on the key-sites more than half the long-lived elements in the periodic chart [M = $Ca^{2+}$, $Pb^{2+}$, $Ba^{2+}$, $Sr^{2+}$, $Mn^{2+}$, $Na^{+}$, $Ce^{3+}$, $La^{3+}$, $Y^{3+}$, $Bi^{3+}$; T = $P^{5+}$, $As^{5+}$, $V^{5+}$, $Si^{4+}$, $S^{6+}$, $B^{3+}$; X = $F^{-}$, $(OH)^{-}$, $Cl^{-}$]. The valid mineral species within the apatite supergroup can be divided into five groups, as follow:

- *Apatite group*: hexagonal and pseudo-hexagonal phosphates, arsenates and vandates containing the same cation at both the M1 and M2 sites.

- *Hedyphane group*: hexagonal and pseudo-hexagonal phosphates, arsenates and sulphates containing different cations at the M1 and M2 sites.
- *Belovite group*: hexagonal and trigonal phosphates with the M1 site split into the M1 and M1´ sites containing different cations.
- *Britholite group*: hexagonal and pseudo-hexagonal silicates, typically with partially ordered M1 and M2 cations.
- *Ellestadite group*: hexagonal and pseudo-hexagonal sulphato-silicates with the ideal ratio $(SiO_4)^{4-}$:$(SO_4)^{2-}$ =1:1.

In this study, we will focus only on fluorapatite $Ca_5(PO_4)_3F$, hydroxyapatite $Ca_5(PO_4)_3OH$ and chlorapatite $Ca_5(PO_4)_3Cl$, which are the most widespread and influential in geological and biological processes (Figure 10):. The crystal structure of apatite was first solved by Mehmel (1930) as hexagonal in the space group $P6_3/m$, and typically all apatites crystallize in that space group [47]. The atomic arrangements of the three apatite phases differ principally in the positions of the occupants of the [0,0,z] anion positions, i.e., fluorine, chlorine, and hydroxyl for the three end-members, respectively [48]. The essential atomic arrangement of these three apatite types is formed of three cation- centred polyhedral: $Ca^{I}$ is coordinated to nine oxygen atoms in the arrangement of a tricapped trigonal prism, as shown in Figure 10b, the $Ca^{II}$ bonds to six oxygen atoms and one anion X (where X is $F^-$, $OH^-$, or $Cl^-$) forming a trigonal prism, and the $PO_4$ tetrahedron (Figure 10c).

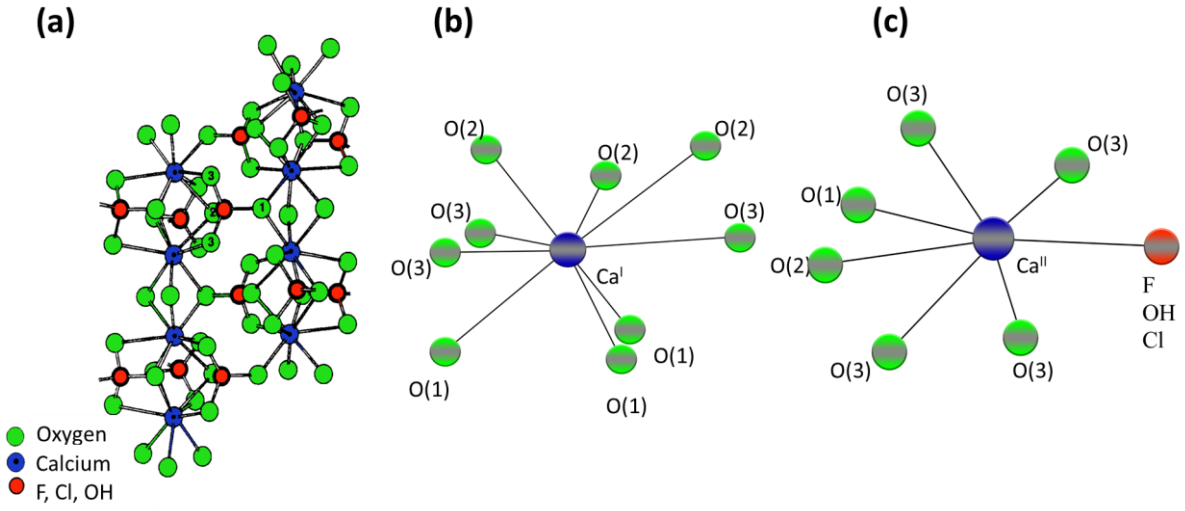


Figure 10. (a) Atomic arrangement in apatite, (b) site of $Ca^{I}$, and (c) $Ca^{II}$ occupancy and its coordination

Besides, Pasero et al. [49] stated that in the apatite structure, the X anion site can be occupied by $O^{2-}$, which would increase the total negative charges and create vacancies, and $H_2O$

molecules, in that case would decrease the total negative charges. The M cation site can be occupied by Cd, Co, K, and almost all rare earth elements (REE) and the T site of the tetrahedron $TO_4$ can be occupied by Be, Cr, Ge, and $Mn^{5+}$.

Because of their physical and chemical properties, obtained due to their exceptional structure, the apatite group minerals offer many applications. Perhaps the most well-known application of apatite, as the major source of phosphorous, and therefore is critical for the production of huge quantities of fertilizers, detergents and phosphoric acid [50]. Natural apatite is present in bones and teeth within mammals [51], hence synthetic apatite exhibits excellent biocompatibility and similar mechanical properties to bones. Apatite was excessively used as a suitable material for filling bone defects, and as a drug delivery system [52, 53]. In addition, the presence of Mn, REE and U in apatite endows the material with fluorescent and luminescence properties [54, 55]. In fact, Owens et al. studied the utilization of synthetic apatite doped with the REE europium in ink jet printing [56]. Natural apatite showed a great efficiency in water treatment. For example, several studies showed that natural apatite emerged as potentially effective for phosphorus (P) removal from wastewater [57-59]. General applications, especially environmental ones, of fluorapatite (FAp) and hydroxyapatite (HAp) will be developed in details in the following sections.

### 3.2.1. Fluorapatite (FAp)

Phosphate rock (phosphorite) is a marine sedimentary rock that contains 18–40% $P_2O_5$. The main mineral in the phosphate rock is apatite, and most commonly, fluorapatite (FAp) $Ca_5(PO_4)_3F$ [60]. FAp belongs to the spatial group $P6_3/m$, its parameters are a = b = 9.462 Å and c = 6.849 Å, a = b = 90°, g = 120°and consists of 3 ions: $F^-$, $Ca^{2+}$, $PO_4^{3-}$ [61].

Thanks to its structure, and the presence of an important number of ionic bonds, FAp is considered as a great host for many substituents, hence it has led it use in many applications. Rare earth ions doped FAp nanoparticles can be used in a wide variety of biomedical applications such as MRI, drug delivery, optical imaging…In fact, a $Ca^{2+}$ substitution in the FAp lattice by a trivalent substituent (i.e. $Sb^{3+}$ or $Nd^{3+}$) is relatively rarely noticed. However, this type of substitution is used in the fabrication of fluorescent lamps. In fact, FAp first industrial use, in a Sb- or Mn-substituted form, remains the production of fluorescent lamps (estimated to 10 tons per day in 1991) [62]. Regarding recent studies, Karthi et al. investigated the fabrication of $Nd^{3+}$ doped FAp coated $Fe_3O_4$ luminomagnetic nanoparticles by

hydrothermal method [63]. The synthesised material showed an excellent multifunctional platform for diagnostics and therapeutic applications. Ye et al. synthesised $Sm^{3+}$ doped FAp phosphors for the first time, via the conventional high-temperature solid-state method in the air atmosphere [64]. This new doped FAp material has a potential application as a near ultraviolet white light emitting diodes. In addition, rare earth ion doped Fap luminescent nanomaterials have wide application in tracing the status of the repair the damaged hard tissue and bio-imaging due to their unique physical and chemical properties. Peng et al. prepared successfully $Yb^{3+}/Ho^{3+}$ doped nano-FAp by hydrothermal method that could provide favourable conditions in cell markers and imaging [65].

FAp is also important in biology, because they form the mineral part of bone and teeth, and take part in the mineralization process. They are used as biocompatible materials for bone replacement and coating of bone prostheses [66]. In fact, Taktak et al. investigated the bioactivity response of a new tricalcium phosphate-FAp ceramic in vitro in Simulated Body Fluid (SBF) to evaluate its biocompatibility in the process of bone regeneration in rabbits [67]. Zeng et al. suggested a new application for europium-doped fluorapatite (Eu-FAp) nanorods as an anticancer drug carrier [68].

FAp is also the main calcium phosphate used in phosphorus chemistry as fertilisers and phosphoric acid ($H_3PO_4$) source. Phosphorus (P) is an essential nutrient for plant growth and food production. In nature, phosphorus is available in the mineral deposits in the form of phosphate rocks. Since the 1950s, the use of phosphorus fertilizer has increased substantially. Phosphate Rock (PR), the only source of phosphate for fertilizer production, is a finite, non-renewable resource [69]. The PR is highly insoluble, so cannot directly be used as a fertilizer and in order to be used as crop nutrients, it must first be processed and converted to a water-soluble form; phosphoric acid [70].

### 3.2.2. Hydroxyapatite (HAp)

Hydroxyapatites (HAp) are a naturally occurring mineral form of calcium apatite, with the general formula $Ca_5(PO_4)_3(OH)$. It crystallizes in the hexagonal crystal system and belongs to the spatial group $P6_3/m$, as shown in Figure 11. The lattice parameters for HAp are a = 9.432 Å and c = 6.881 Å. Besides, the existence of a monoclinic phase of HAp has been confirmed, with a space group P21/b, a = 9.421 Å, b = 2a and c = 6.881 Å [71]. Pure HAp is a stoichiometric apatite phase with a Ca/P molar ratio of 1.67 and the most stable calcium phosphate salt at

normal temperatures and pH between 4 and 12 [72]. Generally, pure HAp powder is white. Hydroxyapatite can be found in teeth and bones of the human body, being one of the few physiologic minerals [73].

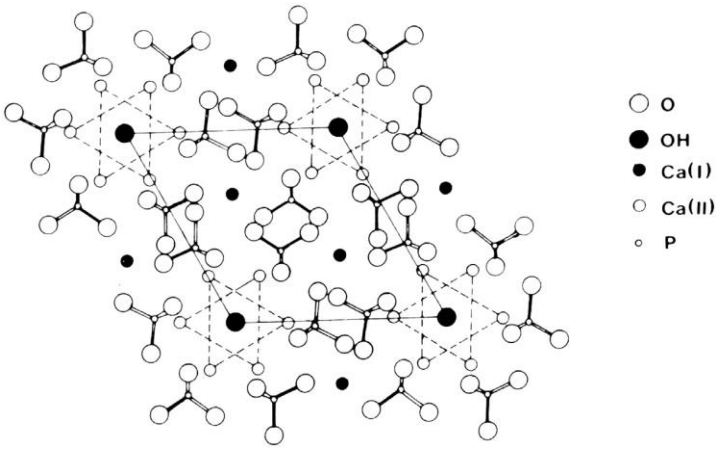


Figure 11. Projection of the constituting ions of hydroxyapatite on the basal (001) plane [74]. Reprinted from Applications of Nanobiomaterials, L. Rigano et al., Nanobiomaterials in Galenic Formulations and Cosmetics, 121-148, Copyright (2016), with permission from Elsevier.

HAp possesses an interesting structure. In fact, it has two types of crystal planes with significantly different charges, positive charges on *a* and *b* planes, and negative charges on *c* planes, respectively. Consequently, the *a* and *b* planes tend to attract the molecules with negative charge, whereas the *c* planes may adsorb those with positive charges [75]. Furthermore, pH values of the medium, where HAp is soaked, play a critical role on the surface charges of HAp. Indeed, negative surface charge is observed on HAp particles in the range of pH 5–8, which becomes even stronger with further increase of pH value [76].

### 3.2.3. Apatite: a material for wastewater treatment

It is almost impossible for living organisms, for both plants and animals, to survive without water, which makes it classified as the most essential resource for human life. Hence, the availability of clean water is a global challenge. However, the quality of water is compromised by pollution caused by agricultural activities, human activities, mining, energy generation, deforestation, industries and urban settlements [77]. Wastewater from the industries are discharged directly or indirectly into the water bodies and surrounding environment or in some cases used for irrigation purposes and, hence, need to be treated before discharge in order to save the life of aquatic animals and human health in general [78]. It has been reported that approximately 300–400 million tons of heavy metals, dyes, solvents and other organic waste

are being deposited into the surrounding environment by industrial plants every year worldwide [79].

As shown above, substitutions are omnipresent in apatite chemistry and a wide variety of ions can be incorporated into the apatite structure. For instance, fluorine can replace hydroxide ion, carbonate may substitute phosphate group and mostly divalent metal ions can be found in lieu of calcium ions; which leads to the formation of mixed metal phosphates easily. This structure particularity allows apatite the capacity to remove heavy metals from aqueous solutions and retain them in the solid phase. In 1981, Suzuki et al. [80] were the first to report the use of HAp for metal ion capture from aqueous solutions. This study confirmed that HAp "traps" heavy metal ions such as Pb, Cd and Cd ions in its main structure by exchange with calcium. Besides, they reported that the HAp structure was maintained and the divalent heavy metal ions were held in the structure. Since then, various studies reported the use of apatite as sorbent materials for heavy metals contaminated water remediation [81-83]. Viipsi et al. [84] investigated HAp and FAp as sorbents in $Cd^{2+}$ and $Zn^{2+}$ binary solutions. They showed that those heavy metal ions sorption is strongly affected by solution pH, in fact the sorbent amount of heavy metals increased with pH. Two mechanism were often suggested for heavy metal capture by HAp are the ion-exchange process and the dissolution-precipitation process. In the first case, the metal attaches to the HAp surface or diffuses inside and provokes calcium release by pushing out the more soluble endogenous calcium ions. The smaller solubility of the heavy metal phosphate pushes the exchange reaction towards release of calcium ions. In the second case, calcium is dissolved first, together with accompanying phosphate ions, and the heavy metal ions precipitate by homogeneous (in solution) or heterogeneous (on the remaining solid HA) nucleation [85]. Elouear et al.[86] investigated the feasibility of using natural Tunisian phosphate rock as sorbent for removal of Pb(II), Cu(II), Cd(II) and Zn(II) from aqueous solutions. However, the affinity and sorption capacity of each metal ion are different. The sorption order is found to Pb(II)>Cd(II)>Cu(II)>Zn(II). They stated that the higher removal of $Pb^{2+}$ was due to its high electronegativity and its ionic radius 1.2 Å is very close to the ionic radius of $Ca^{2+}$ 0.99 Å. $Cd^{2+}$ showed also the same behaviour, with a close ionic radius 0.97 Å and high electronegativity. Besides, $Cu^{2+}$ with a much smaller ionic radius than $Ca^{2+}$, is exchanged to a lesser extent. It has been reported by few studies that cations whose ionic radius were smaller than $Ca^{2+}$ may be incorporated in the apatite lattice to a much lesser degree than those anions of larger ionic radius, which explains the selectivity order of PR towards studied cations.[87] . Apatite was also used in immobilizing soil heavy metals. Indeed, contaminated soil has been dry mixed with HAp and it gave interesting results. In the case of aqueous $Pb^{2+}$ in

lead contaminated soils, it was reduced after reaction with HAp. A theory was proposed in order to explain this result; HAp dissolved and precipitated *hydroxypyromorphite* [$Pb_{10}(PO_4)_6(OH)_2$] [88]. In addition, it was found that lead chemical immobilization by any phosphate source could be related to the formation of pyromorphite $Pb_5(PO_4)_3X$, where X= F, Cl, OH. This lead compound is known to be the most stable Pb compounds under a wide pH range [89].

## 3.3. Overview over synthesis methods of HAp

Due to population growth and an increase of life expectancy with high prevalence of disease, the need for new biomaterials for improving quality of human life continues to be a major focus for researchers. In recent years, bioceramics and biocomposites have been the most promising materials for biomedical applications. Among different classes of bioceramics, HAp nanoparticle is the most emerging one, because HAp has close similarities and mimic the properties of organic mineral component of bone and teeth [90]. In fact, synthetic HAp is thermodynamically stable at physiological pH and osteoconductive. Hence, it has been widely used in hard tissue replacement; as implant coatings and bone substitutes [91]. HAp with correct stoichiometry, morphology and purity had stimulated great interest and a number of synthetic routes for producing HAp powders have been developed [92]. During the past decade, several methods which have been developed to synthesise HAp powders, have claimed to prepare nanoparticles with precise control over its microstructure. These methods can be classified; as either wet chemistry methods or dry methods. An overview of the advantages and disadvantages of each method is detailed as follow.

### ➢ Dry methods

Dry method does not use a solvent, unlike wet methods. This method, although less frequently reported, it is relatively simple and inexpensive compared to the wet treatment methods. In fact, dry method does not require precisely controlled conditions, making them suitable for mass production of powders. The most well-known dry methods adapted by several researchers include solid-state synthesis and mechanochemical process.

- **Solid-state synthesis**

Typically, precursors involve milling and mixing calcium (i.e, $Ca(OH)_2$) and phosphate containing chemical or a previously prepared calcium phosphate (CaP) salt (i.e, β-TCP). Then, they were calcined at a very high temperature (e.g. 1000°C), which leads to the formation of a well-crystallized structure. The solid-state synthesis presents a disadvantage; often the

produced HAp exhibits heterogeneity in its phase composition, attributed to the small diffusion coefficients of ions within the solid phase during the reaction [93]. Indeed, Pramanik et al. [94] investigated the synthesis of HAp particles with a single phase, using powder mixing followed by sintering the cold-compacted pellets at different temperatures up to 1250°C. However, this powder was irregularly shaped, with micron-sized grains. Some attempts have also been made in order to prepare HAp with a regular shape [95]. For instance, Tseng et al. [96] synthesized HAp nanoparticles through a polyethylene glycol (PEG)-assisted reaction at 900°C in an oxygen atmosphere. PEG was used in order to control particle size, crystal phase and degree of aggregation. In fact, the produced HAp with PEG was well dispersed, and much less aggregated than the bare HAp. This can be explained by the fact that the energy required for formation of HAp nanoparticles in the HAp-PEG system should be greater than required for HAp without PEG; because the crystallization of HAp will proceed after the decomposition of PEG-Ca-P complex in the former system, by delaying the phase transition from pure HAp to tricalcium phosphate (TCP).

Nevertheless, the solid-state process is usually the method of choice for commercial production of different powders, few studies have been found regarding this synthesis. As reported, this method suffers from the small diffusion of ions during the reaction. Nowadays, it is crucial to use a method that allows a precise control over the properties of HAp, which is much more important than financial considerations. Therefore, some researchers suggested an alternative approach; called the mechanochemical method.

- **Mechanochemical method**

This method is sometimes known as “mechanical alloying”, because it is a dry method that allows the fabrication of nanocrystalline alloys and ceramics [97]. Both mechanochemical and solid-state methods have the advantages of simplicity and performance of mass production. However, unlike the solid-state method, that gives heterogeneous particles with irregular shape, mechanochemical method gives a well-defined powder structure. The principle of this method consists on grounding the precursor materials on a planetary mill while the molar ratio between the reagents is kept at the stoichiometric ratio [98]. In this process, some of the most important parameters are: the type of reagents, the type of milling medium, the type and diameter of the milling balls, the duration of the milling, … Coreno et al. [99] suggested a synthesis route that involves mixing dry powders of calcium carbonate ($CaCO_3$) and di-ammonium phosphate monobasic ($NH_4H_2PO_4$). It was performed by using a ball to powder weight ratio equals 20:1. After 2 hours of milling, HAp was formed. The crystallinity and the amount of the

hydroxyapatite increase as milling time does. When the milling time was increased to 6h, HAp nanoparticles were obtained, with a particle size between 10 and 50 nm.

### ➢ Wet methods

As mentioned before, HAp powder generated using a typical dry method, is often heterogeneous, and large in size. Consequently, wet methods offer advantages in their ability to control the morphology and the mean size of powder. It is conventionally admitted that they are the most promising techniques for the synthesis of nanosized HAp. The process consists on solution-based reactions, which happen in an organic solvent, more usually in water. It can be conducted at ambient temperature or elevated one depending on the technical route. The main advantage of wet processes is the easy control of growth conditions by just adjusting the reaction parameters. However, the main potential disadvantage is the low preparation temperature compared to dry methods, resulting in the production of CaP phases other than HAp. In fact, various ions in aqueous solution can be incorporated into the crystal structure, inducing some trace impurities.

- **Chemical precipitation**

Knowing that, at room temperature and at pH 4.2, HAp is the least soluble and the most stable of CaP phase in an aqueous solution [100]. Precipitation typically involves a reaction conducted at pH values higher than 4.9 and temperatures can vary between 25°C to temperatures close to the boiling point of water (Usually 90°C). The procedure can be accomplished using calcium (such as calcium hydroxide) and phosphate (e.g. orthophosphoric acid) containing precursors, and a dropwise addition of ammonium hydroxide in order to ensure a constant pH under continuous and gentle stirring, while the molar ratio of Ca/P is kept at stoichiometry according to its ratio in HAp (1.67) [101]. Finally, the resulting precipitate can be aged under atmospheric pressure, where the morphology of the crystal's changes from needle-like to more block-like structure. Then, washed to remove the nitrates and the ammonium hydroxide, filtered, dried and crushes into a powder [102]. Mobasherpour et al. [103] investigated the synthesis of HAp from calcium nitrate hydrated $Ca(NO_3)_2{\cdot}4H_2O$ and di-ammonium hydrogen phosphate solution $(NH_4)_2HPO_4$ by precipitation method. Nanoparticle HAp were successfully synthesized, with increasing the particle size when the sample was heated from 100°C to 1200°C. No other calcium phosphates phases were noticed up to 1200°C. HAp nanoparticles were successfully synthesized by exploring a new approach of precipitation method. This work was reported by Peng et al. [104] using the high-gravity precipitation

technology, that allows the control of the size of HAp nanoparticles by simply tuning the rotating rate during the precipitation process. Structure and morphology characterization of the nano-HAp showed low crystallinity, and size distribution diameters of 1.9 – 14.2 nm and lengths of 4.0 – 36.9 nm, comparable to natural HAp. Nevertheless, a simple precipitation method leads, usually, to non-stoichiometric and poorly crystallized powder. These drawbacks may be due to the vacancies in the crystal lattice, the substitution of diverse ions such as carbonate, potassium and chloride, or the presence of other phases… Consequently, this method requires a very precise control over the processing conditions, such as the pH value, the temperature used during the reaction or the aging step.

- **Sol-gel method**

The sol-gel method was one of the first methods proposed for the wet synthesis of HAp. The regular process consists of the synthesis of a 3D inorganic network by mixing suitable precursors in either an aqueous or an organic solvent, followed by aging at ambient temperature, gelation, drying and finally calcination using post-heat treatment in order to expel organic parts, gaseous products and water molecules from the porous gel [105]. Various precursors can be used in a conventional sol-gel method. However, the most common ones are calcium diethoxide or calcium nitrate reacting with triethylphosphate.[106]. A general reaction may be shown as follows:

$$6\ Ca(NO_3)_2 + 6\ (C_2H_5O)_3P(O) \rightarrow Ca_{10}(PO_4)_6(OH)_2 + \text{by-products}$$

Sol-gel method offers the advantage of an increased control over formation of particular phases and phase purity while HAp synthesis occurs at low temperatures. Hsieh et al. [107] reported the preparation of nanocrystalline HAp according to the reaction above. They showed that fast gelation leads to a high CaO production, meanwhile minor CaO occurs at slow gelation, that can be easily washed out by distilled water. Fathi et al. [108]demonstrated that HAp nanoparticle crystallinity depends on the calcination temperature. They reported the synthesis of HAp powder that exhibits a nanoscaled (25 nm) and carbonated apatitic structure paralleling human bone apatite. In another study, Feng et al. [109] investigated the effect of aging time on the powder growth and agglomeration. TEM micrographs results showed that HAp nanoparticles with increasing particle sizes of 10-15, 15-25 and 50-80 nm can be obtained after 4, 48 and 72 h of aging, respectively. One may find that the main disadvantage of the sol-gel method is the difficulty to hydrolyse phosphate and usually the use of expensive starting chemicals.

### 3.3.1. Hydrothermal method

The hydrothermal process, as one of the most common methods for preparation of HAp, usually refers to those chemical reactions conducted in aqueous solution under high pressure-temperature conditions. This technique was developed in order to mimic the formation of rocks and minerals in the nature. In fact, the word "*hydrothermal*" has a geological origin, and is a self-explanatory word: "*hydro*" meaning water and "*thermal*" meaning heat. Different definitions have been suggested; Laudise [110] defined it as a growth from aqueous solution at ambient or near ambient conditions. In 1985, Rabenau [111] defined hydrothermal synthesis as the heterogeneous reactions in aqueous media above 100°C and 1 bar. According to Byrappa [112], hydrothermal method is a heterogeneous reaction in an aqueous media carried out above room temperature and at pressure greater than 1 atm in a closed system. With the introduction of autoclaves and other novel lining materials for high pressure reactors, this technique was extended to the growth of single crystals [113], thin films [114] and nanostructures [115].

It has been demonstrated that HAp nanoparticles obtained from the hydrothermal conditions are nearly stoichiometric and highly crystalline [116]. In addition, phase purity and Ca/P ratio of HAp precipitate significantly improve with increasing the hydrothermal temperature [117]. A lot of studies have been published regarding the hydrothermal synthesis of HAp, using different experimental conditions. Rod-like HAp may be obtained in acidic [118], relatively neutral [119] or in alkaline conditions [120]. In fact, it can be shown in Figure 12, a typical rod-like HAp nanoparticles synthesized under typical hydrothermal conditions [121].

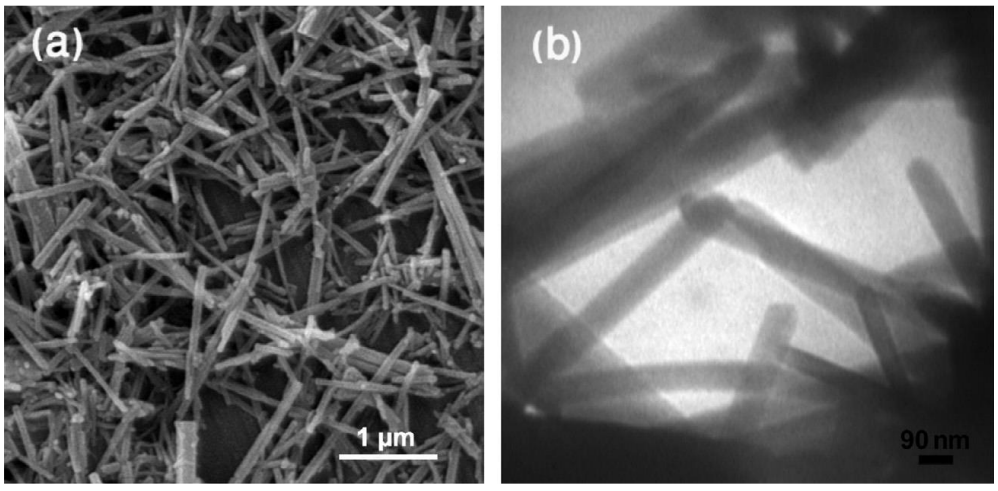


Figure 12. (a) SEM and (b) TEM images of rod-like HAp nanoparticles [121]. Reprinted by permission from *Journal of the Brazilian Chemical Society*, 22, M. Sadat-Shojai et al., Design of experiments for

the optimization of hydrothermal synthesis of hydroxyapatite nanoparticles, 571-582, Copyright (2011), licensed under Creative Commons Attribution License.

### 3.3.2. Surfactant-assisted snythesis

It has been suggested that the formation of rod-like crystals occurs in two main stages; first stage includes the nucleation step in which tiny crystalline nuclei in a supersaturated medium are formed, followed by the growth step in which nuclei continuously grow into the final shape and size [122]. The main parameters affecting the structural and morphological characteristics of HAp nanoparticles are temperature and pH. According to some SEM analysis, it can be concluded that aspect ratio of the fibrous nanoparticles decreases with increasing the pH value. Morphologies may vary from rod-like to spherical nanoparticles, and can be obtained by controlling the driving force of the chemical reaction and under different hydrothermal conditions. According to Figure 13, when the pH value is high, the crystallites can grow to form spherical or short rod-like nano-particles. In contrary, a decrease in pH value of suspension, an anisotropic growth leads to crystallites growing into one-dimensional nanorods or two-dimensional nanoplates. When the pH=4, more complicated shapes, such as three-dimensional microcubes and three-dimensional microfibers are obtained, accompanied with secondary phases of CaP [123].

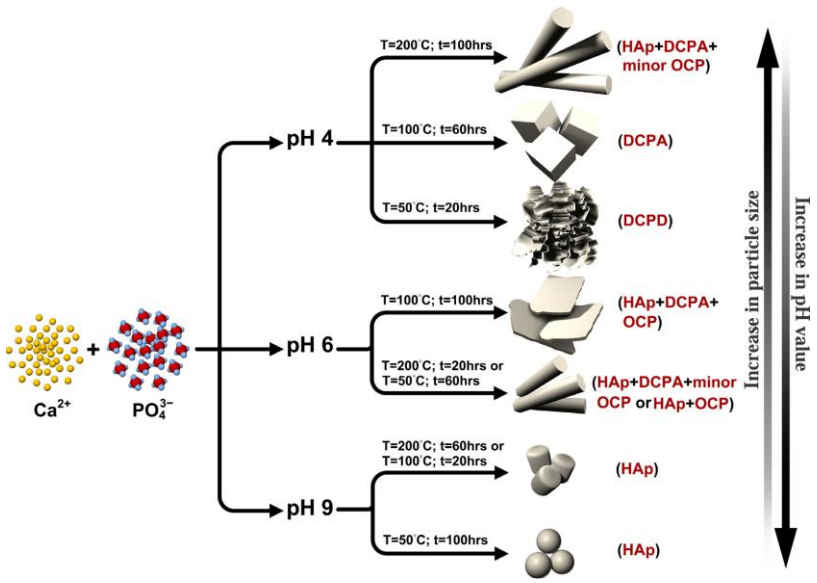


Figure 13. Effect of pH, temperature, and duration of hydrothermal treatment on phase, morphology, and particle size ofthe CaP powder [92]. Reprinted from Acta Biomaterialia, 9, M. Sadat-Shojai et al., Synthesis methods for nanosized hydroxyapatite with diverse structures, 7591- 7621, Copyright (2013), with permission from Elsevier.

Surfactants are usually amphiphilic. They consist of a hydrophilic polar head (high affinity for water), but a hydrophobic tail. Hence, in an aqueous solution, surfactants favour the

migration to the interfaces, and especially the air-liquid interface. At low surfactant concentrations, the molecules are present in solution as separate species. Beyond a critical concentration, the individualised molecules start to self-organize to form molecular aggregates called micelles, measuring between 1 nm and 1 μm, to minimize the contacts between hydrophobic parts of surfactant molecules and water molecules (Figure 14). The concentration at which the molecules begin to form these aggregates is defined as the critical micelle concentration (CMC).

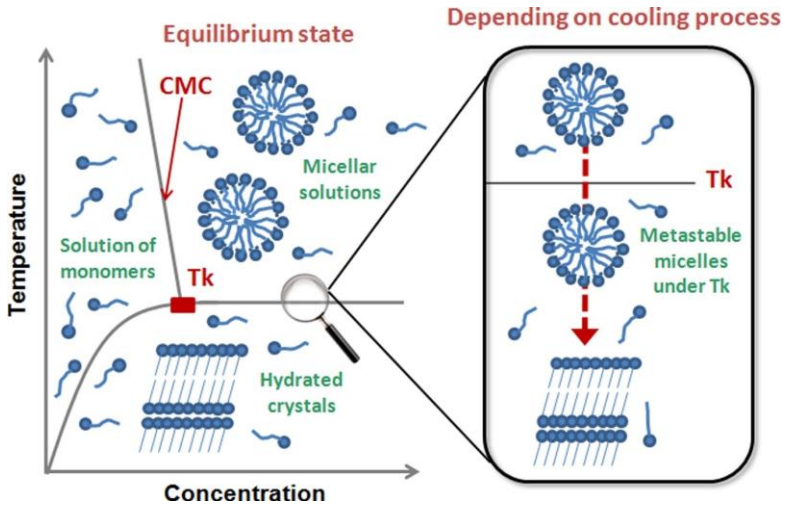


Figure 14. Schematic representation of a surfactant molecule and its behaviour in aqueous solution to minimize the interfacial tension, and the self-assembly after reaching the critical micelle concentration (CMC) [124]. Reprinted from *Colloids and Surfaces A: Physicochemical and Engineering Aspects*, 540, H. Lu et al., Non-equilibrium micelles formed by sugar-based surfactants under their Krafft temperature, 167-176, Copyright (2018), with permission from Elsevier.

Surfactants may be classified into the following large groups based on the ionic charges they carry on the hydrophilic head group:

*(i)* Anionic, with the hydrophilic group carrying a negative charge, such as carboxyl (RCOO−M+) or sulphate ($ROSO^{-3}$ $M^{+}$);

*(ii)* Cationic, with the hydrophilic group bearing a positive charge, as for example, the quaternary ammonium salts ($R_4N^{+}X^{-}$) or amine salts;

*(iii)* Zwitterionic or amphoteric, contains a head with two oppositely charged groups (positive and negative charge)

*(iv)* Non-ionic, where the hydrophilic group has no net electrical charge.

Hydrothermal method presents a drawback; it is not easy to control the morphology and size distribution of nanoparticles. Therefore, in order to improve the procedure, various organic modifiers can be used by different hydrothermal temperatures, and organic surfactants are the

more usual. In fact, three main categories of organic surfactants have been employed in the synthesis; including ionic (cationic and anionic) surfactants, non-ionic surfactants and block-copolymers with different molecular weight.

In order to understand the effect of surfactant on the morphology of HAP, the nucleation mechanism and growth of hydroxyapatite crystals is evaluated. When a surfactant is dissolved in water, cationic and non-ionic surfactant molecules form structures that minimise their surface tension. By increasing surfactant concentration to (and beyond) CMC, surfactant assemblies are present inside the aqueous medium. Depending on the head group size of surfactant, ionic strength and hydrophobic tail, the resulting assemblies are known to have different shapes, such as rod, spherical, worm-like or lamellar [125]. Phosphate precursors are then added to this surfactant solution, which adsorb onto the surfactant assembly surface due to electrostatic attractions between oppositely charged ions. Thereafter, the addition of calcium precursors results in calcium reaching the surface of surfactant assemblies containing phosphate to form layers of calcium phosphate, which is converted to HAP under the chosen synthesis conditions. The surfactant in effect concentrates the phosphate and calcium precursors such that HAP formation occurs on this surface (although not exclusively). The morphology of HAP prepared in the presence of surfactant are, therefore, influenced directly by the properties of the surfactant. Finally, the surfactant is removed by hot-water washing, followed by calcination.

Regarding the use of an ionic surfactant, studies have been reported regarding the synthesis of HAp nanoparticles through a cationic surfactant CTAB. For example, Yan et al. [126] investigated the hydrothermal synthesis of Hap using the surfactant CTAB as regulator of the nucleation and crystal growth. TEM results showed that, after the hydrothermal treatment, the CTAB involved samples, followed by a heat treatment of 16h, transformed to uniformly nano-rods with length up to 150 nm and diameter of 10 nm with aspect ratio of 15. The behaviour of CTAB was explained as follow: in an aqueous system, CTAB would ionize completely and result in a cation with tetrahedral structure. Knowing that the phosphate anion is also a tetrahedral structure, it was suggested that the charge and structure complementarity enhance the surfactant with the ability to control the crystallization process. Bricha et al. [127] studied the effect of various surfactant families; such as cationic (CTAB), anionic (SDS) and non-ionic (Triton X-100), on the preparation of rod-like HAp nanoparticles by hydrothermal synthesis. The results revealed that the average dimensions of the prepared CTAB HAp are 15 nm diameter and 75 nm length, with an aspect ratio of 4.8 approximatively. The synthesized SDS HAp nanoparticles were found to be much thinner and longer with average diameter and

length of about 11 nm and 137 nm, respectively, and an aspect ratio of about 12.4. Regarding the HAp nanoparticles prepared using the non-ionic surfactant Triton X-100, the morphology of those particles varies between the sphere-like shape with dimensions in the range of 19-30 nm and the needle shape with the length and width of 79 nm and 21 nm, respectively, and an aspect ratio of 4.4. It can be concluded that the rod-like morphology was obtained regardless of the surfactant used during the hydrothermal treatment, but the aspect ratio of the crystals was found to be surfactant dependent. In another study, Salarian et al [128]. investigated the effect of temperature on the morphology of HAp nanoparticle through a surfactant assisted hydrothermal method. Results revealed that the morphology and size of HAp particles can be effectively controlled by the presence of the cationic CTAB and the non-ionic PEG surfactants. In addition, the temperature of the hydrothermal treatment plays an important role in controlling the morphology and size of HAp particles. The aspect ratio of rod-like particles increases with the increase in the hydrothermal temperature.

In order to understand the mechanism of action of surfactants on the morphology of the prepared HAp nanoparticles, the example of a cationic (CTAB), anionic (SDS) and non-ionic (Triton X-100) surfactant will be developed. Following the pH used in the study, CTAB molecules dissociate completely in the aqueous solution, forming cationic CTAB. Above the CMC, the cationic charged $CTAB^{+}$ tend to get together in direct cylindrical micelles. Hence, the $PO_4^{3-}$ solution is added to the CTAB solution, $PO_4^{3-}$ ions are directly attracted onto the surface of the cylindrical micelles and decreasing the total charge and the freedom of the $PO_4^{3-}$ ions. Then, the addition of the $Ca^{2+}$ solution leads to the formation of $Ca_9(PO_4)_6$ clusters, following electrostatic interactions, which forces the nucleating and growth of rod-like nano-HAp crystals. A similar interpretation could be suggested to explain the growth of HAp nanoparticles in the presence of anionic surfactants. In fact, the only difference expected when using SDS is the formation of $SDS^{-}$ - $Ca^{2+}$ complexes before the formation of $Ca_9(PO_4)_6$ clusters, when mixing the precursors. However, regarding the use of a non-ionic surfactant, the possibility of electrostatic interactions may be eliminated. In that case, an isotropic colloidal mixture of spherical micelles and hexagonally ordered cylinders is formed above the CMC. For instance, the non-ionic surfactant Triton X-100 consists of a hydrophilic polyethylene oxide group (head) and a hydrophobic hydrocarbon (tail). Lee et al [129] suggested that the polyethylene group could coordinate with $Ca^{2+}$ ions through hydrogen bonds, forming calcium complexes that mediate the reaction with the $PO_4^{3-}$. These intermolecular interactions would enable nucleation and particle growth to proceed, upon mixing the reagent solutions, according to the template micelles (Figure 15).

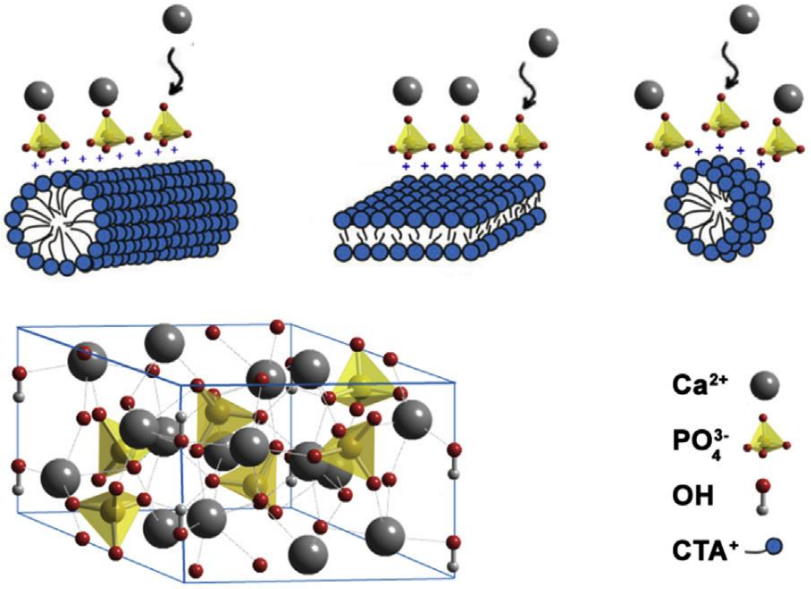


Figure 15. Nucleation and growth of hydroxyapatite crystals over cylindrical, bilayers and spherical surfactant micelle (CTAB case) [130]. Reprinted from Journal of Solid State Chemistry, 276, S. Hajimirzaee et al., Effects of surfactant on morphology, chemical properties and catalytic activity of hydroxyapatite, 345-351, Copyright (2019), with permission from Elsevier.

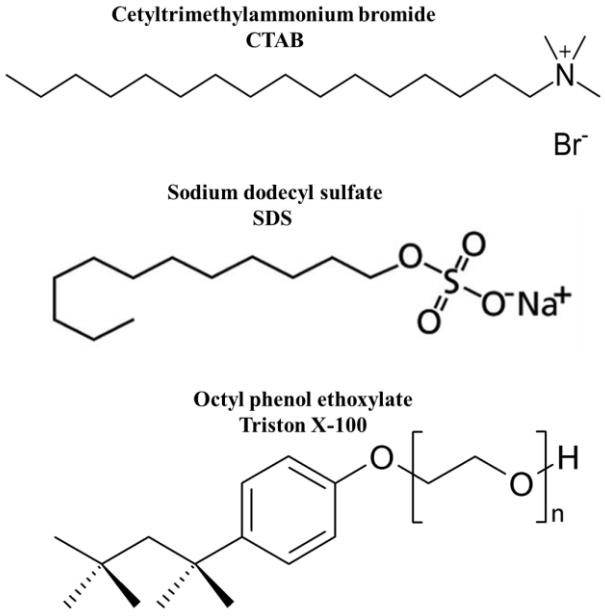


Figure 16. Chemical structure of the cationic (CTAB), anionic (SDS) and non-ionic (Triton X-100) surfactant

In this study we chose the hydrothermal method for the synthesis of nano-sized HAp over other techniques. Hydrothermal synthesis offers many advantages such as relatively mild operating conditions (reaction temperatures < 300 °C), one-step synthetic procedure, environmental friendliness, and good dispersion in solution. In addition, it allowed us to grow

pure phase of crystalline nano-HAp while maintaining control over their composition. Finally, hydrothermal synthesis is inexpensive in terms of the instrumentation, energy and material precursors compared with other solution synthesis methods. Besides, in order to regulate the growth and to achieve control over the size and morphology of the HAp crystals by applying surfactant-assisted hydrothermal technique, by adding a non-ionic surfactant Brij 93. The choice of non-ionic surfactants is due to their properties, effectiveness, economy, and ease of handling and formulating. In fact, it was found that non-ionic surfactants are characterized by weaker adsorption to charged sites, less toxicity to bacteria, poor foaming properties and compatibility with other types of surfactants. Regarding the toxicity of non-ionic surfactants, and in order to follow the green chemistry principles, it was found that high toxicity was shown only by surfactant solutions that contained a benzene ring [131]. Yuan et al. [132] reported that the toxicity of cationic surfactants is the highest, and the toxicity of anionic surfactants is between that of non-ionic surfactants and cationic surfactants. In fact, non-ionic surfactants have minimal irritation to the skin, since they are not electrically charged, this they can't combined with protein. The influence of pH, temperature, time and surfactant concentrations on the structure and composition of HAp formed in a hydrothermal process are investigated by X-ray diffraction (XRD), Fourier Transformed-Infrared Spectroscopy (FTIR), scanning (SEM) and transmission electron microscopy (TEM).

## 3.4. References

[1] D. Cordell, S. White, Tracking phosphorus security: indicators of phosphorus vulnerability in the global food system, *Food Security*, 7 (**2015**) 337-350.
[2] J. Azizi, Gestion des ressources naturelles non renouvelables : Équilibre du marché, impacts socio-économiques et canaux potentiels de malédiction des ressources -Une application au Phosphate, Thesis, (**2018)**.
[3] R. Hakkou, M. Benzaazoua, B. Bussière, Valorization of Phosphate Waste Rocks and Sludge from the Moroccan Phosphate Mines: Challenges and Perspectives, *Procedia Engineering*, 138 (**2016**) 110-118.
[4] A. Alouani, Phosphate Beneficiation Development for Customers' Satisfaction in Sustainable Development Way OCP case Khouribga - Jorf Lasfar, *Procedia Engineering*, 138 (**2016**) 95-103.
[5] S. Belboom, C. Szöcs, A. Léonard, Environmental impacts of phosphoric acid production using di-hemihydrate process: a Belgian case study, *Journal of Cleaner Production*, 108 (**2015**) 978-986.
[6] A.A. El-Asmy, H.M. Serag, M.A. Mahdy, M.I. Amin, Purification of phosphoric acid by minimizing iron, copper, cadmium and fluoride, *Sep Purif Technol*, 61 (**2008**) 287-292.
[7] T.F. Al-Fariss, H.Ö. Özbelge, H.S.H. El-Shall, Process Technology for Phosphoric Acid Production in Saudi Arabia, *Journal of King Saud University - Engineering Sciences*, 4 (**1992**) 239-254.
[8] H. Ben Abdelouahed, N. Reguigui, Radiotracer investigation of phosphoric acid and phosphatic fertilizers production process, *J Radioanal Nucl Chem*, 289 (**2011**) 103-111.
[9] S. Al-Thyabat, P. Zhang, In-line extraction of REE from Dihydrate (DH) and HemiDihydrate (HDH) wet processes, *Hydrometallurgy*, 153 (**2015**) 30-37.
[10] H.-W. Döring, Slack, Phosphoric Acid (Fertilizer Science and Technology Series), 124 (**1969**) 174-175.
[11] S. Manar, Increasing the Filtration Rate of Phosphor-gypsum by Using Mineral Additives, *Procedia Engineering*, 138 (**2016**) 151-163.
[12] H. Essabir, S. Nekhlaoui, M.O. Bensalah, D. Rodrigue, R. Bouhfid, A.e.k. Qaiss, Phosphogypsum Waste Used as Reinforcing Fillers in Polypropylene Based Composites: Structural, Mechanical and Thermal Properties, *J Polym Environ*, 25 (**2017**) 658-666.
[13] R. El Zrelli, L. Rabaoui, N. Daghbouj, H. Abda, S. Castet, C. Josse, P. van Beek, M. Souhaut, S. Michel, N. Bejaoui, P. Courjault-Radé, Characterization of phosphate rock and phosphogypsum from Gabes phosphate fertilizer factories (SE Tunisia): high mining potential and implications for environmental protection, *Environmental Science and Pollution Research*, 25 (**2018**) 14690-14702.
[14] A.-H.T. Kandil, M.F. Cheira, H.S. Gado, M.H. Soliman, H.M. Akl, Ammonium sulfate preparation from phosphogypsum waste, *Journal of Radiation Research and Applied Sciences*, 10 (**2017**) 24-33.
[15] Y. Mi, D. Chen, Y. He, S. Wang, Morphology-Controlled Preparation of α-Calcium Sulfate Hemihydrate from Phosphogypsum by Semi-Liquid Method, *Cryst Res Technol*, 53 (**2018**) 1700162.
[16] A. May, J.W. Sweeney, Evaluation of Radium and Toxic Element Leaching Characteristics of Florida Phosphogypsum Stockpiles, *ASTM International-West Conshohocken*, (**1984**), 140-159.
[17] L. Ajam, M. Ben Ouezdou, H.S. Felfoul, R.E. Mensi, Characterization of the Tunisian phosphogypsum and its valorization in clay bricks, *Construction and Building Materials*, 23 (**2009**) 3240-3247.

[18] M. Azouazi, Y. Ouahidi, S. Fakhi, Y. Andres, J.C. Abbe, M. Benmansour, Natural radioactivity in phosphates, phosphogypsum and natural waters in Morocco, *Journal of Environmental Radioactivity*, 54 (**2001**) 231-242.
[19] B.G. Lottermoser, Recycling, Reuse and Rehabilitation of Mine Wastes, *Elements*, 7 (**2011**) 405-410.
[20] C.E. Roessler, Control of radium in phosphate mining, beneficiation and chemical processing, *International Atomic Energy Agency (IAEA)*, (**1990)**.
[21] P.M. Rutherford, M.J. Dudas, J.M. Arocena, Radioactivity and elemental composition of phosphogypsum produced from three phosphate rock sources, *Waste Management & Research*, 13 (**1995**) 407-423.
[22] K. Grabas, A. Pawełczyk, W. Stręk, E. Szełęg, S. Stręk, Study on the Properties of Waste Apatite Phosphogypsum as a Raw Material of Prospective Applications, *Waste and Biomass Valorization*, 10 (**2019**) 3143-3155.
[23] S.M. El-Bahi, A. Sroor, G.Y. Mohamed, N.S. El-Gendy, Radiological impact of natural radioactivity in Egyptian phosphate rocks, phosphogypsum and phosphate fertilizers, *Appl Radiat Isot*, 123 (**2017**) 121-127.
[24] J.P. Bolivar, R. Garcia-Tenorio, J. Mas, Radioactivity of Phosphogypsum in South-West of Spain, *Radiat Prot Dosim*, 76 (**1998**) 185-189.
[25] O. World Health, Guidelines for drinking-water quality, *World Health Organization-Geneva*, (**2017)**.
[26] J. Yang, W. Liu, L. Zhang, B. Xiao, Preparation of load-bearing building materials from autoclaved phosphogypsum, *Construction and Building Materials*, 23 (**2009**) 687-693.
[27] M. Lysandrou, A. Charalambides, I. Pashalidis, Radon emanation from phosphogypsum and related mineral samples in Cyprus, *Radiation Measurements*, 42 (**2007**) 1583-1585.
[28] L. Rabaoui, R. Balti, R. Zrelli, S. Tlig-Zouari, Assessment of heavy metals pollution in the gulf of Gabes (Tunisia) using four mollusk species, *Mediterranean Marine Science*, 15 (**2013**) 45.
[29] L. Chen, K.Y.H. Gin, Y. He, Effects of sulfate on microcystin production, photosynthesis, and oxidative stress in Microcystis aeruginosa, *Environmental Science and Pollution Research*, 23 (**2016**) 3586-3595.
[30] K.A. Rusch, T. Guo, R.K. Seals, Stabilization of phosphogypsum using class C fly ash and lime: assessment of the potential for marine applications, *J Hazard Mater*, 93 (**2002**) 167-186.
[31] M.A. Taher, Influence of thermally treated phosphogypsum on the properties of Portland slag cement, *Resources, Conservation and Recycling*, 52 (**2007**) 28-38.
[32] M.M. Smadi, R.H. Haddad, A.M. Akour, Potential use of phosphogypsum in concrete, *Cem Concr Res*, 29 (**1999**) 1419-1425.
[33] J.H. Potgieter, S.S. Potgieter, R.I. McCrindle, C.A. Strydom, An investigation into the effect of various chemical and physical treatments of a South African phosphogypsum to render it suitable as a set retarder for cement, *Cem Concr Res*, 33 (**2003**) 1223-1227.
[34] M. Singh, M. Garg, S.S. Rehsi, Purifying phosphogypsum for cement manufacture, *Construction and Building Materials*, 7 (**1993**) 3-7.
[35] Y. Ennaciri, I. Zdah, H. El Alaoui-Belghiti, M. Bettach, Characterization and purification of waste phosphogypsum to make it suitable for use in the plaster and the cement industry, *Chem Eng Commun*, (**2019**) 1-11.
[36] J. Zhou, H. Gao, Z. Shu, Y. Wang, C. Yan, Utilization of waste phosphogypsum to prepare non-fired bricks by a novel Hydration–Recrystallization process, *Construction and Building Materials*, 34 (**2012**) 114-119.
[37] S. Folek, B. Walawska, B. Wilczek, J. Miśkiewicz, Use of phosphogypsum in road construction, 13 (**2011**) 18.

[38] C. Cárdenas-Escudero, V. Morales-Flórez, R. Pérez-López, A. Santos, L. Esquivias, Procedure to use phosphogypsum industrial waste for mineral CO2 sequestration, *J Hazard Mater*, 196 (**2011**) 431-435.
[39] H.-P. Mattila, R. Zevenhoven, Mineral Carbonation of Phosphogypsum Waste for Production of Useful Carbonate and Sulfate Salts, *Frontiers in Energy Research*, 3 (**2015**).
[40] M. Raii, D.P. Minh, F.J.E. Sanz, A. Nzihou, Lead and Cadmium Removal from Aqueous Solution Using an Industrial Gypsum By-product, *Procedia Engineering*, 83 (**2014**) 415-422.
[41] N. Balkaya, H. Cesur, Adsorption of cadmium from aqueous solution by phosphogypsum, *Chem Eng J*, 140 (**2008**) 247-254.
[42] H. Cesur, N. Balkaya, Zinc removal from aqueous solution using an industrial by-product phosphogypsum, *Chem Eng J*, 131 (**2007**) 203-208.
[43] A.G. Werner, Kurze Klassifikation und Beschreibung der verschiedenen Gebirgsarten, (**1787**).
[44] M. Slansky, A. Lallemand, G. Millot, La sédimentation et l'altération latéritique des formations phosphatées du gisement de Taïba (République du Sénégal), *Bulletin du Service de la carte géologique d'Alsace et de Lorraine*, 17 (**1964**) 311-324.
[45] Apatite, *https://enwikipediaorg/wiki/Apatite*.
[46] D. McConnell, A Structural Investigation of the Isomorphism of the Apatite Group, *Am Mineral*, 23 (**1938**) 1-19.
[47] M. Mehmel, 21 Über die Struktur des Apatits. I, in: Zeitschrift für Kristallographie - Crystalline Materials, 1 (**1930)**, 323.
[48] J.M. Hughes, J. Rakovan, The Crystal Structure of Apatite, Ca5(PO4)3(F,OH,Cl), *Reviews in Mineralogy and Geochemistry*, 48 (**2002**) 1-12.
[49] M. Pasero, A.R. Kampf, C. Ferraris, I.V. Pekov, J. Rakovan, T.J. White, Nomenclature of the apatite supergroup minerals, *Eur J Mineral*, 22 (**2010**) 163-179.
[50] S. Samreen, S. Kausar, Phosphorus Fertilizer: The Original and Commercial Sources, (**2019**).
[51] J.D. Pasteris, A mineralogical view of apatitic biomaterials, *Am Mineral*, 101 (**2016**) 2594-2610.
[52] W. Wang, K.W.K. Yeung, Bone grafts and biomaterials substitutes for bone defect repair: A review, *Bioactive Materials*, 2 (**2017**) 224-247.
[53] M. Itokazu, T. Sugiyama, T. Ohno, E. Wada, Y. Katagiri, Development of porous apatite ceramic for local delivery of chemotherapeutic agents, *Journal of Biomedical Materials Research*, 39 (**1998**) 536-538.
[54] M. Czaja, S. Bodył, P. Głuchowski, Z. Mazurak, W. Strek, Luminescence properties of rare earth ions in fluorite, apatite and scheelite minerals, *J Alloys Compd*, 451 (**2008**) 290-292.
[55] C.L. Owens, G.R. Nash, K. Hadler, R.S. Fitzpatrick, C.G. Anderson, F. Wall, Apatite enrichment by rare earth elements: A review of the effects of surface properties, *Adv Colloid Interface Sci*, 265 (**2019**) 14-28.
[56] X. Chen, X. Jin, J. Tan, W. Li, M. Chen, L. Yao, H. Yang, Large-scale synthesis of water-soluble luminescent hydroxyapatite nanorods for security printing, *J Colloid Interface Sci*, 468 (**2016**) 300-306.
[57] N. Bellier, F. Chazarenc, Y. Comeau, Phosphorus removal from wastewater by mineral apatite, *Water Res*, 40 (**2006**) 2965-2971.
[58] S. Troesch, D. Esser, P. Molle, Natural Rock Phosphate: A Sustainable Solution for Phosphorous Removal from Wastewater, *Procedia Engineering*, 138 (**2016**) 119-126.
[59] P. Molle, A. Lienard, A. Grasmick, A. Iwema, A. Kabbabi, Apatite as an interesting seed to remove phosphorus from wastewater in constructed wetlands, *Water Sci Technol*, 51 (**2005**) 193-203.

[60] I. Hore-Lacy, 9 - Production of byproduct uranium and uranium from unconventional resources, in: I. Hore-Lacy (Ed.) Uranium for Nuclear Power, Woodhead Publishing, 2016, pp. 239-251.
[61] N. Leroy, E. Bres, Structure and Substitutions in Fluorapatite, *European Cells and Materials*, 2 (**2001**) 36-48.
[62] B.G. DeBoer, A. Sakthivel, J.R. Cagle, R.A. Young, Determination of the antimony substitution site in calcium fluorapatite from powder X-ray diffraction data, *Acta Crystallographica Section B*, 47 (**1991**) 683-692.
[63] S. Karthi, R. Govindan, A. Gangadharan, G.C. Dannangoda, K.S. Martirosyan, D.K. Sardar, S. Chidangil, E.K. Girija, Luminomagnetic Nd3+ doped fluorapatite coated Fe3O4 nanostructures for biomedical applications, *J Am Ceram Soc*, 102 (**2019**) 2558-2568.
[64] H. Ye, M. He, T. Zhou, Q. Guo, J. Zhang, L. Liao, L. Mei, H. Liu, M. Runowski, A novel reddish-orange fluorapatite phosphor, La6-xBa4(SiO4)6F2: xSm3+ - Structure, luminescence and energy transfer properties, *J Alloys Compd*, 757 (**2018**) 79-86.
[65] K. Peng, Q. Zhang, P. Zou, Y. Wang, J. Li, Synthesis and luminescent properties of rare earth doped upconversion nano-fluorapatite, SPIE, 2018.
[66] I. Denry, O.-M. Goudouri, J. Harless, J.A. Holloway, Rapid vacuum sintering: A novel technique for fabricating fluorapatite ceramic scaffolds for bone tissue engineering, *Journal of Biomedical Materials Research Part B: Applied Biomaterials*, 106 (**2018**) 291-299.
[67] R. Taktak, A. Elghazel, J. Bouaziz, S. Charfi, H. Keskes, Tricalcium phosphate-Fluorapatite as bone tissue engineering: Evaluation of bioactivity and biocompatibility, *Materials Science and Engineering: C*, 86 (**2018**) 121-128.
[68] H. Zeng, X. Li, M. Sun, S. Wu, H. Chen, Synthesis of Europium-Doped Fluorapatite Nanorods and Their Biomedical Applications in Drug Delivery, *Molecules*, 22 (**2017**) 753.
[69] Y. Liu, J. Chen, Phosphorus Cycle☆, in: B. Fath (Ed.) Encyclopedia of Ecology (Second Edition), Elsevier, Oxford, 2014, pp. 181-191.
[70] X.-M. Zhang, C. Hu, Z.-Q. He, Y. Abbas, Y. Li, L.-F. Lv, X.-Y. Hao, G.-S. Gai, Z.-H. Huang, Y.-F. Yang, S.-N. Yun, Microcrystalline Apatite Minerals: Mechanochemical Activation for Agricultural Application, *Minerals*, 9 (**2019**) 211.
[71] G. Ma, X.Y. Liu, Hydroxyapatite: Hexagonal or Monoclinic?, *Crystal Growth & Design*, 9 (**2009**) 2991-2994.
[72] S. Koutsopoulos, Synthesis and characterization of hydroxyapatite crystals: A review study on the analytical methods, *Journal of Biomedical Materials Research*, 62 (**2002**) 600-612.
[73] J.P. Raval, P. Joshi, D.R. Chejara, I.A. Disher, Fabrication and applications of hydroxyapatite-based nanocomposites coating for bone tissue engineering, *Applications of Nanocomposite Materials in Orthopedics*, 3 (**2019**), 71-82.
[74] L. Rigano, N. Lionetti, Nanobiomaterials in galenic formulations and cosmetics, *Nanobiomaterials in Galenic Formulations and Cosmetics*, 6 (**2016**), 121-148.
[75] V. Uskoković, D.P. Uskoković, Nanosized hydroxyapatite and other calcium phosphates: Chemistry of formation and application as drug and gene delivery agents, *Journal of Biomedical Materials Research Part B: Applied Biomaterials*, 96B (**2011**) 152-191.
[76] L. García Rodenas, J.M. Palacios, M.C. Apella, P.J. Morando, M.A. Blesa, Surface properties of various powdered hydroxyapatites, *J Colloid Interface Sci*, 290 (**2005**) 145-154.
[77] T.A. Rangreez, Inamuddin, M. Naushad, H. Ali, Synthesis and characterisation of poly(3,4-ethylenedioxythiophene)-poly(styrenesulfonate) (PEDOT:PSS) Zr(IV) monothiophosphate composite cation exchanger: analytical application in the selective separation of lead metal ions, *International Journal of Environmental Analytical Chemistry*, 95 (**2015**) 556-568.
[78] M. Naushad, Z.A. Alothman, Inamuddin, H. Javadian, Removal of Pb(II) from aqueous solution using ethylene diamine tetra acetic acid-Zr(IV) iodate composite cation exchanger:

Kinetics, isotherms and thermodynamic studies, *Journal of Industrial and Engineering Chemistry*, 25 (**2015**) 35-41.
[79] M.M. Alam, Z.A. Alothman, M. Naushad, T. Aouak, Evaluation of heavy metal kinetics through pyridine based Th(IV) phosphate composite cation exchanger using particle diffusion controlled ion exchange phenomenon, *Journal of Industrial and Engineering Chemistry*, 20 (**2014**) 705-709.
[80] T. Suzuki, T. Hatsushika, Y. Hayakawa, Synthetic hydroxyapatites employed as inorganic cation-exchangers, *Journal of the Chemical Society, Faraday Transactions 1: Physical Chemistry in Condensed Phases*, 77 (**1981**) 1059-1062.
[81] E. Deydier, R. Guilet, P. Sharrock, Beneficial use of meat and bone meal combustion residue: "an efficient low cost material to remove lead from aqueous effluent", *J Hazard Mater*, 101 (**2003**) 55-64.
[82] Chen, J.V. Wright, J.L. Conca, L.M. Peurrung, Effects of pH on Heavy Metal Sorption on Mineral Apatite, *Environmental Science & Technology*, 31 (**1997**) 624-631.
[83] X. Chen, J.V. Wright, J.L. Conca, L.M. Peurrung, Evaluation of heavy metal remediation using mineral apatite, *Water, Air, Soil Pollut*, 98 (**1997**) 57-78.
[84] K. Viipsi, S. Sjöberg, K. Tõnsuaadu, A. Shchukarev, Hydroxy- and fluorapatite as sorbents in Cd(II)–Zn(II) multi-component solutions in the absence/presence of EDTA, *J Hazard Mater*, 252-253 (**2013**) 91-98.
[85] M. Manecki, P.A. Maurice, S.J. Traina, KINETICS OF AQUEOUS Pb REACTION WITH APATITES, *Soil Science*, 165 (**2000**) 920-933.
[86] Z. Elouear, J. Bouzid, N. Boujelben, M. Feki, F. Jamoussi, A. Montiel, Heavy metal removal from aqueous solutions by activated phosphate rock, *J Hazard Mater*, 156 (**2008**) 412-420.
[87] Y. Xu, F.W. Schwartz, S.J. Traina, Sorption of $Zn^{2+}$ and $Cd^{2+}$ on Hydroxyapatite Surfaces, *Environmental Science & Technology*, 28 (**1994**) 1472-1480.
[88] Q.Y. Ma, S.J. Traina, T.J. Logan, J.A. Ryan, In situ lead immobilization by apatite, *Environmental Science & Technology*, 27 (**1993**) 1803-1810.
[89] P. Miretzky, A. Fernandez-Cirelli, Phosphates for Pb immobilization in soils: a review, *Environmental Chemistry Letters*, 6 (**2008**) 121-133.
[90] M. Jarcho, J.F. Kay, K.I. Gumaer, R.H. Doremus, H.P. Drobeck, Tissue, cellular and subcellular events at a bone-ceramic hydroxylapatite interface, *J Bioeng*, 1 (**1977**) 79-92.
[91] H. Oonishi, Orthopaedic applications of hydroxyapatite, *Biomaterials*, 12 (**1991**) 171-178.
[92] M. Sadat-Shojai, M.-T. Khorasani, E. Dinpanah-Khoshdargi, A. Jamshidi, Synthesis methods for nanosized hydroxyapatite with diverse structures, *Acta Biomaterialia*, 9 (**2013**) 7591-7621.
[93] A.-j. Wang, Y.-p. Lu, R.-f. Zhu, S.-t. Li, X.-l. Ma, Effect of process parameters on the performance of spray dried hydroxyapatite microspheres, *Powder Technol*, 191 (**2009**) 1-6.
[94] S. Pramanik, A.K. Agarwal, K.N. Rai, A. Garg, Development of high strength hydroxyapatite by solid-state-sintering process, *Ceram Int*, 33 (**2007**) 419-426.
[95] A.C. Taş, Molten Salt Synthesis of Calcium Hydroxyapatite Whiskers, *J Am Ceram Soc*, 84 (**2001**) 295-300.
[96] Y.-H. Tseng, C.-S. Kuo, Y.-Y. Li, C.-P. Huang, Polymer-assisted synthesis of hydroxyapatite nanoparticle, *Materials Science and Engineering: C*, 29 (**2009**) 819-822.
[97] C.C. Silva, M.P.F. Graça, M.A. Valente, A.S.B. Sombra, Crystallite size study of nanocrystalline hydroxyapatite and ceramic system with titanium oxide obtained by dry ball milling, *Journal of Materials Science*, 42 (**2007**) 3851-3855.
[98] M.H. Fathi, E. Mohammadi Zahrani, Mechanical alloying synthesis and bioactivity evaluation of nanocrystalline fluoridated hydroxyapatite, *J Cryst Growth*, 311 (**2009**) 1392-1403.

[99] J. Coreño A, O. Coreño A, J.J. Cruz R, C. Rodríguez C, Mechanochemical synthesis of nanocrystalline carbonate-substituted hydroxyapatite, *Opt Mater*, 27 (**2005**) 1281-1285.
[100] T. Ikoma, A. Yamazaki, S. Nakamura, M. Akao, Preparation and Structure Refinement of Monoclinic Hydroxyapatite, *J Solid State Chem*, 144 (**1999**) 272-276.
[101] S.K. Swain, D. Sarkar, A comparative study: Hydroxyapatite spherical nanopowders and elongated nanorods, *Ceram Int*, 37 (**2011**) 2927-2930.
[102] S. Ramesh, R. Tolouei, M. Hamdi, J. Purbolaksono, C.Y. Tan, M. Amiriyan, W.D. Teng, Sintering Behavior of Nanocrystalline Hydroxyapatite Produced by Wet Chemical Method, *Current Nanoscience*, 7 (**2011**) 845-849.
[103] I. Mobasherpour, M.S. Heshajin, A. Kazemzadeh, M. Zakeri, Synthesis of nanocrystalline hydroxyapatite by using precipitation method, *J Alloys Compd*, 430 (**2007**) 330-333.
[104] H. Peng, J. Wang, S. Lv, J. Wen, J.-F. Chen, Synthesis and characterization of hydroxyapatite nanoparticles prepared by a high-gravity precipitation method, *Ceram Int*, 41 (**2015**) 14340-14349.
[105] J. Chen, Y. Wang, X. Chen, L. Ren, C. Lai, W. He, Q. Zhang, A simple sol-gel technique for synthesis of nanostructured hydroxyapatite, tricalcium phosphate and biphasic powders, *Mater Lett*, 65 (**2011**) 1923-1926.
[106] A. Milev, G.S.K. Kannangara, B. Ben-Nissan, Morphological stability of hydroxyapatite precursor, *Mater Lett*, 57 (**2003**) 1960-1965.
[107] M.-F. Hsieh, L.-H. Perng, T.-S. Chin, H.-G. Perng, Phase purity of sol–gel-derived hydroxyapatite ceramic, *Biomaterials*, 22 (**2001**) 2601-2607.
[108] M.H. Fathi, A. Hanifi, V. Mortazavi, Preparation and bioactivity evaluation of bone-like hydroxyapatite nanopowder, *J Mater Process Technol*, 202 (**2008**) 536-542.
[109] W. Feng, L. Mu-sen, L. Yu-peng, Q. Yong-xin, A simple sol–gel technique for preparing hydroxyapatite nanopowders, *Mater Lett*, 59 (**2005**) 916-919.
[110] B. Cockayne, The growth of single crystals by R. A. Laudise, *J Appl Crystallogr*, 5 (**1972**) 53.
[111] A. Rabenau, The Role of Hydrothermal Synthesis in Preparative Chemistry, *Angewandte Chemie International Edition in English*, 24 (**1985**) 1026-1040.
[112] K. Byrappa, M. Yoshimura, 2 - History of Hydrothermal Technology, in: K. Byrappa, M. Yoshimura (Eds.) Handbook of Hydrothermal Technology, William Andrew Publishing, Norwich, NY, 2001, pp. 53-81.
[113] L.N. Dem'yanets, L.E. Li, T.G. Uvarova, Zinc oxide: hydrothermal growth of nano- and bulk crystals and their luminescent properties, *Journal of Materials Science*, 41 (**2006**) 1439-1444.
[114] V.V. Kondalkar, R.R. Kharade, S.S. Mali, R.M. Mane, P.B. Patil, P.S. Patil, S. Choudhury, P.N. Bhosale, Nanobrick-like WO3 thin films: Hydrothermal synthesis and electrochromic application, *Superlattices Microstruct*, 73 (**2014**) 290-295.
[115] L. Tan, L. Wang, Y. Wang, Hydrothermal Synthesis of Nanostructures with Different Morphologies and Their Optical Properties, *Journal of Nanomaterials*, 2011 (**2011**) 10.
[116] H. Zhang, M. Zhang, Characterization and thermal behavior of calcium deficient hydroxyapatite whiskers with various Ca/P ratios, *Mater Chem Phys*, 126 (**2011**) 642-648.
[117] K. Kandori, K. Takeguchi, M. Fukusumi, Y. Morisada, Preparation and characterization of calcium hydroxyapatite and balloon-like calcium phosphate particles from forced hydrolysis of Ca(OH)2–triphosphate solution, *Polyhedron*, 28 (**2009**) 3036-3042.
[118] J.S. Earl, D.J. Wood, S.J. Milne, Hydrothermal synthesis of hydroxyapatite, *Journal of Physics: Conference Series*, 26 (**2006**) 268-271.
[119] B. Viswanath, N. Ravishankar, Controlled synthesis of plate-shaped hydroxyapatite and implications for the morphology of the apatite phase in bone, *Biomaterials*, 29 (**2008**) 4855-4863.

[120] X. Guo, P. Xiao, J. Liu, Z. Shen, Fabrication of Nanostructured Hydroxyapatite via Hydrothermal Synthesis and Spark Plasma Sintering, *J Am Ceram Soc*, 88 (**2005**) 1026-1029.
[121] M. Sadat-Shojai, M. Atai, A. Nodehi, Design of experiments (DOE) for the optimization of hydrothermal synthesis of hydroxyapatite nanoparticles, *Journal of the Brazilian Chemical Society*, 22 (**2011**) 571-582.
[122] J.D. Chen, Y.J. Wang, K. Wei, S.H. Zhang, X.T. Shi, Self-organization of hydroxyapatite nanorods through oriented attachment, *Biomaterials*, 28 (**2007**) 2275-2280.
[123] M. Sadat-Shojai, M.-T. Khorasani, A. Jamshidi, Hydrothermal processing of hydroxyapatite nanoparticles—A Taguchi experimental design approach, *J Cryst Growth*, 361 (**2012**) 73-84.
[124] H. Lu, I. Pezron, T. Gaudin, A. Drelich, Non-equilibrium micelles formed by sugar-based surfactants under their Krafft temperature, *Colloids and Surfaces A: Physicochemical and Engineering Aspects*, 540 (**2018**) 167-176.
[125] M. Mujahid, S. Sarfraz, S. Amin, On the Formation of Hydroxyapatite Nano Crystals Prepared Using Cationic Surfactant, *Materials Research*, 18 (**2015**) 468-472.
[126] L. Yan, Y. Li, Z.-X. Deng, J. Zhuang, X. Sun, Surfactant-assisted hydrothermal synthesis of hydroxyapatite nanorods, *Int J Inorg Mater*, 3 (**2001**) 633-637.
[127] M. Bricha, Y. Belmamouni, E.M. Essassi, J.M.F. Ferreira, K.E. Mabrouk, Surfactant-Assisted Hydrothermal Synthesis of Hydroxyapatite Nanopowders, *Journal of Nanoscience and Nanotechnology*, 12 (**2012**) 8042-8049.
[128] M. Salarian, M. Solati-Hashjin, S.S. Shafiei, R. Salarian, Z.A. Nemati, Template-directed hydrothermal synthesis of dandelion-like hydroxyapatite in the presence of cetyltrimethylammonium bromide and polyethylene glycol, *Ceram Int*, 35 (**2009**) 2563-2569.
[129] M.-H. Lee, S.-G. Oh, K.-D. Suh, D.-G. Kim, D. Sohn, Preparation of silver nanoparticles in hexagonal phase formed by nonionic Triton X-100 surfactant, *Colloids and Surfaces A: Physicochemical and Engineering Aspects*, 210 (**2002**) 49-60.
[130] S. Hajimirzaee, S. Chansai, C. Hardacre, C.E. Banks, A.M. Doyle, Effects of surfactant on morphology, chemical properties and catalytic activity of hydroxyapatite, *J Solid State Chem*, 276 (**2019**) 345-351.
[131] K. Jahan, S. Balzer, P. Mosto, Toxicity of nonionic surfactants, 1 (**2008**) 281-290.
[132] Z.Z.X. Yuan C. L. , M. X. Fan, H. Y. Liu, Y. H. Xie and T. Zhu, Study on characteristics and harm of surfactants, *Journal of Chemical and Pharmaceutical Research*, 6 (**2014**).

# 4. Results and discussion

## 4.1. Hydrothermal synthesis of nano-crystalline hydroxyapatite from phosphogypsum waste

| | |
|---|---|
| Title | Hydrothermal synthesis of nano-crystalline hydroxyapatite from phosphogypsum waste |
| Authors | H. Bensalah, M.F. Bekheet, S. Alami Younssi, M. Ouammou and A. Gurlo |
| Journal | Journal of Environmental Chemical Engineering |
| Publisher | Elsevier |
| Publication date | 25 January 2018 |
| Reference | Journal of Environmental Chemical Engineering, 6 (2018) 1347-1352 |
| DOI | 10.1016/j.jece.2018.01.052 |
| My contribution | Design of experiments, hydrothermal synthesis of HAp nano-rods, results analysis and discussion, writing of the manuscript. |

Journal of Environmental Chemical Engineering 6 (2018) 1347–1352

Contents lists available at ScienceDirect

Journal of Environmental Chemical Engineering

journal homepage: www.elsevier.com/locate/jece

# Hydrothermal synthesis of nanocrystalline hydroxyapatite from phosphogypsum waste

Hiba Bensalah[a,b,*], Maged F. Bekheet[b], Saad Alami Younssi[a], Mohamed Ouammou[a], Aleksander Gurlo[b]

[a] Laboratory of Membranes, Materials and Environment, Department of Chemistry, Faculty of Sciences & Technics of Mohammedia BP 146, 20650, University Hassan II of Casablanca, Morocco
[b] Fachgebiet Keramische Werkstoffe, Institut für Werkstoffwissenschaften und–technologien, Technische Universität Berlin, Hardenbergstraße 40, 10623 Berlin, Germany

ARTICLE INFO

*Keywords:*
Phosphogypsum
Hydroxyapatite
Nanorods
Hydrothermal
Surfactant

ABSTRACT

Hydroxyapatite (HAp) nanorods are synthesized from phosphogypsum waste (PG) and potassium dihydrogen phosphate ($KH_2PO_4$) under hydrothermal conditions. The influence of several synthesis parameters such as temperature (100–200 °C), synthesis time (1–15 h), and solution pH (5–11) on product structure and purity is addressed by X-ray diffraction and Fourier Transformed-Infrared Spectroscopy. Phase-pure HAp nanorods with diameter and length of 18 and 63 nm, respectively, are obtained after 10 h at 200 °C and pH ~ 11. The influence of Brij-93 surfactant on the morphology of prepared HAp is investigated by transmission and scanning electron microscopy. The aspect ratio and the mean size of HAp crystals increase to 1013 and 205 × 20 nm, respectively, with increasing the concentration of Brij-93 surfactant to 0.01 mol. Hence, the PG recycling could be accomplished using an easy synthesis route with relatively cheap reactants for the production of nanocrytalline HAp.

## 1. Introduction

Phosphogypsum (PG) is an industrial waste appeared from the production of phosphoric acid where the phosphate ore is dissolved in sulfuric acid [1]:

$$Ca_5(PO_4)_3F + 5H_2SO_4 + 10H_2O \rightarrow 3H_3PO_4 + 5CaSO_4 \cdot 2H_2O + HF \quad (1)$$

About 5 tons of phosphogypsum are produced for every ton of $P_2O_5$ manufactured [2]. Worldwide PG production is huge, and it is estimated that 280 million tons are produced annually in phosphoric acid plants [3]. Until now, only 15% of world PG production is recycled as building materials, agricultural fertilizers or soil stabilization amendments and as setting regulator instead of natural gypsum in the Portland cement industry [4–6]. In fact, 85% of the worldwide production remains at present stored into piles near the factory that occupy considerable land resources, or completely discharged into water, which lead to serious contamination [2]. In consequence, valorizing and minimizing the negative effects of this waste increasingly grab the attention of researchers all around the world.

Since hydroxyapatite ($Ca_{10}(PO_4)_6(OH)_2$, HAp) is the major mineral constituent of human hard tissues such as bones and teeth, synthetic hydroxyapatite has received large attention as bone and teeth implants [7,8]. HAp has been extensively used also as a catalyst [9–12], catalyst support [13,14], biosensor [15–17] and adsorbent for several heavy elements, organic dyes and fluoride ions [18–21]. Recent studies showed that the nanostructured HAp exhibits multi-adsorbing sites, large surface area, and high biocompatibility [8,17,22]. In enamel HAp is present as highly crystalline nanorods with length and diameter of 100–1000 nm and 33–65 nm, respectively [23,24]. Thus, the synthesis of nanosized HAp materials with control over size and morphology of crystals is essential for a variety of applications. HAp was previously synthesized by various methods such as solid-state reaction [25], co-precipitation [7], sol-gel process [26], hydrothermal methods [22,27], and microwave synthesis route [21]. Some of these synthesis techniques have some drawbacks such as long reaction times, agglomeration, uncontrolled particle size and non-stoichiometric products. Among all these synthesis methods, the hydrothermal method, that can combine moderate temperatures with high pressures, is often used to prepare nanocrystalline HAp with controlled size and morphology [22,27]. Moreover, as surfactants are found to be the best shape directing agents allowing control over size and morphology of nanocrystals [28], they have also been explored in the HAp synthesis. For example, Wang et al.

*Abbreviations:* PG, phosphogypsum; HAp, hydroxyapatite

* Corresponding author at: Laboratory of Membranes, Materials and Environment, Department of Chemistry, Faculty of Sciences & Technics of Mohammedia BP 146, 20650, University Hassan II of Casablanca, Morocco.
*E-mail address:* hiba.bensalah@ceramics.tu-berlin.de (H. Bensalah).

https://doi.org/10.1016/j.jece.2018.01.052
Received 2 August 2017; Received in revised form 11 December 2017; Accepted 25 January 2018

succeeded to regulate the growth of HAp crystals by the addition of cationic surfactant hexadecyltrimethylammonium bromide (CTAB) [22].

Accordingly, the aim of this work is to convert industrial waste PG into nanocrystalline HAp and to achieve control over the size and morphology of the HAp crystals by applying surfactant-assisted hydrothermal technique. A nonionic Brij-93 ($C_{18}H_{35}(OCH_2CH_2)_2OH$) surfactant, containing polar polyoxyethylene groups separated by hydrophobic polyethylene chain, is applied in this study. The influence of pH, temperature, time and surfactant concentrations on the structure and composition of HAp formed in a hydrothermal process are investigated by X-ray diffraction (XRD), Fourier Transformed-Infrared Spectroscopy (FTIR), scanning (SEM) and transmission electron microscopy (TEM).

## 2. Experimental

### 2.1. Materials

The phosphogypsum (PG) waste samples used in this study were collected from the production of phosphoric acid factory in Morocco. The powder was washed several times with distilled water, then dried overnight in oven and sieved with 50 µm sieve. Potassium dihydrogen phosphate ($KH_2PO_4$) as phosphate source, sodium hydroxide pellets for pH adjustment, and polyethylene glycol oleyl ether $C_{22}H_{44}O_3$ (Brij-93 with average Mn ~ 357) as non-ionic surfactant, were obtained from Sigma-Aldrich (Germany). Distilled water (DIW) was used for all syntheses.

### 2.2. HAp synthesis

The hydrothermal synthesis was performed in distilled water according to the following procedure: (i) 0.3 M solution of potassium dihydrogen phosphate was prepared by dissolving 2 g $KH_2PO_4$ in 50 mL $H_2O$ at room temperature under continuous stirring; (ii) 2 g of PG was added to $KH_2PO_4$ solution with continuous stirring at room temperature for 30 min; (iii) the solution pH was adjusted between 5 and 11 by dropwise addition of 1 M NaOH solution; (iv) 0.003–0.01 mol of the surfactant Brij 93 was added to the mixture; (v) the obtained solutions were transferred into 120 mL Teflon lined steel autoclaves and the hydrothermal synthesis was carried out at 100, 150 and 200 °C for different holding time (i.e. 1, 2, 6 and 15 h); (vi) the synthesis products were washed several times with distilled hot water and ethanol in order to remove the side products, then the products were collected by centrifugation and dried at 70 °C for 24 h in air.

The conversion to hydroxyapatite was achieved according to the reaction below:

$$10\ (CaSO_4,\ ½\ H_2O) + 6\ KH_2PO_4 \rightarrow Ca_{10}(PO_4)_6(OH)_2 + 3K_2SO_4 + 7H_2SO_4 + 3H_2O \quad (2)$$

### 2.3. Characterization methods

The structural characterization was performed using a Bruker AXS D8 ADVANCE X-ray diffractometer (Bruker, Germany) equipped with a Lynx Eye 1D detector with CoKα radiation. This device operated in a Bragg–Brentano geometry. Data were collected between 10 and 80° 2θ, with a step time of 3 s/0.02°. The characterization of the synthesized HAp for each parameter was carried out by X-ray diffraction using a PHILIPS PW 1830 diffractometer (PHILIPS, Netherlands) with CuKα radiation. Data were collected in the 2θ range of 15–80°, with a step size of 0.04. Rietveld refinement was performed using the FULLPROF program [29] and profile function 7 (Thompson-Cox-Hastings pseudo-Voigt convoluted with axial divergence asymmetry function) [30]. The resolution function of the instrument was obtained from the structure refinement of $LaB_6$ standard. The functional groups of raw PG and elaborated HAp were analysed by attenuated total reflection (ATR) method using Fourier transform infrared spectrometer on Bruker EQUINOX 55 (Bruker, Germany). The morphology of elaborated HAp at different surfactant dosages was studied via scanning electron microscopy (SEM) on a Zeiss Gemini Leo 1530 (Zeiss, Germany). Samples were placed on conducting carbon pads and then sputtered with a thin layer of gold to prevent sample charging. Transmission electron microscopy (TEM) characterization was performed on a TECNAI $G^2$20 S-TWIN (FEI, Oregon, USA) with $LaB_6$ electron gun, operated at 200 kV. A Gatan MS794 P CCD camera and Digital Micrograph software package were used for image recording and evaluation.

## 3. Results and discussion

### 3.1. Composition and structure of phosphogypsum waste

In the first step phosphogypsum sample was characterized by powder X-ray diffraction in order to determine the crystalline phases in the sample. The Rietveld refinement of the XRD data showed that the sample contains 56.9 wt% hemi-hydrate gypsum $CaSO_4.½\ H_2O$ (*I*2, No. 5, $Z = 12$, $a = 12.0220(4)$, $b = 6.9312(5)$, $c = 12.6867(4)$ Å and $\beta = 90.18(1)^\circ$), 42.2 wt% anhydrous $CaSO_4$ (*Amma*, No. 63, $Z = 4$, $a = 7.0016(5)$, $b = 7.0068(3)$, $c = 6.2431(3)$ Å) and 0.9 wt% of quartz $SiO_2$ ($P3_221$, No. 154, $Z = 3$, $a = b = 4.8949$ and $c = 5.4361$ Å). Fig. 1 shows the observed, calculated and the difference profile for the final cycle of the structure refinement.

The results of the structure refinement were confirmed by FT-IR characterization (Fig. 2). The hemi-hydrate gypsum $CaSO_4.½\ H_2O$ and anhydrous $CaSO_4$ are identified by absorption bands characteristic to sulfate $SO_4^{2-}$ group such as the doublet bands at 592 and 656 $cm^{-1}$ associating to the asymmetrical $\nu_4$ vibrations, the band at 1005 corresponding to asymmetrical $\nu_1$ vibrations and the doublet at 1082 and 1112 $cm^{-1}$ corresponding to the asymmetrical $\nu_3$ vibrations. The presence of water in hemi-hydrate gypsum were also confirmed by its absorption band appear at 1619 $cm^{-1}$ corresponding to its $\nu_2$ vibrations and doublet bands at 3550 and 3610 $cm^{-1}$ corresponding to its $\nu_1$ vibrations. The presence of hemi-hydrate calcium sulfate ($CaSO_4.½\ H_2O$) as main phase in the raw PG sample is in a good agreement with previous studies [31].

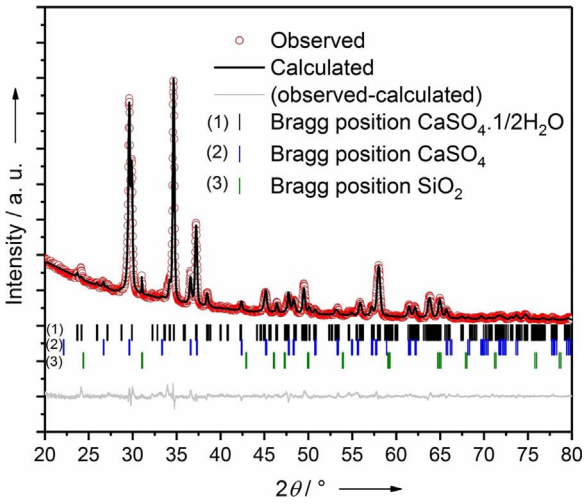


**Fig. 1.** Structure refinement from XRD data of phosphogypsum waste sample showing observed (red dots), calculated (black solid line) intensities and differences (grey solid line). Tick marks refer to the reflections of $CaSO_4.1/2H_2O$ (1), anhydrous $CaSO_4$ (2) and quartz $SiO_2$ (3).

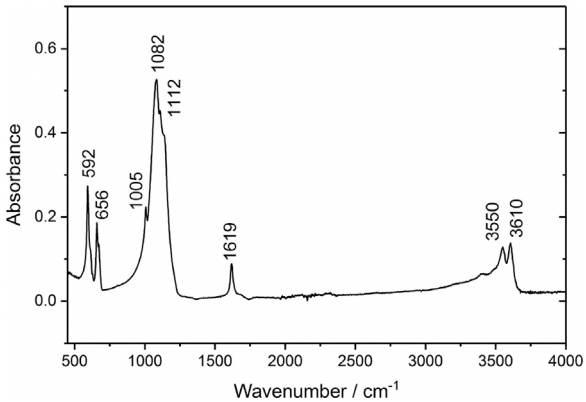


**Fig. 2.** ATR-FTIR spectrum of phosphogypsum waste.

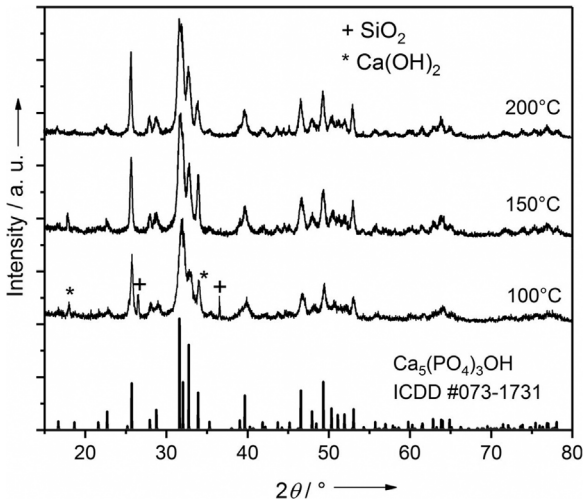


**Fig. 3.** XRD patterns of the materials synthesized at pH 11 at 100, 150 and 200 °C for 15 h.

### 3.2. Hydrothermal synthesis of hydroxyapatite

In the next step we studied the influence of temperature on the synthesis of phase pure HAp. Fig. 3 displays the XRD patterns of the materials synthesized at pH 11 at 100, 150 and 200 °C for 15 h. The XRD results reveal that nanocrystalline HAp is obtained already at 100 °C, however, with side phases ($Ca(OH)_2$ and quartz $SiO_2$), the latter was already present in the starting PG material (Fig. 1). With increasing the temperature to 150 °C, $SiO_2$ phase was disappeared and only $Ca(OH)_2$ was observed in addition to the HAp phase. The disappearance of $SiO_2$ can be explained by its high solubility in NaOH solution under hydrothermal conditions at temperatures above 150 °C, which it is good agreement with previous studies [32]. At 200 °C, phase pure nanocrystalline HAp was obtained, all impurity phases from the starting PG material were effectively removed being dissolved under the synthesis conditions.

The influence of synthesis time and pH were also studied. Fig. 4a shows the XRD patterns of the specimens synthesized at 200 °C and pH 11 for different synthesis times. Fig. 4b shows the XRD patterns of the specimens synthesized at 200 °C for 15 h at different pH. All the reflections in Fig. 4a can be assigned to either HAp or $Ca(OH)_2$ phase. The reflections corresponding to $Ca(OH)_2$ phase were found to decrease with increasing synthesis time, thus after 15 h only HAp phase was observed. On the other hand, $CaSO_4$ phase was detected in addition to HAp when the pH decreased from 11 to 5 when the synthesis was performed at 200 °C for 15 h (Fig. 4b). These results suggest that the hydrothermal conversation of PG into HAp at 200 °C and pH 11 for 15 h takes place in two steps; (i) the complete hydrolysis of $CaSO_4$ into $Ca(OH)_2$ phase and then (ii) the reaction of formed $Ca(OH)_2$ with free $PO_4^{3-}$ anions in the solution. Therefore, at low pH ($\leq 9$) $CaSO_4$ phase was observed in XRD patterns because there are no sufficient free hydroxide ions in the solution to hydrolyze all $CaSO_4$ in PG. As the concentration of hydroxide ions increases in the solution at pH 11, all $CaSO_4$ in PG transformed to $Ca(OH)_2$ phase (Fig. 4a). However, the second step, which involves conversion of formed $Ca(OH)_2$ phase into HAp, is time dependent and 15 h is required for complete reaction.

To confirm the crystal structure of HAp and to determine the unit cell parameters, Rietveld refinements of the XRD data were performed. Fig. 5 shows the observed, calculated and the difference profile for the final cycle of the structure refinement of HAp sample synthesized at 200 °C and pH 11 for 15 h. The using of sphere model with isotropic peak broadening for all XRD reflections in the first refinement attempts resulted in bad fitting (convergence factors $R_{wp}$ = 16.5%) as shown in Fig. 5a. Close inspection of the fitted XRD pattern revealed that the width of all 00 *l* reflections being significantly narrower, which suggests preferential crystalline growth along the *c* direction. This result is consistent with the rod-like crystals as seen in Fig. 8 and Fig. 9. The using of needle-like coherent domains for Rietveld refinement gave better fittings (convergence factors $R_{wp}$ = 14.12%). The determined structural parameters (space group $P6_3/m$, No. 176, Z = 2, $a = b$ = 9.4073(6) and $c$ = 6.8895(5)) from the structure refinements in this work were found in good agreement with previously reported values [27], which confirms the formation of stoichiometric hydroxyapatite under the present experimental conditions.

### 3.3. HAp nanorods synthesized with Brij-93 surfactant

In the next step, we investigated the influence of Brij-93 surfactant on the crystallization and morphology of the HAp crystals. Fig. 6 displays the XRD patterns of hydrothermally synthesized samples without and with different concentration of Brij-93 surfactant (0.003, 0.006, and 0.01 mol) at pH 11 and 200 °C for 15 h. Although all the reflections in the XRD patterns of the four samples could be indexed to the hexagonal structure of HAp, the intensities and width of 00 *l* reflections are varied for the four samples. This result indicates that the crystallites size along the *c* direction in the three samples are different. This is also consistent with previous studies about hydrothermally synthesized hexagonal HAp rods, which were grown along the *c* axis [22]. These 00 *l* reflections were found more intense and narrow for the samples synthesized with Brij-93 surfactant which indicates the increase in the crystallite size of HAp. The influence of Brij-93 surfactant on the crystal size of HAp nanorods were further confirmed by TEM characterizations (Fig. 9) and discussed in details below.

To confirm the removal the surfactant residues after hydrothermal synthesis, all samples were characterized by FTIR spectroscopy (Fig. 7). As can be seen from Fig. 7b–e, the absorption bands appearing at 560 and 602 $cm^{-1}$ corresponds to $\nu_4$ mode of phosphate group ($PO_4^{3-}$), while the band at 960 $cm^{-1}$ is due to its $\nu_1$ mode. The two strong bands at 1022 and 1095 $cm^{-1}$ are also assigned to $\nu_3$ mode of phosphate group. The weak absorption bands at 723, 865 and doublet at 1410 and 1456 $cm^{-1}$ correspond to $\nu_4$, $\nu_2$ and $\nu_3$ modes of $CO_3^{2-}$, respectively [33]. The observation of these characteristic bands indicates the partial substitution of $PO_4^{3-}$ group in HAp lattice by $CO_3^{2-}$ group, which is due to the entrapment of atmospheric carbon dioxide during preparation [34,35]. The presence of carbonates in the prepared HAp may indicate their high biocompatibility as HAp present in human bone has 4–6 wt% carbonates [36]. The broad band at 3100–3500 could be assigned to adsorbed water, while the weak band at 3540 corresponds to the stretching vibration of $OH^-$ group in the HAp lattice. For Brij-93 (Fig. 7a), characteristic absorption bands at 2900 and 1100 $cm^{-1}$ are attributed to C—H and C—O stretching vibrations. These absorption bands were not observed in the spectra of HAp (Fig. 7b–e), which indicates that Brij-93 is discarded during the washing process with hot water and ethanol.

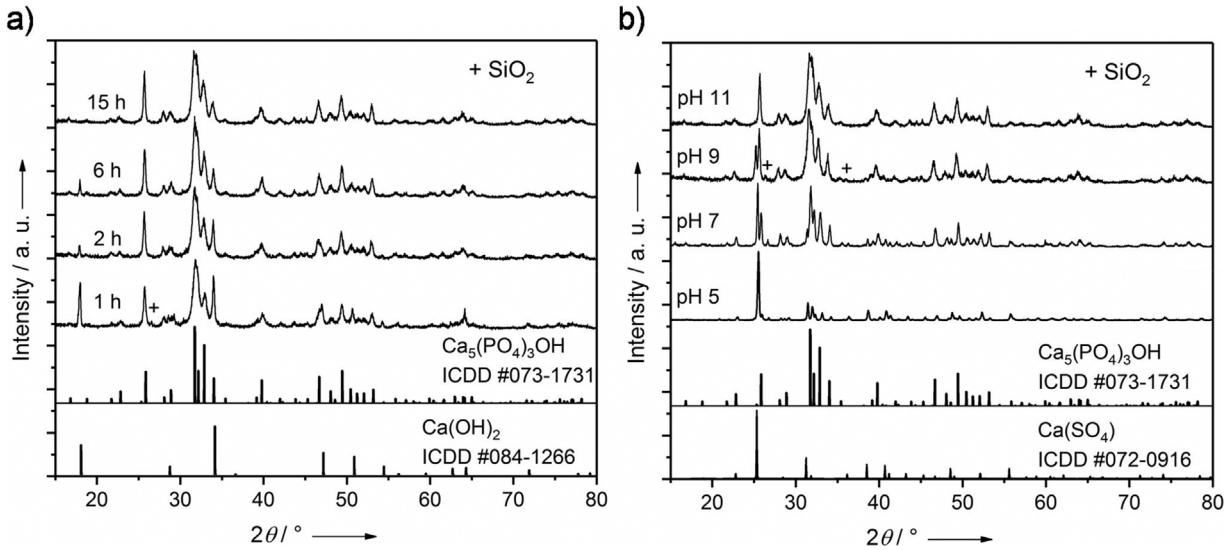


**Fig. 4.** XRD patterns of the materials synthesized at 200 °C: (a) at constant pH 11 and for times between 1 and 15 h; (b) at constant time (15 h) and pH between 5 and 11.

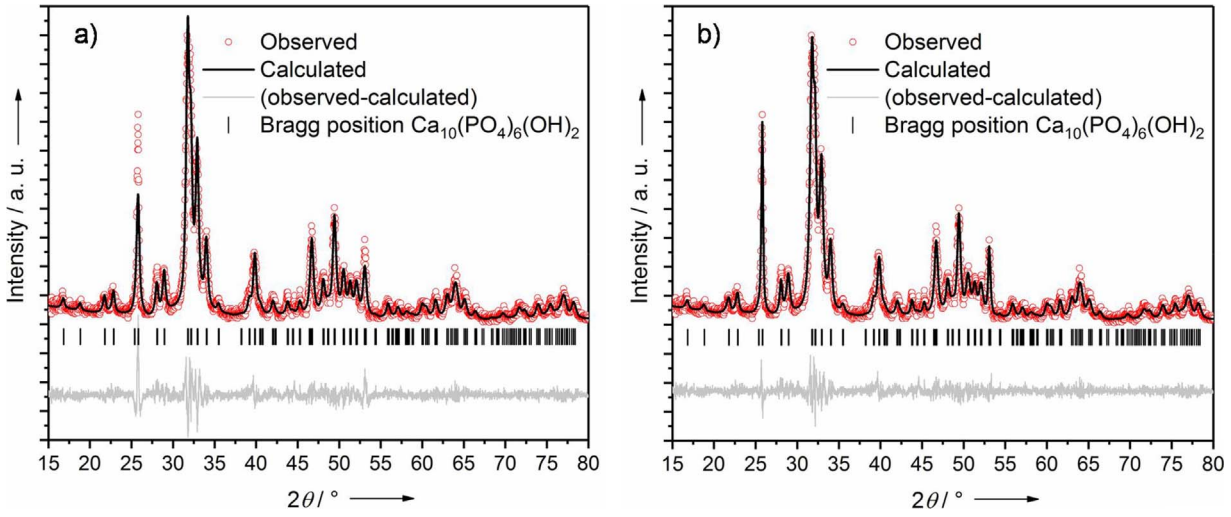


**Fig. 5.** Structure refinement from XRD data of HAp sample, hydrothermally synthesized at 200 °C, pH 11 for 15 h, using a single-phase model (a) with isotropic peak widths for all reflections and (b) with anisotropic peak broadening for all 00 *l* reflections. Observed (red dots), calculated (black solid line) intensities and differences (grey solid line) are shown. Tick marks refer to the reflections of HAp.

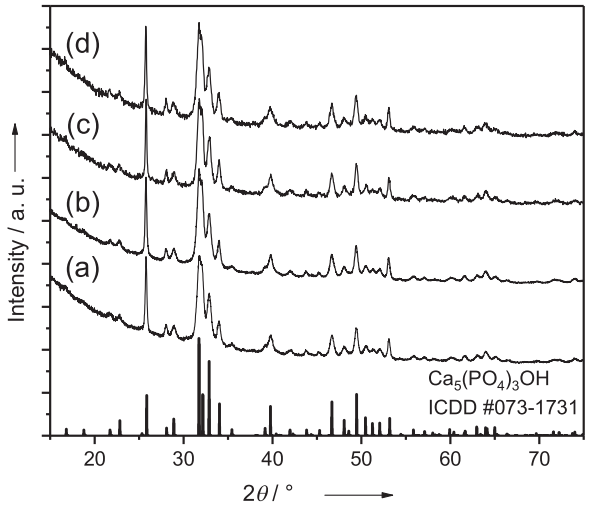


**Fig. 6.** XRD patterns of materials synthesized at pH 11 and 200 °C for 15 h without (a) and with 0.003 (b), 0.006 (c) and 0.01 (d) mol of Brij-93 surfactant.

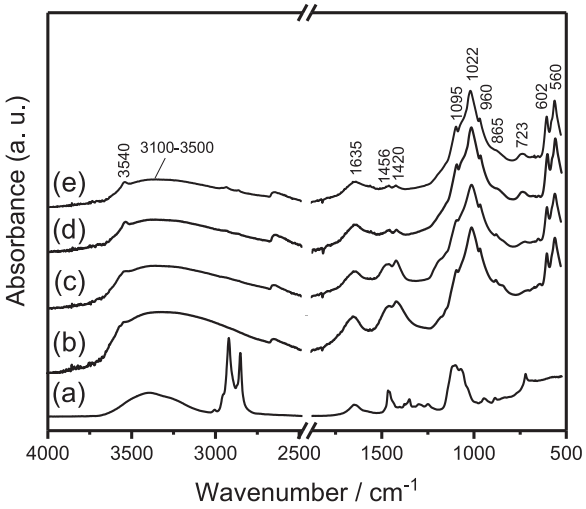


**Fig. 7.** FTIR spectra of Brij-93 surfactant (a) and the materials synthesized at pH 11 and 200 °C for 15 h without (b) and with 0.003 (c), 0.006 (d) and 0.01 (e) mol of Brij-93 surfactant.

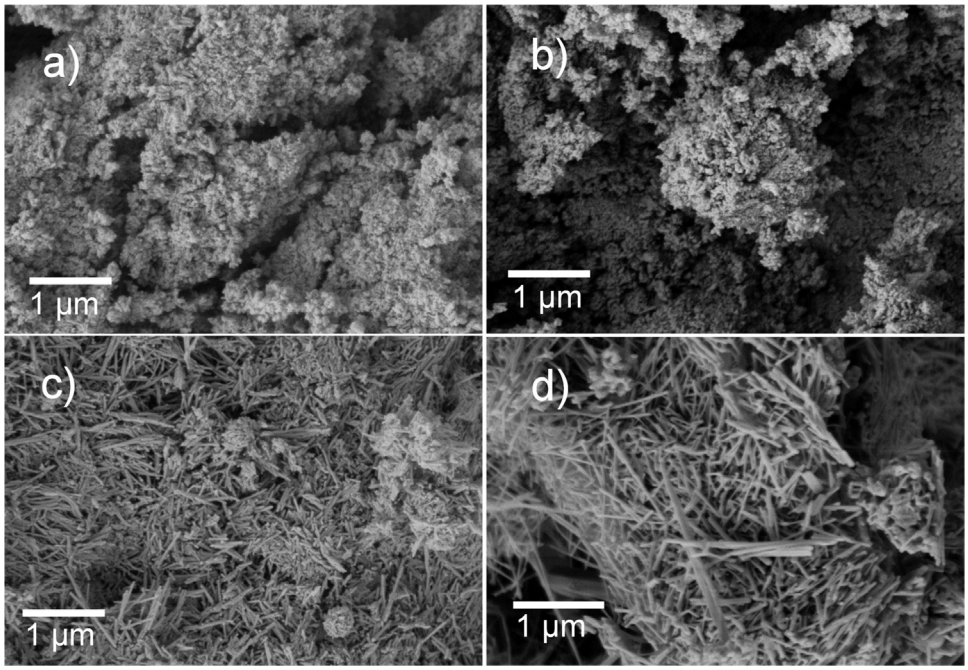


**Fig. 8.** SEM micrographs of HAp materials synthesized at 200 °C and pH 11 for 15 h without (a) and with 0.003 (b), 0.006 (c) and 0.01 (d) mol of Brij-93 surfactant.

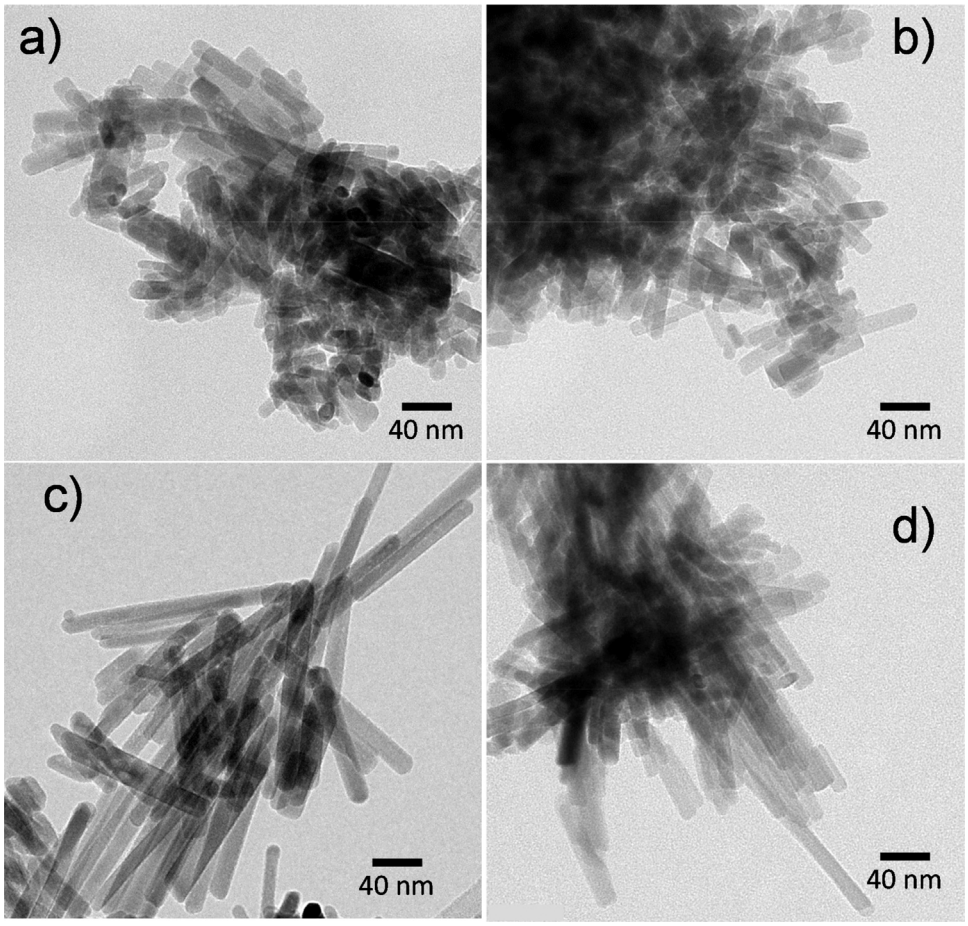


**Fig. 9.** TEM micrographs of HAp materials synthesized at 200 °C and pH 11 for 15 h without (a) and with 0.003 (b), 0.006 (c) and 0.01 (d) mol of Brij-93 surfactant.

The influence of Brij-93 surfactant on the morphology of synthesized HAp particles was further investigated by SEM (Fig. 8a–d) and TEM (Fig. 9a–d) inspection. As shown in Fig. 8a–d and Fig. 9a–d, all HAp materials consist of uniform rod-like particles with different aspect ratio (i.e. particle length/particle diameter). The HAp nanorods synthesized without Brij-93 surfactant (Fig. 8a and Fig. 9a) are smaller and highly agglomerated in comparison with those synthesized with the surfactant (Fig. 8b–d); they have small aspect ratio of 3.5, where the crystal diameter and length are 18 and 63 nm, respectively. The Brij surfactant leads to an increase in the aspect ratio of HAp nanocrystals

(Fig. 9b–d), finally resulting in nanorods with aspect ratio about 10–13 and the mean size around 200–205 × 16–20 nm (Fig. 9c–d). Similar effect was observed previously in the synthesis of Co−B−N−H nanowires with Brij surfactant and was attributed to in which the Brij was chemically capped at the surface of the growth particles acting as an assembly director leading to the preferential growth in one direction preventing simultaneously the agglomeration of nanorods [37].

## 4. Conclusion

Nanocrystalline hydroxyapatite (HAp) was successfully synthesized from industrial waste phosphogypsium (PG) and potassium dihydrogen phosphate $KH_2PO_4$ by hydrothermal method. The purity and morphology of prepared HAp strongly depends on the conditions of hydrothermal synthesis. XRD data reveal that phase-pure HAp is hydrothermally obtainable in strong alkaline medium (i.e. pH = 11) at 200 °C after sufficient long time (15 h). SEM and TEM characterizations showed that the prepared HAp consists of uniform rod-like nanoparticles with different aspect ratios depending on the concentration of the Brij-93 surfactant used in the synthesis. The Brij-93 surfactant capped at the surface of the HAp crystals leads to the preferential growth in one direction preventing simultaneously the agglomeration of nanorods.

## Acknowledgment

The financial support by the Otto Bayer Fellowship, application number: F-2017-BS-0121 is greatly acknowledged. This publication reflects the views only of the author, and the Commission cannot be held responsible for any use, which may be made of the information contained therein. We thank Dr. Franziska Schmidt for SEM and Sören Selve for TEM characterization.

## References

[1] T.Z. Guo, R.F. Malone, K.A. Rusch, Stabilized phosphogypsum: class C fly ash: Portland type II cement composites for potential marine application, Environ. Sci. Technol. 35 (2001) 3967–3973.
[2] H. Tayibi, M. Choura, F.A. Lopez, F.J. Alguacil, A. Lopez-Delgado, Environmental impact and management of phosphogypsum, J. Environ. Manage. 90 (2009) 2377–2386.
[3] J.K. Yang, W.C. Liu, L.L. Zhang, B. Xiao, Preparation of load-bearing building materials from autoclaved phosphogypsum, Constr. Build. Mater. 23 (2009) 687–693.
[4] N. Degirmenci, Utilization of phosphogypsum as raw and calcined material in manufacturing of building products, Constr. Build. Mater. 22 (2008) 1857–1862.
[5] C. Papastefanou, S. Stoulos, A. Ioannidou, A. Manolopoulou, The application of phosphogypsum in agriculture and the radiological impact, J. Environ. Radioact. 89 (2006) 188–198.
[6] N. Degirmenci, A. Okucu, A. Turabi, Application of phosphogypsum in soil stabilization, Build. Environ. 42 (2007) 3393–3398.
[7] M. Jarcho, C.H. Bolen, M.B. Thomas, J. Bobick, J.F. Kay, R.H. Doremus, Hydroxylapatite synthesis and characterization in dense polycrystalline form, J. Mater. Sci. 11 (1976) 2027–2035.
[8] H. Zhou, J. Lee, Nanoscale hydroxyapatite particles for bone tissue engineering, Acta Biomater. 7 (2011) 2769–2781.
[9] J.W. Jaworski, S. Cho, Y. Kim, J.H. Jung, H.S. Jeon, B.K. Min, K.Y. Kwon, Hydroxyapatite supported cobalt catalysts for hydrogen generation, J. Colloid Interf. Sci. 394 (2013) 401–408.
[10] N. Razavi, B. Akhlaghinia, Hydroxyapatite nanoparticles (HAP NPs): a green and efficient heterogeneous catalyst for three-component one-pot synthesis of 2,3-dihydroquinazolin-4(1H)-one derivatives in aqueous media, New J. Chem. 40 (2016) 447–457.
[11] J. Xu, T. White, P. Li, C.H. He, Y.F. Han, Hydroxyapatite foam as a catalyst for formaldehyde combustion at room temperature, J. Am. Chem. Soc. 132 (2010) 13172–13173.
[12] M. Zahouily, Y. Abrouki, B. Bahlaouan, A. Rayadh, S. Sebti, Hydroxyapatite: new efficient catalyst for the Michael addition, Catal. Commun. 4 (2003) 521–524.
[13] K. Mori, T. Hara, T. Mizugaki, K. Ebitani, K. Kaneda, Hydroxyapatite-supported palladium nanoclusters: a highly active heterogeneous catalyst for selective oxidation of alcohols by use of molecular oxygen, J. Am. Chem. Soc. 126 (2004) 10657–10666.
[14] A. Venugopal, M.S. Scurrell, Hydroxyapatite as a novel support for gold and ruthenium catalysts–behaviour in the water gas shift reaction, Appl. Catal. A-Gen. 245 (2003) 137–147.
[15] Y.Y. Li, X.H. Lv, D. Wu, H.M. Ma, R. Feng, Y.L. Wang, B. Du, Q. Wei, Screen printed biosensor for hydrogen peroxide based on prussian blue modified hydroxyapatite, J. Inorg. Organomet. Polym. 23 (2013) 917–922.
[16] L.M. Lu, L. Zhang, X.B. Zhang, S.Y. Huan, G.L. Shen, R.Q. Yu, A novel tyrosinase biosensor based on hydroxyapatite-chitosan nanocomposite for the detection of phenolic compounds, Anal. Chim. Acta 665 (2010) 146–151.
[17] S.P. Wang, Y. Lei, Y. Zhang, J. Tang, G.L. Shen, R.Q. Yu, Hydroxyapatite nanoarray-based cyanide biosensor, Anal. Biochem. 398 (2010) 191–197.
[18] V.E. Badillo-Almaraz, J.A. Flores, H. Arriola, F.A. Lopez, L. Ruiz-Ramirez, Elimination of fluoride ions in water for human consumption using hydroxyapatite as an adsorbent, J. Radioanal. Nucl. Chem. 271 (2007) 741–744.
[19] Y.A. Feng, J.L. Gong, G.M. Zeng, Q.Y. Niu, H.Y. Zhang, C.G. Niu, J.H. Deng, M. Yan, Adsorption of Cd (II) and Zn (II) from aqueous solutions using magnetic hydroxyapatite nanoparticles as adsorbents, Chem. Eng. J. 162 (2010) 487–494.
[20] C. Srilakshmi, R. Saraf, Ag-doped hydroxyapatite as efficient adsorbent for removal of Congo red dye from aqueous solution: synthesis, kinetic and equilibrium adsorption isotherm analysis, Micropor. Mesopor. Mater. 219 (2016) 134–144.
[21] E. Hasret, M. Ipekoglu, S. Altintas, N.A. Ipekoglu, Microwave-assisted synthesis of hydroxyapatite for the removal of lead(II) from aqueous solutions, Environ. Sci. Pollut. Res. 19 (2012) 2766–2775.
[22] Y.J. Wang, S.H. Zhang, K. Wei, N.R. Zhao, J.D. Chen, X.D. Wang, Hydrothermal synthesis of hydroxyapatite nanopowders using cationic surfactant as a template, Mater. Lett. 60 (2006) 1484–1487.
[23] B. Kerebel, G. Daculsi, L.M. Kerebel, Ultrastructural studies of enamel crystallites, J. Dent. Res. 58 (1979) 844–851.
[24] L.J. Wang, X.Y. Guan, H.Y. Yin, J. Moradian-Oldak, G.H. Nancollas, Mimicking the self-organized microstructure of tooth enamel, J. Phys. Chem. C 112 (2008) 5892–5899.
[25] I.H. Arita, V.M. Castano, D.S. Wilkinson, Synthesis and processing of hydroxyapatite ceramic tapes with controlled porosity, J. Mater. Sci. Mater. Med. 6 (1995) 19–23.
[26] U. Vijayalakshmi, S. Rajeswari, Influence of process parameters on the sol-gel synthesis of nano hydroxyapatite using various phosphorus precursors, J. Sol-Gel Sci. Technol. 63 (2012) 45–55.
[27] Y. Fujishiro, H. Yabuki, K. Kawamura, T. Sato, A. Okuwaki, Preparation of needle-like hydroxyapatite by homogeneous precipitation under hydrothermal conditions, J. Chem. Technol. Biotechnol. 57 (1993) 349–353.
[28] M.S. Bakshi, How surfactants control crystal growth of nanomaterials, Cryst. Growth Des. 16 (2016) 1104–1133.
[29] J. Rodriguez-Carvajal, Fullprof: a program for Rietveld refinement and pattern matching analysis, Collected Abstract of Powder Diffraction Meeting, Toulouse, France, 1990.
[30] L.W. Finger, D.E. Cox, A.P. Jephcoat, A correction for powder diffraction peak asymmetry due to axial divergence, J. Appl. Crystallogr. 27 (1994) 892–900.
[31] N. Barka, A. Assabbane, A. Nounah, L. Laanab, Y.A. Ichou, Removal of textile dyes from aqueous solutions by natural phosphate as a new adsorbent, Desalination 235 (2009) 264–275.
[32] D.A. Crerar, G.M. Anderson, Solubility and solvation reactions of quartz in dilute hydrothermal solutions, Chem. Geol. 8 (1971) 107–122.
[33] S. Gunasekaran, G. Anbalagan, S. Pandi, Raman and infrares spectra of carbonates of calcite structure, J. Raman Spectrosc. 37 (2006) 892–899.
[34] T.A. Kuriakose, S.N. Kalkura, M. Palanichamy, D. Arivuoli, K. Dierks, G. Bocelli, C. Betzel, Synthesis of stoichiometric nano crystalline hydroxyapatite by ethanol-based sol-gel technique at low temperature, J. Cryst. Growth 263 (2004) 517–523.
[35] Z.H. Cheng, A. Yasukawa, K. Kandori, T. Ishikawa, FTIR study of adsorption of CO2 on nonstoichiometric calcium hydroxyapatite, Langmuir 14 (1998) 6681–6686.
[36] D.K. Lee, J.Y. Park, M.R. Kim, D.J. Jang, Facile hydrothermal fabrication of hollow hexagonal hydroxyapatite prisms, CrystEngComm 13 (2011) 5455–5459.
[37] F. Yang, Y.Z. Li, W. Chu, C. Li, D.G. Tong, Mesoporous Co-B-N-H nanowires: superior catalysts for decomposition of hydrous hydrazine to generate hydrogen, Catal. Sci. Technol. 4 (2014) 3168–3179.

## 4.2. Removal of cationic and anionic textile dyes with Moroccan natural phosphate

| | |
|---|---|
| Title | Removal of cationic and anionic textile dyes with Moroccan natural phosphate |
| Authors | H. Bensalah, M.F. Bekheet, S. Alami Younssi, M. Ouammou and A. Gurlo |
| Journal | Journal of Environmental Chemical Engineering |
| Publisher | Elsevier |
| Publication date | 11 April 2017 |
| Reference | Journal of Environmental Chemical Engineering 5 (2017) 2189–2199 |
| DOI | 10.1016/j.jece.2017.04.021 |
| My contribution | Design of experiments, processing of materials, collecting and interpreting UV-VIS data, simulation of adsorption isotherms and kinetics, results analysis and discussion, writing of the manuscript. |

Journal of Environmental Chemical Engineering 5 (2017) 2189–2199

Contents lists available at ScienceDirect

Journal of Environmental Chemical Engineering

journal homepage: www.elsevier.com/locate/jece

# Removal of cationic and anionic textile dyes with Moroccan natural phosphate

Hiba Bensalah[a,b,*], Maged F. Bekheet[b], Saad Alami Younssi[a], Mohamed Ouammou[a], Aleksander Gurlo[b]

[a] Laboratory of Membranes, Materials and Environment, Department of Chemistry, Faculty of Sciences & Technics of Mohammedia BP 146, 20650, University Hassan II of Casablanca, Morocco

[b] Fachgebiet Keramische Werkstoffe/Chair of Advanced Ceramic Materials, Institut für Werkstoffwissenschaften und—Technologien, Technische Universität Berlin, Hardenbergstraße 40, 10623 Berlin, Germany

ARTICLE INFO

*Keywords:*
Natural phosphate
Adsorption
Desorption
Congo Red
Rhodamine 6G
Isotherm
Kinetics

ABSTRACT

Moroccan natural phosphate was tested as an effective adsorbent for the removal of cationic dye rhodamine 6G (Rh6G) as well as anionic dye congo red (CR) from wastewater. The X-ray diffraction, FTIR and EDX characterizations reveal that the sample contains 98 wt% fluoroapatite ($Ca_5(PO_4)_3F$) with 1 wt% quartz ($SiO_2$) and 1 wt% calcium carbonate ($CaCO_3$). Nitrogen sorption analysis shows that the BET specific surface area ($S_{BET}$) and BJH pore volumes of the sample are 18.8 $m^2/g$ and 0.1 $cm^3/g$, respectively. Batch adsorption experiments of the dyes from aqueous solution were conducted, taking into account the influence of initial dye concentration (100–400 mg/L), adsorbent dosage (1–20 g/L), contact time (5–300 min) and solution pH (3–12). The Langmuir isotherm model best represents the equilibrium adsorption process of the two dyes. The calculated maximum adsorbed quantity $q_{max}$ of CR and Rh6G at dosage 20 g/L and pH value of 5.2 were found 19.81 and 6.84 mg/g, respectively. The adsorption of Rh6G and CR on natural phosphate was found to follow the pseudo-second-order model. Natural phosphate was also tested as an effective adsorbent for a simulated dye effluent under industrial conditions of temperature and pH. Desorption studies were conducted using HCl as an eluent and the highest elution efficiency for both dyes was obtained with a 0.1 M solution. Accordingly, it is demonstrated in this work that natural phosphate is a very efficient adsorbent for both cationic and anionic dyes from contaminated water, and represents a great low-cost alternative to commercial adsorbents due to its abundance as a natural resource in Morocco.

## 1. Introduction

In daily life, we are surrounded by color in all forms; colorful clothes, cars, food even our medicines are often colored. This is the main reason behind the success of the dyestuffs industry [1,2]. However, it does not remain without a hazardous effects on the health of human and other living species, since several billion tons of industrial wastewater effluents are annually discharged into rivers and seas [3]. These organic dyes are highly toxic, mutagenic and carcinogenic [4,5]. In addition, it has been proved that textile effluents decrease the penetration of light in water resources such as river and lakes, and therefore photosynthetic activity, causing oxygen shortage that is a serious hazard to aquatic living organisms [6]. However, the wastewater of textile industries is very difficult to treat, since the containing dyes are extremely soluble in water and very stable to light, heat and oxidizing agents, which makes the separation of dyes from aqueous solutions very difficult [7,8]. Fortunately, several methods have proved to be reliable in removing dyes from colored effluents, such as membrane filtration, coagulation–flocculation, biological treatment, electrochemical process, photo-degradation and adsorption [9–15]. Among these methods, the adsorption process by solid adsorbents receives more attention because of its simplicity, low cost and adsorbents efficiency. According to the US Environmental Protection Agency, activated carbon is one of the best commercial adsorbents for the removal of organic dyes from industrial wastewater [16]. However, it is still an expensive sorbent, which limits its widespread use. Hence, the development of new low-cost and effective adsorbents, such as natural materials, biomass from agriculture and waste materials from

*Abbreviations:* Rh6G, Rhodamine 6G; CR, Congo Red

* Corresponding author at: Laboratory of Membranes, Materials and Environment, Department of Chemistry, Faculty of Sciences & Technics of Mohammedia BP 146, 20650, University Hassan II of Casablanca, Morocco.

*E-mail address:* hiba.bens@hotmail.fr (H. Bensalah).

http://dx.doi.org/10.1016/j.jece.2017.04.021
Received 1 December 2016; Received in revised form 8 April 2017; Accepted 11 April 2017
Available online 19 April 2017

industry, has been investigated. Numerous non-conventional low-cost adsorbents such as clay [17], pine sawdust [18], cotton waste [19] or biomass [20] have shown excellent adsorption abilities. For instance, chitosan-based sorbent showed exceptional removal capacity of reactive blue 2 and direct red 81 dyes in comparison to activated carbon [21]. Therefore, low-cost sorbents offer a promising alternative to commercial sorbents and efforts are being made in order to improve their performance in real industrial conditions.

In this study, Moroccan natural phosphate was selected as the low-cost adsorbent due to its abundance. In fact, Morocco is the largest phosphate producer in the world; it contains about 75% of the world's estimated reserves. Fluoroapatite $Ca_{10}(PO_4)_6F_2$ is the major phase that constitutes the Moroccan natural phosphate. This material, that has a sedimentary origin, has been used in water treatment and has shown great effectiveness as a catalyst as well as ceramic support of a microfiltration membrane [22,23]. Only two studies were found using natural phosphate as an adsorbent for cationic and anionic dyes [22,23]. However, the natural phosphate showed good adsorption capacities of only cationic dyes such as methylene blue (MB), crystal violet (CV) and basic yellow 28 (BY 28), whereas in the case of anionic dyes such as reactive yellow 125 (RY 125) and methyl orange (MO), it showed a low adsorption affinity. Furthermore, some factors that could affect the adsorption capability, such as the surface charges of the phosphate adsorbents at different pH values and the amount of impurity phases, have not been sufficiently investigated thus far.

Accordingly, the main goal of the present work was to investigate the ability of natural phosphate to adsorb organic cationic and anionic dyes as well as a simulated dye effluent. In fact, to simulate the wastewater produced by real textile industries, a synthetic dye effluent was prepared. The cationic dye used in this study is rhodamine 6G, an azo dye with an amino group and a molecular weight of 479.02 g/mol. The anionic dye is congo red, a diazo sulfonated dye with molecular weight of 696.665 g/mol. The simulated dye effluent was prepared from a congo red solution and NaCl. The adsorption capacity and operation parameters including adsorbent dosage, solution pH, adsorption time and initial dye concentration were studied. The results were analyzed regarding four adsorption isotherms and kinetic models to understand the mechanism of adsorption on the dye molecules onto the natural phosphate. In order to have a better understanding of the adsorption mechanisms and to make this method more environmentally friendly, desorption studies were also carried out by testing different eluents.

## 2. Experimental

### 2.1. Materials

Analytical grade congo red CR (dye content ≥35%), ammonium hydroxide solution (30–32%), hydrochloric acid solution (37%), sulfuric acid (95–99%), ethanol (96%) and sodium hydroxide pellets were purchased from Sigma-Aldrich (Germany). Rhodamine 6G (Rh6G) was purchased from Merck. The adsorbent used in this study was a natural phosphate rock from Khouribga, Morocco. It was washed several times with distilled water, dried in an oven overnight at 100 °C, ball-milled and sieved to particles size d < 63 μm. The solution of simulated dye effluent was prepared by dissolving a known amount of salt, NaCl (Chem-Lab, Belgium), in a congo red solution.

### 2.2. Characterization methods

The natural phosphate sample was characterized using a Bruker AXS D8 ADVANCE X-ray diffractometer (Bruker, Germany) with a Bragg–Brentano geometry equipped with a Lynx Eye 1D detector (CoKα1 radiation wavelength 0.178901 nm and CoKα2 radiation wavelength 0.17929 nm). Measurements were carried out between 15 and 80° 2θ value, with a step time of 3 s/0.02° at 35 kV and 40 mA. Rietveld refinement was performed using the FULLPROF program [24] and profile function 7 (Thompson-Cox-Hastings pseudo-Voigt convoluted with axial divergence asymmetry function) [25]. The resolution function of the instrument was obtained from the structure refinement of LaB6 standard. The morphology of the natural phosphate was studied via scanning electron microscopy (SEM) on a Zeiss Gemini Leo 1530 (Zeiss, Germany) equipped with energy dispersive X-ray spectroscopy (EDAX). Samples were placed on conducting carbon pads and then sputtered with a thin layer of gold to prevent sample charging. The particle size distribution was measured using Helos H1505 particle size analyzer with wet dispersion unit SUCELL2 (Sympatec, Germany). The powder samples were dispersed using either mechanical stirrer or mechanical stirrer coupled with ultrasonication. The functional groups of the natural phosphate were analysed by attenuated total reflection (ATR) method using Fourier transform infrared spectrometer (FT-IR) on Bruker EQUINOX 55 (Bruker, Germany). The pore size and specific surface area were studied with nitrogen sorption analysis. Gas adsorption isotherms were recorded at 77 K on a QuadraSorb Station 4 apparatus (Quantachrome, USA) after degassing for 10 h at 200 °C under vacuum. Surface area was determined using the Brunauer, Emmet and Teller (BET) method. All nitrogen sorption data were analyzed using the Quantachrome/QuadraWin software. Zeta potential of natural phosphate in 0.1 N HCl solution as a function of pH was determined using StabiSizer PMX 200 CS equipment (Particle Metrix, Germany).

### 2.3. Adsorption experiments

#### 2.3.1. Batch equilibrium studies

Aqueous stock solutions of Rh6G and CR were prepared by dissolving a known amount of the dyes in distilled water to the concentration of 1000 mg/L. The experimental solutions were diluted to different concentrations in 1L flasks. The adsorption tests were performed in 100 flasks in which 20 mL of dye solutions with different concentrations (100–400 mg/L) were placed. The adsorbent dosages were varied from 1 g/L to 30 g/L and pH values of the solutions were gradually adjusted between 3 and 12 by using HCl (1 M) and $NH_4OH$ (1 M) solutions. The agitation speed of 400 rpm at room temperature was maintained for all experiments. Once the adsorption equilibrium is reached, the adsorbent was separated from the solutions by centrifugation at 5000 rpm for 10 min. The initial and final concentrations of Rh6G and CR were determined from their UV–vis absorbance according to the calibration method. UV/VIS/NIR spectrometer (Perkin Elmer Lambda 9) was used at λ = 526 and 497 μm for Rh6G and CR, respectively. The removal efficiency of each dye $R_e$ (%) and the equilibrium adsorption capacity $q_e$ (mg/g) were calculated as follows:

$$R_e = \frac{(C_i - C_e)}{C_i} \times 100\% \quad (1)$$

$$q_e = \frac{(C_i - C_e)V}{m} \quad (2)$$

where $C_i$ and $C_e$ are the initial and equilibrium concentration (mg/L), respectively, of the dyes solution, $m$ is the weight of adsorbent (g) and V is the volume of dyes solutions (L).

#### 2.3.2. Adsorption isotherms experimental

Different models, namely, Langmuir, Freundlich, Dubinin–Radushkevich (D–R) and Tempkin isotherm, were used to study the adsorption isotherms of the organic dyes onto the natural phosphate. The linear form of Langmuir isotherm model [26] is given by Eq. (A.$_3$). The separation factor $R_L$, which represents the type of Langmuir isotherm, is calculated by Eq. (A.$_4$). The logarithmic form of Freundlich model [27] is represented by Eq. (A.$_5$). The Dubinin–Radushkevich D–R model [28] is given by Eqs. (A.$_6$) and (A.$_7$). The last model Tempkin [29] is described in Eq. (A.$_8$).

*2.3.3. Adsorption kinetics experimental*

The adsorption kinetics of natural phosphate with two different dyes were done by using similar procedure as for equilibrium experiments. The experiments were conducted by adding 200 mg of the natural phosphate powder into 20 mL of dye solution with initial concentration $C_i$ = 100 mg/L. The aqueous solutions were taken after different contact times and separated by centrifuging for UV–vis absorbance measurements. The adsorption quantity $q_t$ (mg/g) of the dye onto the phosphate at time $t$ was calculated according to Eq. (A.$_9$).

The pseudo-first-order [30], pseudo-second-order [31], intra-particle diffusion [32], and Elovich kinetic [33] models were used to analyze the kinetic data. These models are represented by Eqs. (A.$_{10}$)–(A.$_{13}$), respectively.

*2.3.4. Simulated dye effluent adsorption*

Simulated dye effluents were prepared in an aqueous solution of CR (100 mg/L) with different NaCl concentration (10–1000 mM). The adsorption experiments were carried out by stirring 400 mg of natural phosphate powder into 20 mL of simulated dye solution placed in 50 mL flasks for 120 min. The pH value and the temperature of the solution were kept constant at 5.6 and 80 °C, respectively.

*2.3.5. Desorption studies*

Batch mode was employed for CR and Rh6G desorption studies. A specific amount of natural phosphate was stirred in 250 mL of aqueous dye solutions (100 mg/L) at pH = 5.2 for 120 min. Once the equilibrium was reached, the loaded adsorbent was washed several times with distilled water to remove unadsorbed traces of dyes, then dried overnight in a drying cabinet at 70 °C. Desorption experiments were conducted for 120 min using 50 ml of 0.1 M each of HCl, NaOH, $H_2SO_4$ and Ethanol as eluents. The amount of dye desorbed was calculated from the initial concentrations of CR and Rh6G loaded on natural phosphate and final CR and Rh6G concentrations in the eluent.

## 3. Results and discussion

### 3.1. Adsorbent characterization

In the first step the crystal structure of crystalline phases in the phosphate sample was characterized by powder X-ray diffraction. The Rietveld refinement of the XRD data showed that the sample contains 98 wt% fluoroapatite ($Ca_5(PO_4)_3F$, $P6_3/m$, No. 176, $Z$ = 2, $a = b$ = 9.3394(3) and $c$ = 6.8991(2) Å) with 1 wt% of quartz ($SiO_2$, $P3_221$, No. 154, $Z$ = 3, $a = b$ = 4.8944(6) and $c$ = 5.4357(10) Å) and 1 wt% of calcium carbonate ($CaCO_3$, $R\text{-}3c$, No. 167, $Z$ = 6, $a = b$ = 4.9892(5) and $c$ = 17.0607(16) Å). Fig. 1a shows the observed, calculated and the difference profile for the final cycle of the structure refinement. The lattice parameter $c$ of $Ca_5(PO_4)_3F$ phase is in good agreement with the literature data ($a = b$ = 9.372 and $c$ = 6.888 Å) [34], while the slight decrease in lattice parameter $a$ indicates the substitution of $Ca^{2+}$ cations in $Ca_5(PO_4)_3F$ phase with smaller cations such as $Na^+$, $Mg^{2+}$ and $Al^{3+}$ or substitution of $PO_4^{3+}$ by $CO_3^{2-}$ anions [35]. The presence of $Na^+$, $Mg^{2+}$ and $Al^{3+}$ cations in the specimen was confirmed by EDS analysis (Fig. 2b). The existence of minor quartz $SiO_2$ phase in the natural Moroccan phosphate is consistent with previous studies [22,36].

Analysis of microstructural parameters by Rietveld refinement revealed that the fluoroapatite $Ca_5(PO_4)_3F$ phase has a crystallite size of 49 nm and microstrain of 1.6 × $10^{-3}$ induced during ball milling.

The results of the structure refinement were confirmed by FT-IR characterizations (Fig. 1b). The doublet absorption bands at 562 and 600 $cm^{-1}$ correspond to the asymmetrical $\nu_4$ vibrations of the phosphate $PO_4^{3-}$ group, while the bands at 967 and 1027 $cm^{-1}$ correspond to the asymmetrical $\nu_1$ and $\nu_3$ vibrations [37,38]. The doublet appears at 1423 and 1455 that corresponds to $\nu_3$ vibrations of the carbonate group ($CO_3^{2-}$), while the absorption band at 867 $cm^{-1}$ corresponds to the vibration of $HPO_4^{2-}$ [37,38]. The band at 3400 $cm^{-1}$ is attributable to the stretching vibration of the lattice $OH^-$ ions. All these bands confirm the presence of $Ca_5(PO_4)_3F$ and $CaCO_3$ phases in the natural phosphate sample and are in good agreement with previous studies [39].

The SEM micrograph (Fig. 2a) shows that the natural phosphate sample is composed of irregular porous particles, which have a strong tendency to aggregate. The particles aggregation was also analysed by measuring the particle size distribution with and without treating the suspension by ultrasonication as shown in Fig. 3a. The using of ultrasonic treatment in addition to the mechanical stirrer resulted in the separation of the aggregated particles. Therefore, the mean particle diameter shifts to smaller size than that dispersed only mechanically and without ultrasonic treatment, and the fine powder below 10 μm is observed as well.

Fig. 3b shows the $N_2$ adsorption isotherm of natural phosphate. The adsorption isotherm can be classified as a Type IV isotherm, commonly related to mesoporous materials, as established by the International Union of Pure and Applied Chemistry (IUPAC) [40]. The isotherm exhibits a type H3 hysteresis loop, which does not exhibit any limiting adsorption at high $p/p^\circ$. This type of hysteresis is commonly related to slit-shaped pores that result from the aggregation of plate-like particles [40]. The BET specific surface area ($S_{BET}$) and BJH pore volumes of the sample were found to be 18.8 $m^2/g$ and 0.1 $cm^3/g$, respectively.

### 3.2. Effect of pH on dye adsorption

It is known that the pH of the solutions can affect the surface charge of the adsorbent as well as the degree of ionization and the chemical structure of the organic dyes. Thus, the dye adsorption process would not be possible without taking into account the pH of the solution. Fig. 4a shows the effect of pH on adsorption of cationic dye Rh6G and anionic dye CR. It was observed that the adsorption capacities of the two dyes changed significantly over the pH range of 3–12. With increasing solution pH the adsorption capacities of cationic dyes increased, while the adsorption of the anionic dye decreased. These results can be interpreted by analysing the zeta potential of the natural phosphate (Fig. 4b). The phosphate species varied in the aqueous solutions with pH as following: the monovalent anion ($H_2PO_4^-$) predominate at 0.12 < pH < 5.21, while the divalent anion ($HPO_4^{2-}$) form at 5.21 < pH < 10.67 and the trivalent anion ($PO_4^{3-}$) appears at 10.67 < pH < 12 [41]. At the initial low pH (pH = 3–4), the zeta potential was positive, due to the protonation of these negatively surface functional groups, that the negatively charged sulfonic groups ($-SO_3^-$) of anionic dyes CR could be electrostatically attracted by the phosphate surface. As a matter of fact, electrostatic attraction constitutes the main force to adsorb phosphate at lower pH. Therefore, the cationic dye Rh6G showed low adsorption capacities at lower pH due to the repulsion between the positively charged groups ($=NCH_2CH_3)^+$ of the dyes and the phosphate surface. The point of zero charge $pH_{PZC}$ of phosphate is found to be 4.8 and above this pH value, the surface of the natural phosphate became negatively charged. Therefore, the adsorption of cationic dyes increased, while the adsorption of anionic dyes decreased at higher pH. However, the adsorption capacity of anionic dye CR on the phosphate surface is still higher than those of cationic dye Rh6G even at higher pH values and dosage which indicated that the electrostatic attraction is not only the mechanism for CR adsorption and other banding forces took over such as hydrogen bonds and van der Waals forces [42–44].

### 3.3. Effect of adsorbent dosage

For the condition of pH 5.2, an initial dye-solution concentration of 100 mg/L, and a contact time of 2 h, the effects of the amount of natural phosphate (1–30 g) on adsorption and removal of Rh6G and CR are shown in Fig. 5. It was noticed that a rapidly increase in removal

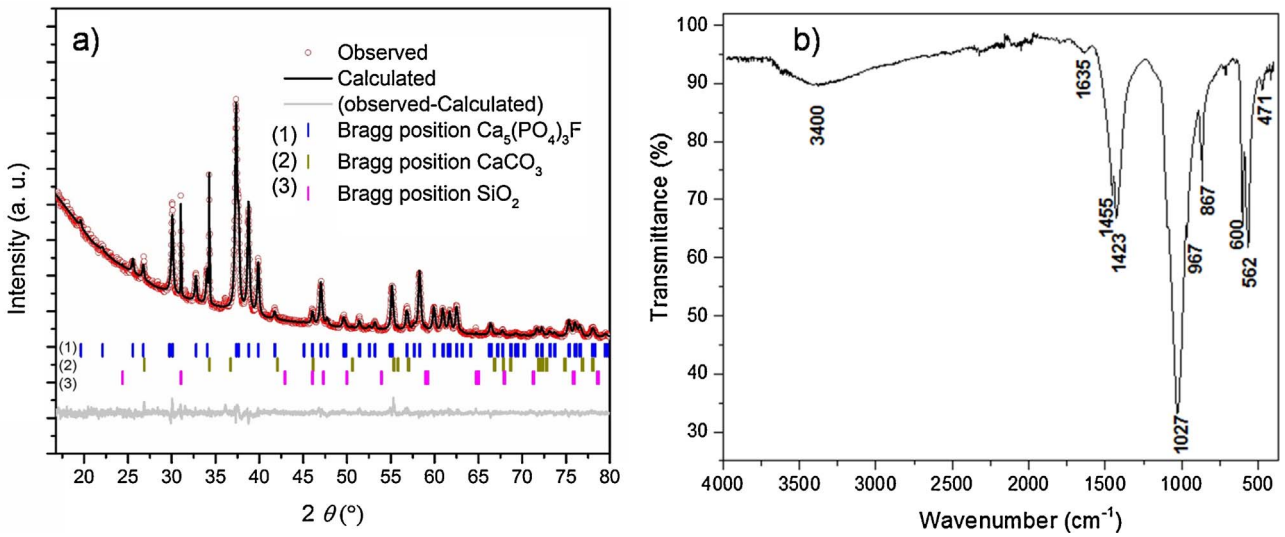


**Fig. 1.** (a) Structure refinement from XRD data of the natural Moroccan phosphate showing observed (red dots) and calculated (black solid line) intensities. Tick marks refer to the reflections of $Ca_5(PO_4)_3F$ (1), quartz $SiO_2$ (2) and $CaCO_3$ (3). (b) FT-IR spectrum of natural Moroccan phosphate.

efficiencies of the two dyes up to ~95% occurred in the first stage when the adsorbent dosage was progressively increased from 1.0 to 6 and 20 g/L for CR and Rh6G, respectively, and then the removal efficiency did not change significantly with a further increase in adsorbent dose. This increase in the removal efficiency of the organic dyes is due to the formation of a large number of active adsorption sites as the amount of adsorbent increased [45]. On the other hand, the slight increase in the removal efficiency at doses more than 20 g/L for Rh6G and 10 g/L for CR can explained by the reduction of the active adsorption sites due to the partial aggregation of adsorbent particles at higher adsorbent doses [46]. Meanwhile, the equilibrium adsorption capacity decreased for the two dyes with increasing of adsorbent dose. This effect can be attributed to the unsaturation of the adsorption sites of the adsorbent due to the limited concentration of dyes molecules if compared with amount of adsorbent [42]. However, the highest removal efficiency of dyes were observed at 20 g/L for Rh6G and 10 g/L for CR, thus these adsorbent doses were chosen for further experiments.

### 3.4. Adsorption isotherms

The adsorption isotherms describe the adsorption behaviour of an adsorbate onto an adsorbent when the adsorption process reaches an equilibrium state. The analysis of adsorption isotherm by fitting the experimental data using different isotherm models is important step to design and optimise the adsorption system [42,47]. Langmuir, Freundlich, Dubinin–Radushkevich (D–R) and Tempkin isotherm are the most widely used models to describe dye adsorption at solid-liquid interfaces. Therefore, we applied the four models in this study to analyze the adsorption equilibrium process of Rh6G and CR with initial concentration range of 100–400 mg/L onto natural phosphate dosage of 20 g/L at equilibrium time of 2 h and pH value of 5.2. Fig. 6 shows the fitting of experimental adsorption data of the two dyes at equilibrium using Langmuir, Freundlich, Dubinin–Radushkevich (D–R) and Tempkin isotherm, respectively. The constants calculated for the four isotherm models according to Eq. (A.3), Eq. (A.5), Eq. (A.6) and Eq. (A.8) as well as the standard deviations ($R^2$) values of the fitting are listed in Table 1. As shown in Fig. 6a and listed in Table 1, the Langmuir isotherm gives the best fitting for the two dyes Rh6G and CR with $R^2 > 0.996$. For more confirmation of Langmuir isotherm, the separation factor $R_L$ was calculated according to Eq. (A.4) and listed in Table 1. Of note that the separation factor $R_L$ should be $0 < R_L < 1$ for appropriate Langmuir isotherm [48]. The values of $R_L$ of the two dyes were found to be in the range from 0.0004 to 0.03, confirming the suitability of Langmuir model. This leads to the conclusion that the adsorption of Rh6G and CR onto natural phosphate is a monolayer process and the surface is relatively homogeneous. The using of the Freundlich model (Fig. 6b), which describes the multilayer adsorption process on heterogeneous surface [27], gives lower $R^2$ values than the

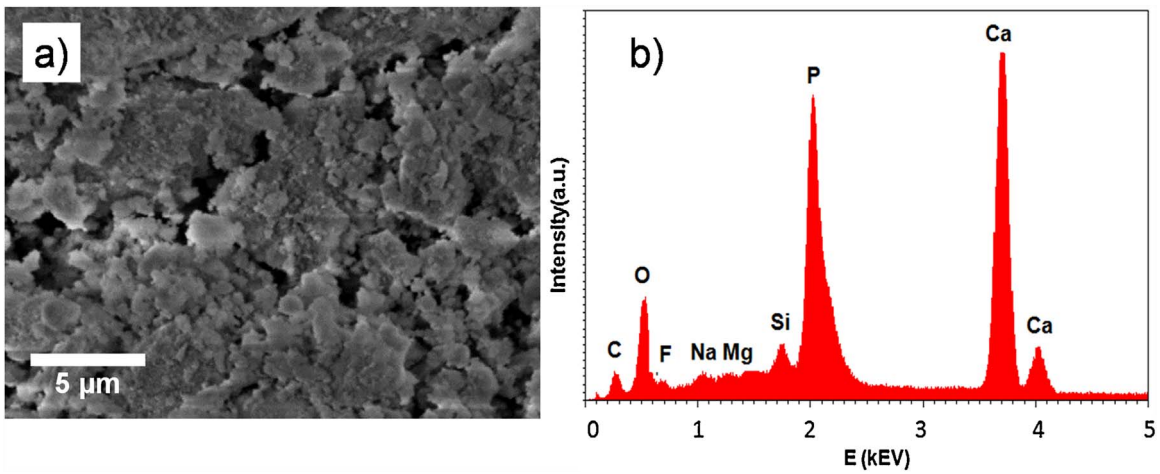


**Fig. 2.** (a) SEM micrograph and (b) EDS spectra of natural Moroccan phosphate.

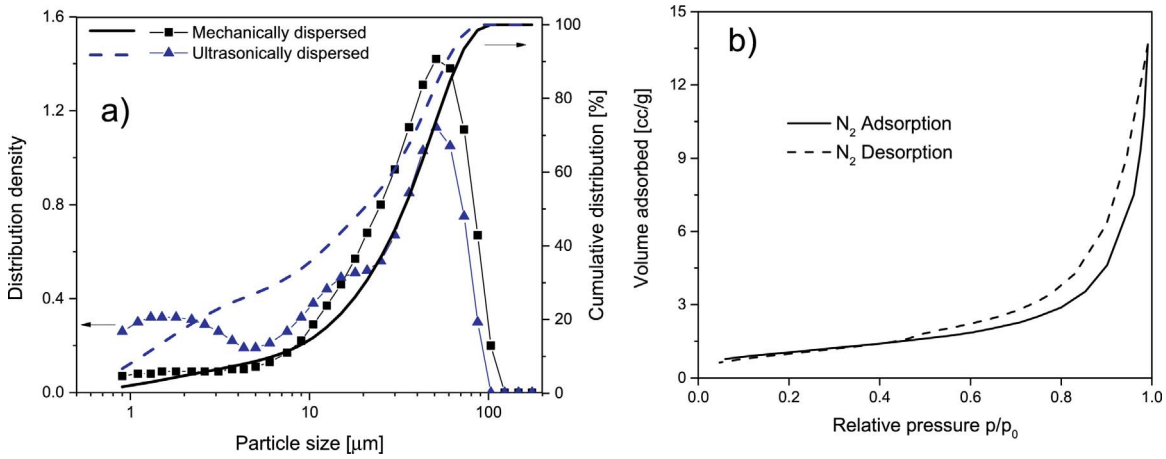


**Fig. 3.** (a) Particle size distribution and (b) Nitrogen adsorption-desorption isotherms of natural Moroccan phosphate.

Langmuir isotherms (Table 1). This points out that the adsorption of Rh6G and CR onto natural phosphate is not a multilayer process. Dubinin–Radushkevich (D–R) isotherm is most widely used model to determine whether the adsorption is a chemical or physical process [28]. Moreover, the maximum adsorbed quantity and mean adsorption free energy can be calculated from this model according to Eq. (A.$_7$). However, Fig. 6c shows that the experimental adsorption data are not well fitted with the Dubinin–Radushkevich model. In addition, as listed in Table 1, the obtained values of $R^2$ are less than 0.76. Finally, we applied Tempkin isotherm in order to study the interaction between the dyes molecules during the adsorption process. The adsorption heat $b = -\Delta H$ of the adsorbates (dyes) molecules can be calculated from this model according to Eq. (A.$_8$). As shown in Fig. 6d and Table 1, the using of Tempkin isotherm to fit the experimental data resulted in positive values of adsorption heat $b$ suggesting that the adsorption is an exothermic process [42].

In summary, the Langmuir isotherm model best represents the equilibrium adsorption process of the two dyes by comparing the values of $R^2$ for the four isotherm models (Table 1). The calculated maximum adsorbed quantity $q_{max}$ of CR and Rh6G were found 19.81 and 6.84 mg/g, respectively. The obtained $q_{max}$ of Rh6G dye is quite similar to those observed of other cationic dyes such as methylene blue over natural phosphate in the previous studies [39,49]. However, the maximum adsorbed quantity of the anionic dye CR onto the natural phosphate is two times more than that of cationic dyes Rh6G. Furthermore, $q_{max}$ of CR onto natural phosphate is higher than that found using activated carbon (6.72 mg/g) [50]. Therefore, in comparison to commercial adsorbents, natural phosphate can be a good adsorbent for anionic dyes such as CR.

### 3.5. Adsorption kinetics

The effects of contact times on adsorption capacity and removal efficiency of natural phosphate for Rh6G and CR with initial dye-solution concentration of 100 mg/L at dosage 10 g/L and pH 5.2 are shown in Fig. 7. This figure shows that the adsorption capacities and removal efficiency increased with rising contact time for the two dyes. The adsorption process reached equilibrium with removal efficiency $R_e > 99$ of CR and $R_e > 75$ of Rh6G dye from the aqueous solution within 40 and 90 min, respectively. The equilibrium adsorption capacities of Rh6G and CR dye onto the natural phosphate were 7.481 and 9.926 mg/g, respectively. The better adsorption of CR over natural phosphate can be attributed to the fact that CR is a sulfonated anionic dye, which has negatively charged sulfonic group ($-SO_3^-$), and can bind easily through electrostatic attraction with protonated groups on natural phosphate surface at this pH value. In contrast, Rh6G has positively charged groups $(=NCH_2CH_3)^+$; that weakened the interaction with natural phosphate, which explains the lower removal capacity in this case.

Four different kinetic models, namely, pseudo-first-order, pseudo-second–order, Elovich model and intra-particle diffusion models according to Eqs. (A.$_{10}$)–(A.$_{13}$), respectively, were used to analyze the experimental kinetic data for the adsorption of Rh6G and CR dyes onto the natural phosphate as shown in Fig. 8. The constants and $R^2$ values

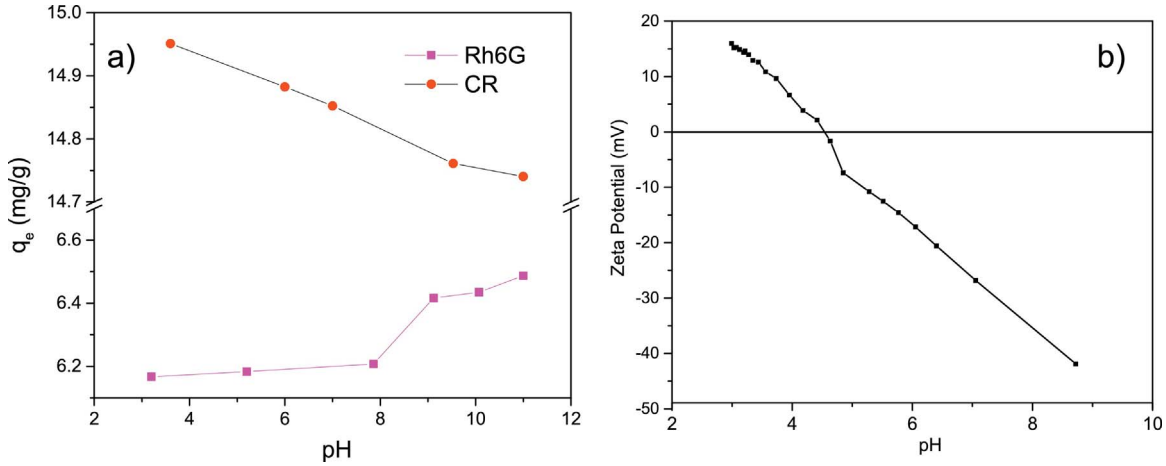


**Fig. 4.** (a) Effect of pH solution on the adsorption capacity on cationic dye Rh6G (solid squares) as well as anionic dye CR (solid circles) onto natural phosphate (Ci = 100 mg/L, $t$ = 2 h and dosage = 14 g/L for Rh6G and 20 g/L for CR). (b) Zeta potential of natural phosphate as function of pH showing $pH_{PZC}$ = 4.8.

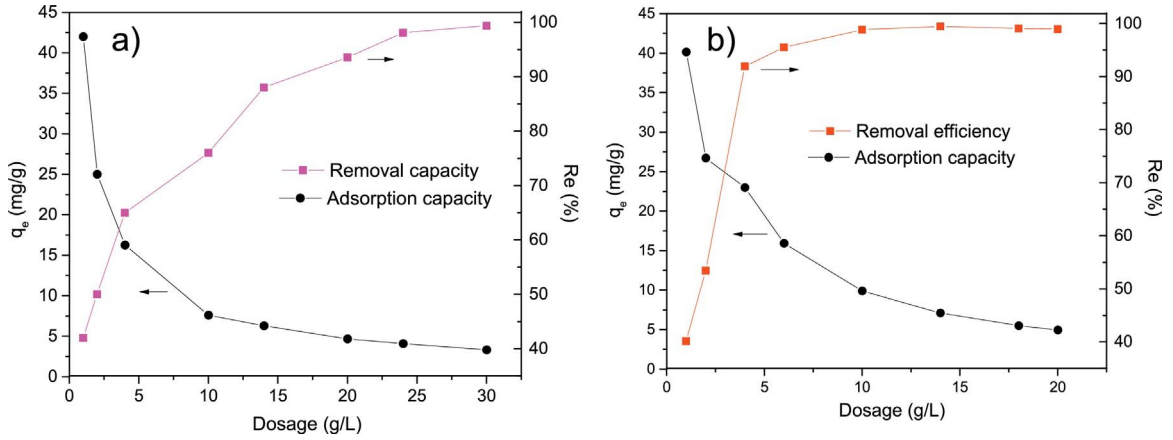


**Fig. 5.** Effect of adsorbent dose on the adsorption capacity (solid circles) and removal efficiency (solid squares) of Rh6G (a) and CR (b) dyes onto natural phosphate (pH = 5.2, $C_i$ = 100 mg/L, $t$ = 2 h).

calculated for the four kinetic equations are listed in Table 2. Fig. 8a shows that the fitting of the experimental kinetic data according to the pseudo-first-order model is not linear and the standard deviation of the fitting $R^2$ is less than 0.96. Moreover, the calculated values of adsorption capacities $q_e$ at equilibrium for the two dyes do not agree with the experimental values, which indicate that the adsorption process cannot be represented by the pseudo-first order model. In contrast, plotting $t/q_t$ versus $t$ gave good linear fitting with high $R^2$ (i.e $R^2 > 0.99$) for the two dyes (see Fig. 8b and Table 2). Additionally, the calculated $q_e$ values from this model are conforming to the experimental values determined from Fig. 7a. These results suggest that the time dependence for the adsorption of Rh6G and CR by natural phosphate is well described by a pseudo-second-order model in which a molecule of dye is adsorbed onto two sites of the natural phosphate surface, while the dye concentration is constant [31]. As illustrated in Fig. 8c, the using of the intra-particle diffusion model, a plot of the amount of adsorbed dye $q_t$ versus the square root of time $t^{1/2}$, shows that the distribution of the experimental points of the two dyes are not linear over the whole time range and, instead, can be divided into three linear regions. This multilinear curve indicates that the adsorption

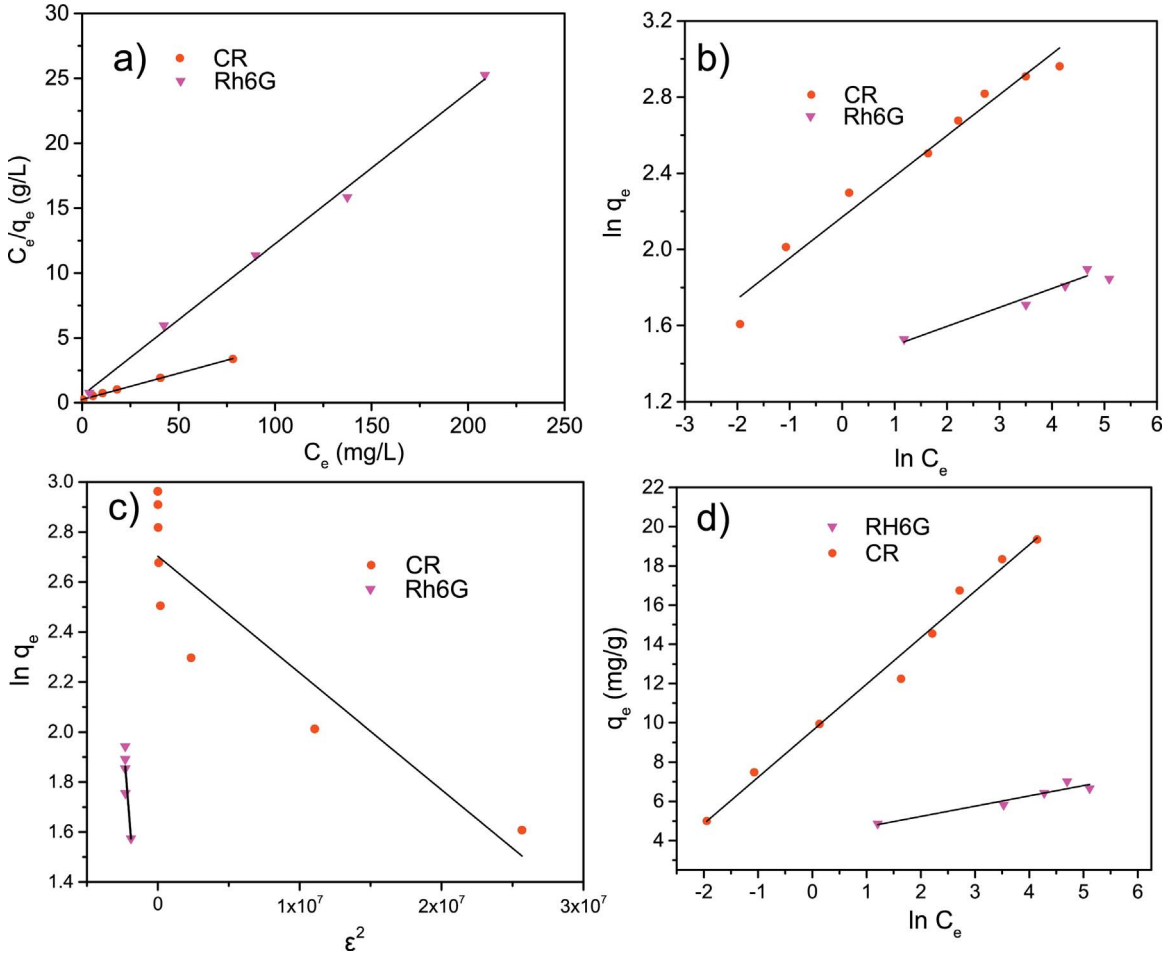


**Fig. 6.** Isotherm models of (a) Langmuir, (b) Freundlich, (c) Dubinin–Radushkevich model, and (d) Tempkin for adsorption of Rh6G (solid triangles) and CR (solid circles) onto natural phosphate (pH = 5.2, $C_i$ = 100–400 mg/L, Dosage = 20 g/L, $t$ = 2 h). The black lines represent the linear fitting of the experimental data.

**Table 1**
The adsorption isotherm parameters for the adsorption of CR and Rh6G onto natural phosphate with Langmuir, Freundlich, Dubinin–Radushkevich model, and Tempkin models.

| Isotherm models/parameters | CR | Rh6G |
|---|---|---|
| Langmuir | | |
| $q_{max}$ (mg/g) | 19.81 | 6.84 |
| $k_L$ (L/mg) | 0.46 | 4.68 |
| $R^2$ | 0.997 | 0.996 |
| $R_L$ | 0.004–0.02 | 0.01–0.03 |
| Freundlich | | |
| $k_F$ ((mg/g)(L/mg)$^{1/n}$) | 8.76 | 4.23 |
| $n$ | 4.663 | 10.0675 |
| $R^2$ | 0.963 | 0.941 |
| D-R | | |
| $q_m$ (mg/g) | 14.93 | 6.44 |
| $k_D$ (mol$^2$/kJ$^2$) | $4.67 \times 10^{-2}$ | 0.713 |
| E (kJ/mol) | 3.272 | 0.837 |
| $R^2$ | 0.787 | 0.712 |
| Temkin | | |
| $k_T$ (L/mg) | 5.73 | 2.75 |
| $b$ (kJ/mol) | 1.04 | 4.73 |
| $R^2$ | 0.985 | 0.895 |

process of the dye is a multi-step process. In the first step, the high rate of dyes adsorption $K_1$ is caused by the surface adsorption due to the boundary layer effect. In the second step, the intra-particle diffusion control the adsorption rate, therefore, the adsorption rate $K_2$ becomes smaller than $K_1$. Finally, the adsorption rate $K_3$ gradually decreased in the third stage until adsorption equilibrium is reached. However, the intercept of the line fails to pass through the origin at the first stage, and the standard deviation of fitting $R^2$ for the third region is quite low for both dyes. The results suggest that intra-particle diffusion is not the only rate-limiting step during the dye adsorption process onto the natural phosphate surface. Finally, as shown in Fig. 8d, the using of Elovich kinetic model gave the worst linear fitting of the experimental kinetic data of Rh6G and CR, with $R^2 < 0.81$. Moreover, the calculated initial adsorption rate α and Elovich desorption constant $\beta$ according to this model are not realistic, indicating that Elovich adsorption kinetics of both cationic and anionic dyes onto natural phosphate is not suitable.

### 3.6. Simulated dye effluent adsorption

Large amounts of salt are used in textile industry as an electrolyte for transport, adsorption and fixation of the dye molecules on the fabric. During the dyeing process, it leads to maximum exhaustion of dye molecules [51]. In order to study the influence of salt on the adsorption process, adsorption experiments were conducted using an aqueous solution of CR dye, at varying concentrations of NaCl (0, 10, 100, 500 and 1000 mM), while keeping the other parameters constant. It is evident from Fig. 9 that the presence of salt in solution can significantly affect the dye adsorption. The removal efficiency of CR dye from the simulated dye effluent slightly decreased from 98.5 to 88.4% with increasing NaCl concentration from 0 to 100 mM. With further increase in the NaCl concentration to 1000 mM, the removal efficiency decreased sharply to 35.5%. This can be explained by: (i) the neutralization of the negatively charged dye molecules as well as the charged surface of natural phosphate by NaCl and (ii) the interaction of the salt with the adsorbate molecules [52]. As a result, the attraction force between the dye molecules and phosphate surface are decreased, and thus, the adsorption capacity is also decreased. These results confirm that the natural phosphate could be good adsorbent for anionic dyes such as CR from industrial wastewater with low concentration of NaCl (< 100 mM).

### 3.7. Desorption of CR and Rh6G

In the adsorption process, the recovery of the adsorbent as well as the disposal of the adsorbates are very important. Therefore, batch desorption experiments were carried out using 0.1 M solution of several desorbing agents (NaOH, HCl, $H_2SO_4$, and ethanol). Desorption efficiencies are compared in Fig. 10a. The use of basic solution of NaOH resulted in low desorption efficiency (< 7.6%) of both dyes, while ethanol showed moderate desorption efficiency of 22.1% and 19.3% for CR and Rh6G, respectively. On the other hand, HCl showed the highest recovery efficiencies of 48.3% and 34.9% for CR and Rh6G, respectively. In Fig. 10b, the study of the efficiency of HCl as an eluent at different concentrations is shown. For both dyes, the maximum elution was found at 0.1 M of HCl solution. It is also noteworthy that an increase in HCl concentration leads to a decrease in desorption percentage. This could be due to the deterioration of actives site on the natural phosphate surface at higher HCl concentrations [53].

## 4. Conclusions

Natural phosphate is found to be an effective low-cost adsorbent for the removal of cationic dye rhodamine 6G (Rh6G) as well as anionic dye congo red (CR) from contaminated water. The Rietveld refinement of the XRD data shows that the sample contains fluoroapatite $Ca_5(PO_4)_3F$ with minor amount of $SiO_2$ and $CaCO_3$. The adsorption efficiency of the anionic dye CR decreased with an increasing pH, in the opposite of the cationic dye Rh6G. The Langmuir model demonstrated

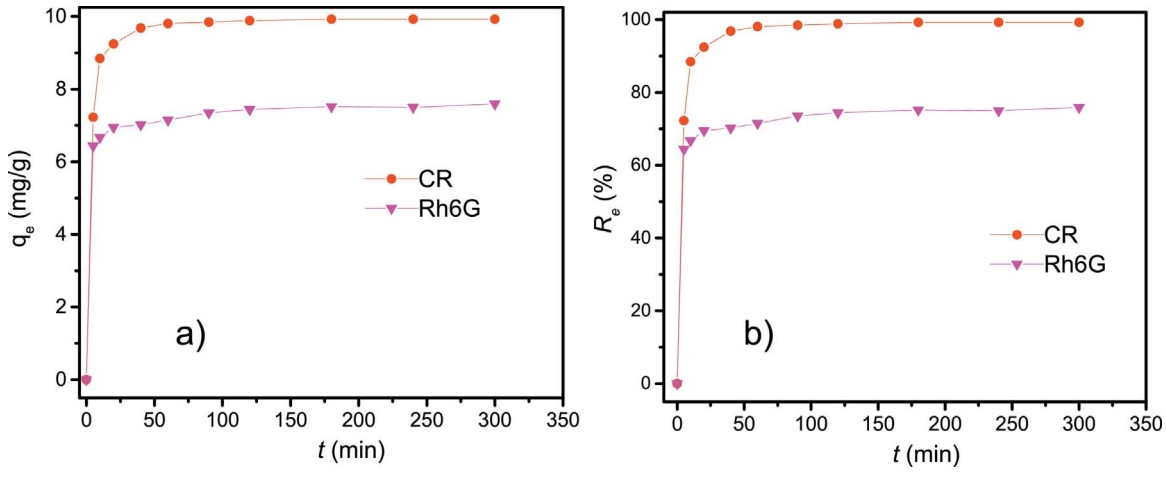


**Fig. 7.** Effect of contact time on the adsorption capacity (a) and removal efficiency (b) of CR (solid circles) and Rh6G (solid triangles) dyes onto natural phosphate at room temperature (pH = 5.2, $C_i$ = 100 mg/g, dosage = 10 g/L).

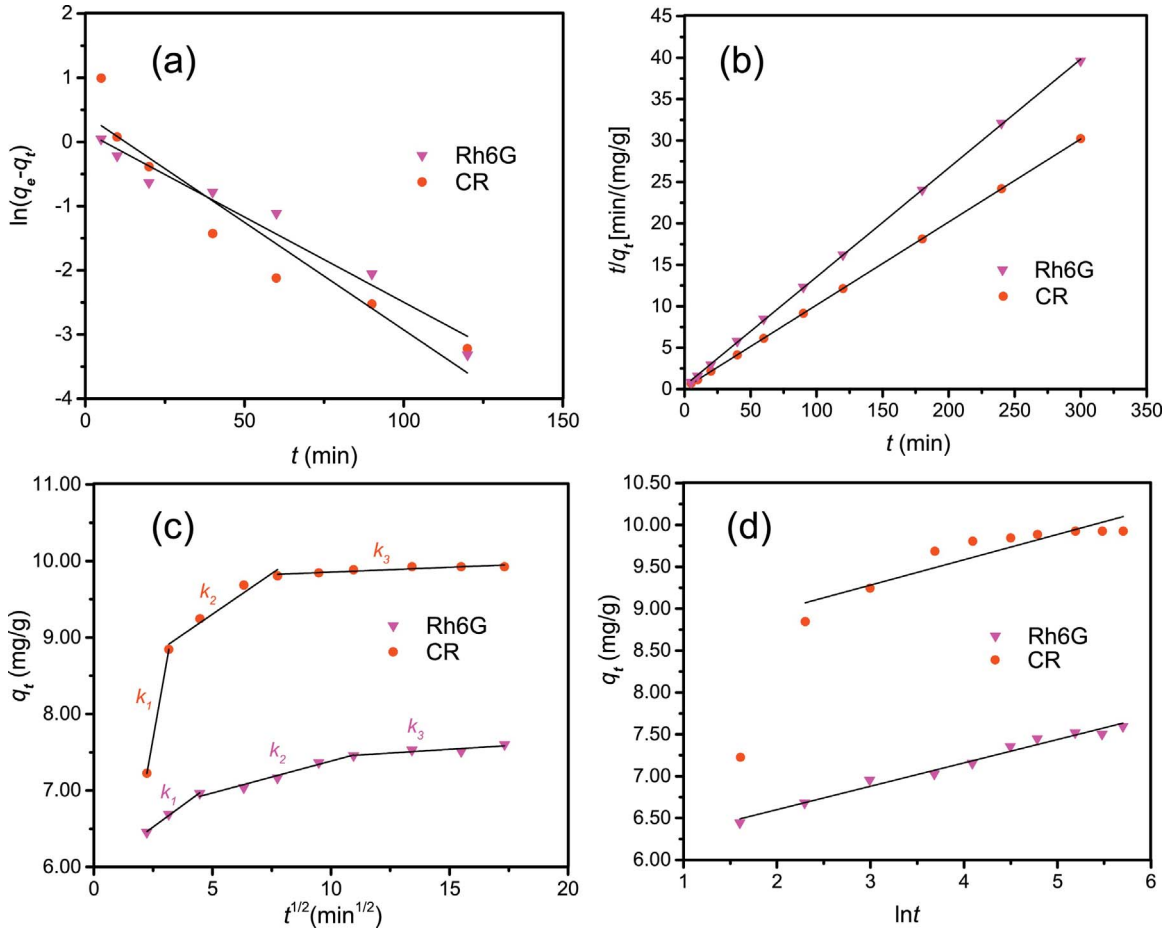


**Fig. 8.** Kinetic models of (a) pseudo-first-order, (b) pseudo-second–order, (c) intra-particle diffusion and (d) Elovich model for adsorption of Rh6G (triangles) and CR (circles) onto natural phosphate at room temperature (pH = 5.2, $C_i$ = 100 mg/g, dosage = 10 g/L). The black lines represent the linear fitting of the experimental data.

**Table 2**
The adsorption kinetics parameters for the adsorption of CR and Rh6G onto natural phosphate with pseudo-first-order, pseudo-second–order, Elovich model and intra-particle diffusion models.

| Kinetics models/parameters | CR | Rh6G |
|---|---|---|
| Pseudo-first-order | | |
| $q_e$ (exp) (mg/g) | 9.926 | 7.481 |
| $q_e$ (cal) (mg/g) | 1.5223 | 1.1635 |
| $k_1$ (1/min) | 0.0335 | 0.0265 |
| $R^2$ | 0.891 | 0.954 |
| Pseudo-second-order | | |
| $q_e$ (cal) (mg/g) | 9.983 | 7.611 |
| $q_e$ (exp) (mg/g) | 9.926 | 7.481 |
| $k_2$ (g/(mg min)) | 0.0733 | 0.0548 |
| $R^2$ | 0.999 | 0.999 |
| Elovich | | |
| α (mg/(g min)) | $3.15 \times 10^{11}$ | $6.85 \times 10^{8}$ |
| β (g/mg) | 3.304 | 3.581 |
| $R^2$ | 0.816 | 0.978 |
| Intra-particule diffusion | | |
| $k_1$ (mg/(g $min^{1/2}$)) | 1.7491 | 0.2273 |
| $C_1$ | 3.3147 | 5.9412 |
| $(R_1)^2$ | 0.985 | 0.993 |
| $k_2$ (mg/(g $min^{1/2}$)) | 0.2127 | 0.0835 |
| $C_2$ | 8.2416 | 6.5371 |
| $(R_2)^2$ | 0.937 | 0.964 |
| $k_3$ (mg/(g $min^{1/2}$)) | 0.0127 | 0.0197 |
| $C_3$ | 9.2785 | 7.231 |
| $(R_3)^2$ | 0.902 | 0.698 |

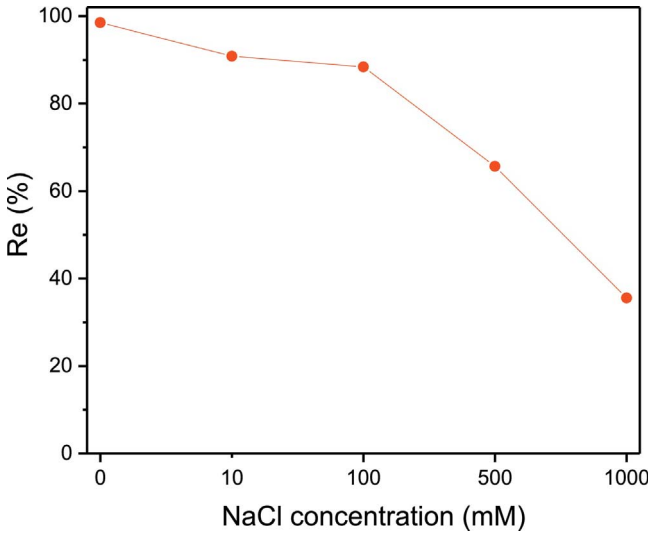


**Fig. 9.** Effect of NaCl concentration on removal efficiency of CR from simulated dye effluent (CR+ NaCl) onto natural phosphate ($t$ = 2 h, dosage = 20 g/L, pH = 5.6 and T = 80 °C).

that a monolayer adsorption process occurs on the homogeneous surface of the natural phosphate without considering the interaction between adsorbate molecules. The calculated maximum adsorbed quantity $q_{max}$ of CR and Rh6G were found 19.81 and 6.84 mg/g, respectively, which was superior to other conventional adsorbents such as activated carbon [50]. The pseudo-second-order equation was

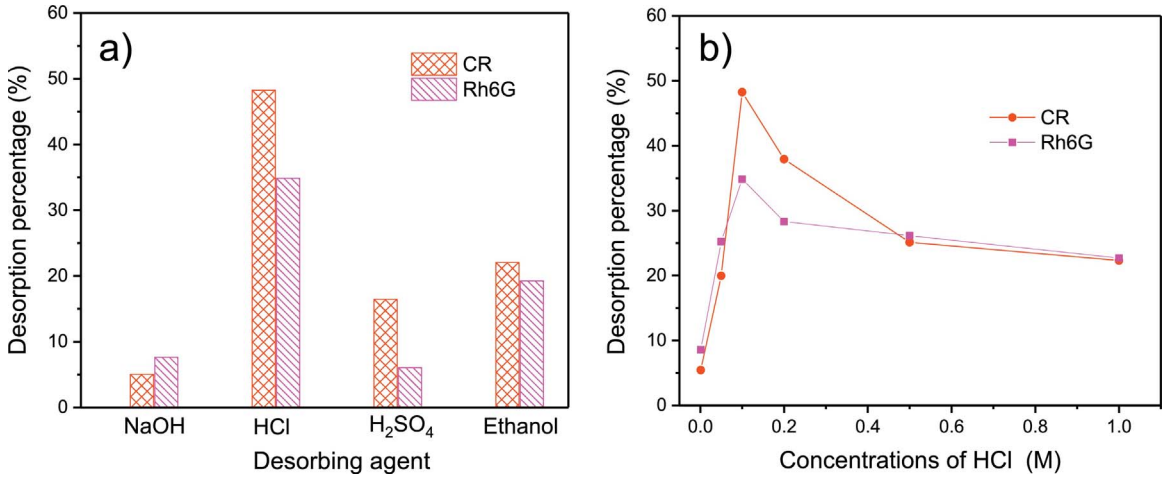


**Fig. 10.** Desorption of CR and Rh6G dyes from loaded natural phosphate using (a) various desorbing agents (0.1 M) and (b) HCl at various concentrations.

followed for the adsorption of CR and Rh6G on natural phosphate. The elution of CR and Rh6G from natural phosphate was the highest at 0.1 M HCl. This work proved that Moroccan natural phosphate is a promising low-cost adsorbent for both cationic and anionic dyes.

## Acknowledgments

The financial support by the European Commission through EU-Metalic II by Erasmus Mundus program is greatly acknowledged. This publication reflects the views only of the author, and the Commission cannot be held responsible for any use, which may be made of the information contained therein. We would like to kindly thank Dr. Gabriele Steinborn for Zeta potential measurements, Artur Hejczyk for particle size distribution measurements and Christina Eischenauer for nitrogen sorption measurements.

## Appendix A

*Adsorption isotherm and kinetics equations*

The linear form of Langmuir isotherm model is calculated by:

$$\frac{C_e}{q_e} = \frac{1}{q_m k_L} + \frac{1}{q_m} C_e \qquad \text{Eq. (A.3)}$$

where $q_m$ (mg/g) is the Langmuir maximum adsorption of the dyes per unit weight of the adsorbent and $k_L$ (L/mg) is the Langmuir isotherm constant related to the rate of adsorption.

The separation factor $R_L$, which represents the type of Langmuir isotherm, is calculated by:

$$R_L = \frac{1}{1 + k_L C_i} \qquad \text{Eq. (A.4)}$$

The logarithmic form of Freundlich model is represented by:

$$\ln q_e = \ln k_f + \frac{1}{n} \ln C_e \qquad \text{Eq. (A.5)}$$

where $k_f$ and $n$ are the Freundlich isotherm coefficients, indicating the adsorption capacity and adsorption intensity, respectively.

The Dubinin–Radushkevich D–R model is given by:

$$\text{Eq. (A.6)} \quad \ln q_e = \ln q_m - k_D \varepsilon^2$$

In this model, $q_m$ (mg/g) and $k_D$ ($mol^2/kJ^2$) are D-R isotherm constants related to the maximum adsorption quantity and the adsorption free energy, respectively. The Polanyi potential ε can be defined as:

$$\varepsilon = RT \ln\left(1 + \frac{1}{C_e}\right) \qquad \text{Eq. (A.7)}$$

The Tempkin model is described as:

$$q_e = \frac{RT}{b} \ln k_T + \frac{RT}{b} \ln C_e \qquad \text{Eq. (A.8)}$$

Where $q_e$ is expressed in terms of the adsorption heat $b$ (equal to $-\Delta H$, kJ/mol) and the Tempkin isotherm constant $k_T$ (L/mg).

The adsorption quantity $q_t$ (mg/g) of the dye onto the phosphate at time $t$ was calculated according to:

$$q_t = \frac{(C_i - C_t)V}{m} \qquad \text{Eq. (A.9)}$$

where $C_t$ (mg/L) is the concentration of the dye solution at time $t$.

**Pseudo-first-order model:**

Eq. (A.10) $\ln(qe - q_t) = \ln q_e - K_1 t$

**Pseudo-second-order model:**

$$\frac{t}{q_t} = \frac{1}{K_2 {q_e}^2} + \frac{t}{q_e} \quad \text{Eq. (A.11)}$$

**Intra-particle diffusion model:**

Eq. (A.12) $q_t = K_i t^{1/2} + C$

where $K_1$ (1/min), $K_2$ (g/(mg min), and $K_i$ (mg/(g $\min^{1/2}$) represent the kinetic rate constant of pseudo-first-order adsorption, pseudo-second-order adsorption, and Intra-particle diffusion at stage $i$, respectively. The intercept constant $C_i$ (mg/g) indicates the effect of boundary layer thickness of molecular diffusion.

**Elovich kinetic model:**

$$q_t = \frac{1}{\beta}\ln(\alpha\beta) + \frac{1}{\beta}\ln t \quad \text{Eq. (A.13)}$$

α (mg/g/min) and β (g/mg) refers to initial adsorption rate and the Elovich desoprtion constant in Elovich kinetic model.

## References

[1] A. Afkhami, R. Moosavi, Adsorptive removal of Congo red a carcinogenic textile dye, from aqueous solutions by maghemite nanoparticles, J. Hazard. Mater. 174 (2010) 398–403.
[2] H. Zollinger, Color Chemistry, VCH Publishers, New York, 1987.
[3] S.G. Liu, Y.Q. Ding, P.F. Li, K.S. Diao, X.C. Tan, F.H. Lei, Y.H. Zhan, Q.M. Lib, B. Huang, Z.Y. Huang, Adsorption of the anionic dye Congo red from aqueous solution onto natural zeolites modified with N,N-dimethyl dehydroabietylamine oxide, Chem. Eng. J. 248 (2014) 135–144.
[4] L. Giorgetti, H. Talouizte, M. Merzouki, L. Caltavuturo, C. Geri, S. Frassinetti, Genotoxicity evaluation of effluents from textile industries of the region Fez-Boulmane, Morocco: a case study, Ecotox. Environ. Saf. 74 (2011) 2275–2283.
[5] M. Iqbal, Vicia faba bioassay for environmental toxicity monitoring: a review, Chemosphere 144 (2016) 785–802.
[6] S.S. Phugare, D.C. Kalyani, S.N. Surwase, J.P. Jadhav, Ecofriendly degradation, decolorization and detoxification of textile effluent by a developed bacterial consortium, Ecotox. Environ. Saf. 74 (2011) 1288–1296.
[7] S.V. Mohan, S.V. Ramanaiah, P.N. Sarma, Biosorption of direct azo dye from aqueous phase onto Spirogyra sp 102: Evaluation of kinetics and mechanistic aspects, Biochem. Eng. J. 38 (2008) 61–69.
[8] L.L. Lian, L.P. Guo, C.J. Guo, Adsorption of Congo red from aqueous solutions onto Ca-bentonite, J. Hazard. Mater. 161 (2009) 126–131.
[9] J.W. Zhang, L. Wang, G.L. Zhang, Z.Y. Wang, L.S. Xu, Z. Fan, Influence of azo dye-TiO2 interactions on the filtration performance in a hybrid photocatalysis/ultra-filtration process, J. Colloid Interface Sci. 389 (2013) 273–283.
[10] A. Babarinde, K. Ogundipe, K.T. Sangosanya, B.D. Akintola, A.O. Elizabeth Hassan, Comparative study on the biosorption of Pb(II), Cd(II) and Zn(II) using Lemon grass (Cymbopogon citratus): kinetics, isotherms and thermodynamics, Chem. Int. 2 (2) (2016) 89–102.
[11] A. Szygula, E. Guibal, M.A. Palacin, M. Ruiza, A.M. Sastre, Removal of an anionic dye (Acid Blue 92) by coagulation-flocculation using chitosan, J. Environ. Manage. 90 (2009) 2979–2986.
[12] A.R. Khataee, G. Dehghan, Optimization of biological treatment of a dye solution by macroalgae Cladophora sp using response surface methodology, J. Taiwan Inst. Chem. Eng. 42 (2011) 26–33.
[13] A.I. del Rio, J. Fernandez, J. Molina, J. Bonastre, F. Cases, Electrochemical treatment of a synthetic wastewater containing a sulphonated azo dye. Determination of naphthalenesulphonic compounds produced as main by-products, Desalination 273 (2011) 428–435.
[14] M. Dogan, Y. Ozdemir, M. Alkan, Adsorption kinetics and mechanism of cationic methyl violet and methylene blue dyes onto sepiolite, Dyes Pigm. 75 (2007) 701–713.
[15] M.A. Jamal, M. Muneer, M. Iqbal, Photo-degradation of monoazo dye blue 13 using advanced oxidation process, Chem. Int. (2015) 12–16.
[16] F. Derbyshire, M. Jagtoyen, R. Andrews, A. Rao, I. Martin-Gullon, E.A. Grulke, Carbon materials in environmental applications, Chem. Phys. Carbon 27 (2001) 1–66.
[17] A.A. Adeyemo, I.O. Adeoye, O.S. Bello, Adsorption of dyes using different types of clay: a review, Appl. Water Sci. (2015) 1–26.
[18] W.H. Zou, H.J. Bai, S.P. Gao, K. Li, Characterization of modified sawdust, kinetic and equilibrium study about methylene blue adsorption in batch mode, Korean J. Chem. Eng. 30 (2013) 111–122.
[19] E. Ekrami, F. Dadashian, M. Arami, Adsorption of methylene blue by waste cotton activated carbon: equilibrium, kinetics, and thermodynamic studies, Desalin. Water Treat. 57 (2016) 7098–7108.
[20] O.S. Bello, K.A. Adegoke, A.A. Olaniyan, H. Abdulazeez, Dye adsorption using biomass wastes and natural adsorbents: overview and future prospects, Desalin. Water Treat. 53 (2015) 1292–1315.
[21] G. Crini, Recent developments in polysaccharide-based materials used as adsorbents in wastewater treatment, Prog. Polym. Sci. 30 (2005) 38–70.
[22] I. Barrouk, S.A. Younssi, A. Kabbabi, M. Persin, A. Albizane, S. Tahiri, New ceramic membranes from natural Moroccan phosphate for microfiltration application, Desalin. Water Treat. 55 (2015) 53–60.
[23] I. Barrouk, S.A. Younssi, A. Kabbabi, M. Persin, A. Albizane, S. Tahiri, Elaboration and characterization of ceramic membranes made from natural and synthetic phosphates and their application in filtration of chemical pretreated textile effluent, J. Mater. Environ. Sci. 6 (2015) 2190–2197.
[24] J. Rodriguez-Carvajal, Fullprof: a program for Rietveld refinement and pattern matching analysis, Collected Abstract of Powder Diffraction Meeting Toulouse, France (1990).
[25] L.W. Finger, D.E. Cox, A.P. Jephcoat, A correction for powder diffraction peak asymmetry due to axial divergence, J. Appl. Crystallogr. 27 (1994) 892–900.
[26] I. Langmuir, The constitution and fundamental properties of solids and liquids. Part I. Solids, J. Am. Chem. Soc. 38 (1916) 2221–2295.
[27] H.M.F. Freundlich, Uber die adsorption in losungen, Z. Phys. Chem. 57 (1906) 385–470.
[28] M.J.C. Calagui, D.B. Senoro, C.C. Kan, J.W.L. Salvacion, C.M. Futalan, M.W. Wan, Adsorption of indium(III) ions from aqueous solution using chitosan-coated bentonite beads, J. Hazard. Mater. 277 (2014) 120–126.
[29] S.J. Allen, Q. Gan, R. Matthews, P.A. Johnson, Comparison of optimised isotherm models for basic dye adsorption by kudzu, Bioresour. Technol. 88 (2003) 143–152.
[30] S. Langergen, B.K. Svenska, Zur theorie der sogenannten adsoption geloester stoffe, Veteruskapsakad Handl. 24 (1898) 1–39.
[31] Y.S. Ho, G. McKay, Pseudo-second order model for sorption processes, Process Biochem. 34 (1999) 451–465.
[32] W.J. Weber, J.C. Morris, Kinetics of adsorption on carbon from solution, J. Sanit. Eng. Div. 89 (1963) 31–60.
[33] N. Yeddou, A. Bensmaili, Kinetic models for the sorption of dye from aqueous solution by clay-wood sawdust mixture, Desalination 185 (2005) 499–508.
[34] J.C. Trombe, Decomposition and reactivity of some hydroxylated and carbonated apatites, Ann. Chim. Fr. 8 (1973) 251–269.
[35] I. Nikcevic, V. Jokanovic, M. Mitric, Z. Nedic, D. Makovec, D. Uskokovic, Mechanochemical synthesis of nanostructured fluorapatite/fluorhydroxyapatite and carbonated fluorapatite/fluorhydroxyapatite, J. Solid State Chem. 177 (2004) 2565–2574.
[36] S. Asri, A. Laghzizil, A. Alaoui, A. Saoiabi, R. M'Hamdi, K. El Abbassi, A. Hakam, Structure and thermal behaviors of Moroccan phosphate rock (Bengurir), J. Therm. Anal. Calorim. 95 (2009) 15–19.
[37] R.A. Nyquist, R.O. Kagel, Infrared Spectra of Inorganic Compounds (3800–45 $cm^{-1}$), Academic Press, New York, London, 1971.
[38] K. Nakamoto, Infrared and Raman Spectra of Inorganic and Coordination Compounds, John Wiley & Sons, New York, 1978.
[39] N. Barka, A. Assabbane, A. Nounah, L. Laanab, Y.A. Ichou, Removal of textile dyes from aqueous solutions by natural phosphate as a new adsorbent, Desalination 235 (2009) 264–275.
[40] K.S.W. Sing, D.H. Everett, R.A.W. Haul, L. Moscou, R.A. Pierotti, J. Rouquerol, T. Siemieniewska, Reporting physisorption data for gas solid systems with special reference to the determination of surface-area and porosity (Recommendations 1984), Pure Appl. Chem. 57 (1985) 603–619.
[41] Y. Yao, B. Gao, M. Inyang, A.R. Zimmerman, X.D. Cao, P. Pullammanappallil, L.Y. Yang, Removal of phosphate from aqueous solution by biochar derived from anaerobically digested sugar beet tailings, J. Hazard. Mater. 190 (2011) 501–507.
[42] Q.J. Du, J.K. Sun, Y.H. Li, X.X. Yang, X.H. Wang, Z.H. Wang, L.H. Xia, Highly enhanced adsorption of congo red onto graphene oxide/chitosan fibers by wet-chemical etching off silica nanoparticles, Chem. Eng. J. 245 (2014) 99–106.
[43] J. Li, D.H.L. Ng, P. Song, C. Kong, Y. Song, P. Yang, Preparation and characterization of high-surface-area activated carbon fibers from silkworm cocoon waste for congo red adsorption, Biomass Bioenergy 75 (2015) 189–200.
[44] X.J. Jia, J.S. Wang, J.S. Wu, Y.C. Du, B.X. Zhao, D. den Engelsen, Bouquet-like calcium sulfate dihydrate: a highly efficient adsorbent for Congo red dye, RSC Adv.

5 (2015) 72321–72330.
[45] R.R. Mohammed, M.R. Ketabchi, G. McKay, Combined magnetic field and adsorption process for treatment of biologically treated palm oil mill effluent (POME), Chem. Eng. J. 243 (2014) 31–42.
[46] J.S. Wang, R.T. Peng, J.H. Yang, Y.C. Liu, X.J. Hu, Preparation of ethylenediamine-modified magnetic chitosan complex for adsorption of uranyl ions, Carbohydr. Polym. 84 (2011) 1169–1175.
[47] B. Royer, N.F. Cardoso, E.C. Lima, J.C.P. Vaghetti, N.M. Simon, T. Calvete, R.C. Veses, Applications of Brazilian pine-fruit shell in natural and carbonized forms as adsorbents to removal of methylene blue from aqueous solutions-kinetic and equilibrium study, J. Hazard. Mater. 164 (2009) 1213–1222.
[48] T.W. Weber, R.K. Chakravorti, Pore and solid diffusion models for fixed-bed adsorbers, AIChE J. 20 (1974) 228–238.
[49] A. Achkoun, J. Naja, R. M'Hamdi, Elimination of cationic and anionic dyes by natural phosphate, J. Chem. Chem. Eng. 6 (2012) 721–725.
[50] C. Namasivayam, D. Kavitha, Removal of Congo Red from water by adsorption onto activated carbon prepared from coir pith, an agricultural solid waste, Dyes Pigm. 54 (2002) 47–58.
[51] S.A. Avlonitis, I. Poulios, D. Sotiriou, M. Pappas, K. Moutesidis, Simulated cotton dye effluents treatment and reuse by nanofiltration, Desalination 221 (2008) 259–267.
[52] A.W.M. Ip, J.P. Barford, G. McKay, Reactive Black dye adsorption/desorption onto different adsorbents: effect of salt, surface chemistry, pore size and surface area, J. Colloid Interface Sci. 337 (2009) 32–38.
[53] M.R. Malekbala, M.A. Khan, S. Hosseini, L.C. Abdullah, T.S.Y. Choong, Adsorption/desorption of cationic dye on surfactant modified mesoporous carbon coated monolith: equilibrium, kinetic and thermodynamic studies, J. Ind. Eng. Chem. 21 (2014) 369–377.

# 4.3. Azo dye adsorption on an industrial waste-transformed hydroxyapatite adsorbent: Kinetics, isotherms, mechanism and regeneration studies

| | |
|---|---|
| Title | Azo dye adsorption on an industrial waste-transformed hydroxyapatite adsorbent: Kinetics, isotherms, mechanism and regeneration studies |
| Authors | H. Bensalah, S. Alami Younssi, M. Ouammou, A. Gurlo and M.F. Bekheet |
| Journal | Journal of Environmental Chemical Engineering |
| Publisher | Elsevier |
| Publication date | 23 February 2020 |
| DOI | 10.1016/j.jece.2020.103807 |
| My contribution | Design of experiments, processing of materials, collecting and interpreting UV-VIS data, simulation of adsorption isotherms and kinetics, results analysis and discussion, writing of the manuscript. |

Journal of Environmental Chemical Engineering 8 (2020) 103807

Contents lists available at ScienceDirect

Journal of Environmental Chemical Engineering

journal homepage: www.elsevier.com/locate/jece

# Azo dye adsorption on an industrial waste-transformed hydroxyapatite adsorbent: Kinetics, isotherms, mechanism and regeneration studies

Hiba Bensalah[a,b,*], Saad Alami Younssi[b], Mohamed Ouammou[b], Aleksander Gurlo[a], Maged F. Bekheet[a]

[a] Fachgebiet Keramische Werkstoffe / Chair of Advanced Ceramic Materials, Institut für Werkstoffwissenschaften und -technologien, Technische Universität Berlin, Hardenbergstraße 40, 10623, Berlin, Germany

[b] Laboratory of Membranes, Materials and Environment, Department of Chemistry, Faculty of Sciences & Technics of Mohammedia BP 146, 20650, University Hassan II of Casablanca, Morocco

ARTICLE INFO

*Keywords:*
Waste-transformed adsorbents
Hydroxyapatite
Azo dye
Mechanism
Regeneration
Waste management

ABSTRACT

Nanocrystalline hydroxyapatite (HAp) with high surface area was synthesized by surfactant-assistant hydrothermal method from an industrial waste phosphogypsum. X-ray diffraction (XRD), transmission electron microscopy (TEM) and nitrogen sorption characterizations revealed that HAp crystals grow as needle-like particles along the *c* direction with surface area of 86 and 135 $m^2/g$ for the samples synthesized without and with Brij-93 surfactant, respectively. Adsorption of anionic azo dye Congo Red (CR) were conducted on both samples, taking into account the influence of initial dye concentration (100–500 mg/L), adsorbent dosage (0.5–30 g/L), contact time (5–180 min) and solution pH (2–12). Kinetic studies showed that the adsorption of CR followed pseudo-second-order model, i.e., chemisorption is the rate controlling step. Freundlich isotherm was found to be most suitable model for the adsorption of CR, i.e. adsorption is multilayer process. The calculated maximum adsorption capacity of synthesized B93-HAp adsorbent using Brij-93 surfactant was found to be 139 mg/g at pH 5.5 and dosage of 2 g/L. Two predominant mechanisms were observed for CR adsorption, electrostatic attraction and hydrogen bonding as revealed by Fourier transformed infrared spectroscopy (FTIR) and X-ray photoelectron spectroscopy (XPS) studies. The multi-cycle sorption/desorption tests indicated that waste-transformed adsorbent could be regenerated and reused up to 6 cycles. Therefore, this work shows that the conversion of waste materials into adsorbents has a two-fold environmental benefit for both waste management and wastewater treatment.

## 1. Introduction

Phosphogypsum (PG) is a solid industrial waste produced during the production of phosphoric acid from phosphate rock by the wet process. About 3 − 5 tons of PG is generated for every ton of phosphoric acid produced [1]. Taking into consideration that the fertilizer industry is very important for the Moroccan economic and social area, with an annual production of 4.4 million tons of phosphoric acid ($H_3PO_4$) and a PG generation of approximatively 15 million tons [2]. This enormous quantity of waste is totally discharged into Atlantic Ocean, causing environmental problems to the aquatic fauna and flora via eutrophication. While only 15 % of world PG production is being utilized in agriculture, road engineering, cement and plaster industry [3–5]; it is of prime importance to valorize this hazardous waste by transforming it into useful nanomaterial.

A great attention has been paid to the development of smart and efficient nanomaterials for wastewater treatment applications. A thorough review of the literature reported a large variety of nanomaterials used efficiently in the removal of a wide range of pollutants in contaminated water [6,7]. Adsorption is one of the most attractive techniques for the treatment of wastewater due to its versatility, low energy consumption, simplicity and high efficiency compared to other conventional techniques [8–12]. Commercial activated carbon has been widely reported as one of the most efficient adsorbent of several contaminants [13]. Although these commercial adsorbents provide high removal rates, they present also a great drawback; their high cost which

*Abbreviations:* PG, phosphogypsum; HAp, hydroxyapatite; B93-HAp, surfactant-modified hydroxyapatite; CR, congo red

* Corresponding author at: Fachgebiet Keramische Werkstoffe / Chair of Advanced Ceramic Materials, Institut für Werkstoffwissenschaften und -technologien, Technische Universität Berlin, Hardenbergstraße 40, 10623, Berlin, Germany.

*E-mail address:* hiba.bensalah@ceramics.tu-berlin.de (H. Bensalah).

https://doi.org/10.1016/j.jece.2020.103807
Received 24 November 2019; Received in revised form 10 February 2020; Accepted 23 February 2020
Available online 24 February 2020

limits their application in large scale systems [14]. Therefore, the search for alternative low-cost and efficient adsorbents is an urgent need. The use of wastes has attracted the attention of many researchers due to their abundance, low price, good mechanical and chemical resistance [15]. The use of waste materials as adsorbents is in line with the principles of green chemistry and with the increasingly stringent environmental regulation that discourages disposal practices or discharge into water.

Although low-cost adsorbents present higher economic feasibility over commercial ones, it is stated in literature that they usually show less adsorption capacity [16,17]. It is challenging to design novel adsorbents which have both high adsorption capacity, rapid rate and at the same time meet the standards of low cost and minimal environmental impact. Morphology of the material is an important factor in heterogeneous chemical reactions and adsorption [18]. In addition, it has been reported that the adsorption properties of the adsorbent depend on their shape, internal surface area and pore size distribution [19]. The surface modification of these materials, in order to increase their surface area, seems to be necessary before application in adsorption. It does not only provide novel binding properties for dyes or increase the surface area, but also prevents the bare nanoparticles from aggregation.

Many studies focus on azo dyes removal because they constitute by far the largest group of colorants and the most important class of commercial inorganic dyes [20]. Despite their wide applications, they may react under reductive conditions and form mutagenic and carcinogenic aromatic amines, which represents a serious hazard [21].

Accordingly, we succeeded in converting industrial waste phosphogypsum (PG) into nano-crystalline hydroxyapatite (HAp) using a new surfactant-assistant hydrothermal synthesis. Nano-sized hydroxyapatite $Ca_{10}(PO_4)_6(OH)_2$ is attracting more interest as a promising adsorbent due to its specific structure conferring ionic exchange property and adsorption affinity towards many pollutants like anionic and cationic proteins, heavy metals, phenol, and azo dyes [22,23]. HAp possesses crystal surface rich in calcium ions with positive charge and phosphate ions with negative charge that can bind with other atoms resulted in a great adsorption ability [24]. Several studies have been reported on azo dyes adsorption of HAp, among them reactive yellow 4 [25], reactive yellow 84 [26] and methylene blue [27]. Few reports exist regarding the adsorption of Congo Red dye using HAp as an adsorbent [28–30]. However, the adsorption rate is relatively low for almost all bare HAp materials, which may be due to the low specific surface area of these adsorbents. To the best of our knowledge, there are only two studies using waste transformed adsorbent from PG for the removal of lead ions [31] and fluoride from aqueous solution [32], but it has not been approached for azo dyes.

In this work, hydrothermal method was used to synthesize low-cost HAp adsorbents with high surface area from an industrial PG waste. The obtained HAp nanoparticles were characterized by XRD, TEM and nitrogen sorption analysis. The adsorption behavior of CR onto the obtained adsorbents was studied, taking into account experimental parameters such as initial concentration, contact time, pH, and adsorbent dosage. In addition, the equilibrium isotherms, adsorption kinetics, and desorption/regeneration studies of CR were also investigated. Moreover, the adsorption mechanisms of CR onto the adsorbent surface were studied using FTIR and XPS characterizations, in order to improve our understanding of azo dyes adsorption by this low-cost adsorbent. The results of this study offer new insights on the conversion of a waste and its use for the removal of azo dyes.

## 2. Experimental section

### 2.1. Materials

The phosphogypsum (PG) waste samples, used in the synthesis of HAp adsorbents, were obtained from the production of phosphoric acid factory in the area of Jorf Lasfar, Morocco. The PG samples were washed several times with deionized water and sieved ($< 50$ µm) after drying overnight in oven at 100 °C. Potassium dihydrogen phosphate ($KH_2PO_4$), sodium hydroxide (NaOH) pellets, polyethylene glycol oleyl ether $C_{22}H_{44}O_3$ (Brij-93 average Mn ~357). Congo Red Dye content ≥35 %, sulfuric acid (95–99 %), ethanol (96 %) and hydrochloric acid solution (37 %) were purchased from Merck (Sigma Aldrich, Germany).

### 2.2. Synthesis HAp and B93-HAp adsorbents

The two adsorbents used in this study: HAp and surfactant modified B93-HAp, were synthesized by a hydrothermal method [33] applying the following procedure: 2 g of $KH_2PO_4$ was dissolved in 50 ml of $H_2O$, followed by the addition of 2 g of PG with continuous stirring at room temperature for 30 min. For the preparation of B93-HAp adsorbent, 0.01 mol of the surfactant Brij 93 was added to the mixture. After complete dispersion of the powders in water, the pH value of the solution was increased to 11 by dropwise addition of 1 M NaOH solution. The obtained solutions were then transferred into 120 mL Teflon lined steel autoclaves and heated at 200 °C for 15 h. To remove the by-products, the synthesis adsorbents were washed several times with distilled hot water and ethanol before drying at 70 °C for 24 h in air.

### 2.3. Adsorbents characterization

X-ray diffraction patterns of HAp and B93-HAp adsorbents were obtained in a Bruker AXS D8 ADVANCE X-ray diffractometer (Bruker, Germany) equipped with a Lynx Eye 1D detector in Bragg–Brentano geometry using CoKα radiation. Measurements were carried out between 10 and 80° 2θ value, with a step time of 3 s/0.02° at 35 kV and 40 mA. The attenuated total reflection (ATR) method using Fourier transform infrared spectrometer (FT-IR, Bruker EQUINOX 55) was used to characterize the adsorbents before and after adsorption experiments. The specific surface area was studied with nitrogen sorption analysis. Gas adsorption isotherms were recorded at 77 K on a QuadraSorb Station 4 apparatus after degassing for 10 h at 200 °C under vacuum. Surface area was determined using the Brunauer, Emmet and Teller (BET) method. All nitrogen sorption data were analyzed using the Quantachrome/QuadraWin software. Zeta potential of nano particles of HAp and B93-HAp was measured in 0.1 N HCl solution as a function of pH using StabiSizer PMX 200 CS equipment. The XPS characterization was performed on K-Alpha ™ + X-ray Photoelectron Spectrometer (XPS) System (Thermo Scientific) coupled with Hemispheric 180° dual-focus analyzer and 128-channel detector. The X-ray monochromator is Micro focused Al-Kα radiation. For the measurement, the dried adsorbents B93-HAp before and after adsorption are ground into fine powders and are directly loaded on the sample holder. The data is collected with X-ray spot size of 400 µm, 20 scans for survey, and 50 scans for regions in vacuum ($10-7$ mbar). The XPS spectra were calibrated to C1 s at 284.8 eV. Transmission electron microscopy (TEM) characterization was performed on a TECNAI G220 STWIN (FEI, Oregon, USA) with LaB6 electron gun, operated at 200 kV. A Gatan MS794 P CCD camera and Digital Micrograph software package were used for image recording and evaluation.

### 2.4. Batch adsorption experiments

Aqueous stock solution of CR with concentration 1000 mg/L was prepared by dissolving a 1 g of the dyes in 1 L distilled water. The experimental solutions were diluted to different concentrations (100–500 mg/L) in 1 L flasks. Table 1 shows the summary of experimental design for these adsorption tests. Batch adsorption experiments for both adsorbents were performed in amber Erlenmeyer flasks, where a pre-established mass of each material were placed in contact with 50 mL of CR solution. The samples were continuously stirred on a multi-position magnetic stirrer (RT 10 IKAMAG, IKA, Germany) at 150 rpm

**Table 1**
Experimental design for adsorption test.

| Investigated parameters | Initial conc. (mg/L) | Adsorbent dosage (g/L) | pH | Contact time (min) |
|---|---|---|---|---|
| Dose | 300 | 0.5–30 | 5.5 | 120 |
| Contact time | 300 | 2 | 5.5 | 0–180 |
| pH | 300 | 2 | 2–12 | 120 |

for different range of time. In order to optimize the adsorption parameters, the effect of adsorbent dosage (0.5–30 g/L), time (5–180 min) and pH values (2–12), were studied by varying one parameter and keeping the others constant. The solution pH, adjusted by gradually addition of HCl (1 M) and $NH_4OH$ (1 M) solutions, was measured by pH meter (FiveEasy, METTLER TOLEDO, USA). After adsorption equilibrium was achieved, the supernatant was separated from the sorbent by centrifugation at 5000 rpm for 10 min. Each of the experiments was carried out three times under similar conditions at 25 °C and an average of the data from the experiments, with error bars showing the values of standard deviation, is shown in the results and discussion section.

The initial and final concentrations of CR were determined from their UV–vis absorbance according to the calibration method. UV/VIS/NIR spectrometer (Perkin Elmer Lambda 9) was used at λ = 497 μm for CR.

The removal efficiency of each dye $R_e$ (%) and the equilibrium adsorption capacity $q_e$ (mg/g) were calculated as follows:

$$R_e = \frac{(C_i - C_e)}{C_i} \times 100\% \quad (1)$$

$$q_e = \frac{(C_i - C_e)V}{m} \quad (2)$$

where $C_i$ and $C_e$ are the initial and equilibrium mass concentration (mg/L), respectively, of the dyes solution, $m$ is the mass of adsorbent (g) and V is the volume of dyes solutions (L).

The experimental data were fitted by non-linear Langmuir, Freundlich and Temkin isotherm models (Eqs. (A1)–(A3), respectively) in order to determine the equilibrium parameters of the systems. Origin Pro 8.0 software (OriginLab, USA) was used to perform the calculations.

In batch adsorption systems, several models describing the diffusion of solutes at the surface have been reported, the pseudo-first order, the pseudo-second order and Elovich kinetic models (Eqs. (A5)–(A7), respectively) have been widely used to describe the rate of adsorption in liquid-solid interactions.

### 2.5. Desorption and regeneration studies

The dye-loaded adsorbent B93-HAp was used for desorption studies. Prior to that, the adsorbent was washed gently with distilled water to remove any non-adsorbed traces of CR, before drying overnight at 80 °C. The eluents used in this study were HCl, NaOH, $H_2SO_4$, Ethanol and $H_2O$. The concentration of the desorbed CR in eluents was determined from the initial concentrations of CR loaded on the adsorbent B93-HAp and final CR concentrations in the eluent after filtration, and measured using a UV/VIS/NIR spectrometer (Perkin Elmer Lambda 9). Each of the desorption experiments was repeated three times and the average values of desorption amount were plotted with error bars showing the values of standard deviation.

Recovery studies were conducted in HCl solution (0.1 M) for CR. Prior to that, B93-HAp was loaded with dye by mixing 100 mg of the adsorbent in 50 mL of 300 mg/L of dye solution for 120 min at 298 K. Then, it was filtrated by centrifugation from the solution, and the adsorption capacity of CR was determined. The dye-loaded B93-HAp was washed with distilled water, then dried overnight at 80 °C. Subsequently, it was mixed with HCl solution (0.1 M) for 120 min. This process cycle was renewed six times (Fig. 1).

**Polyethylene glycol oleyl ether**
**Brij 93**

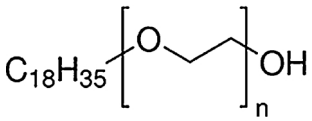


**Fig. 1.** Chemical structure of the non-ionic surfactant Brij 93.

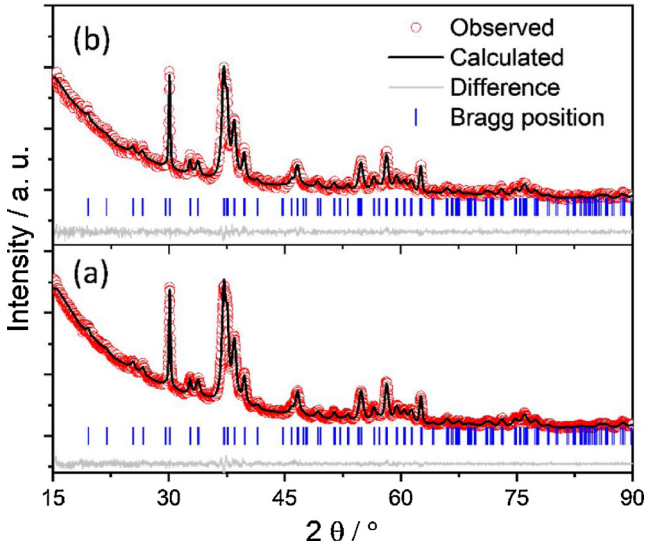


**Fig. 2.** Structure refinement from XRD data of HAp sample, hydrothermally synthesized at 200 °C, pH 11 for 15 h (a) without surfactant and (b) with 0.01 mol of the surfactant Brij 93 using anisotropic peak broadening for all 00 l reflections. Observed (red dots), calculated (black solid line) intensities and differences (grey solid line) are shown. Tick marks refer to the reflections of HAp.

## 3. Results and discussions

### 3.1. Phase composition and crystallite size and morphology of HAp and B93-HAp adsorbents

The crystallinity and phase purity of the obtained HAp and B93-HAp samples were first examined using X-ray diffraction technique (XRD). As shown in Fig. 2a–b, Rietveld refinement of the XRD patterns revealed that both samples composed of phase-pure nanocrystalline HAp $Ca_{10}(PO_4)_6OH_2$ (space group $P6_3/m$). No other crystalline phases were observed in the XRD patterns. The obtained lattice parameters from structure refinement for $Ca_{10}(PO_4)_6OH_2$ phase in HAp sample ($a = b = 9.4092(3)$ and $c = 6.8906(3)$) were found very close to those of that in B93-HAp sample ($a = b = 9.4098(6)$ and $c = 6.8914(7)$), which suggests that Brij-93 surfactant doesn't influence the purity or stoichiometry of the obtained HAp phase. Moreover, these lattice parameters are in good agreement with previously reported values [33], indicating stoichiometric composition of obtained hydroxyapatite in this work. Both samples exhibit anisotropic size broadening that can be will fitted using of needle-like coherent domains for Rietveld refinement. The size of HAp crystallites grown in the $c$ direction were found to be 54.7 and 59.0 nm for HAp and B93-HAp samples, respectively, while an average crystallite size of 17 ± 6 nm was determined in other directions for both samples. These results indicate that the HAp is preferentially grown along the $c$ direction in both samples and Brij-93 surfactant catalyse the growth of these HAp needles.

The rod-like crystals morphology of the obtained HAp was further confirmed by TEM characterization. Fig. 3a–b show the TEM micrograph of HAp and B93-HAp samples, respectively. The HAp nanorods

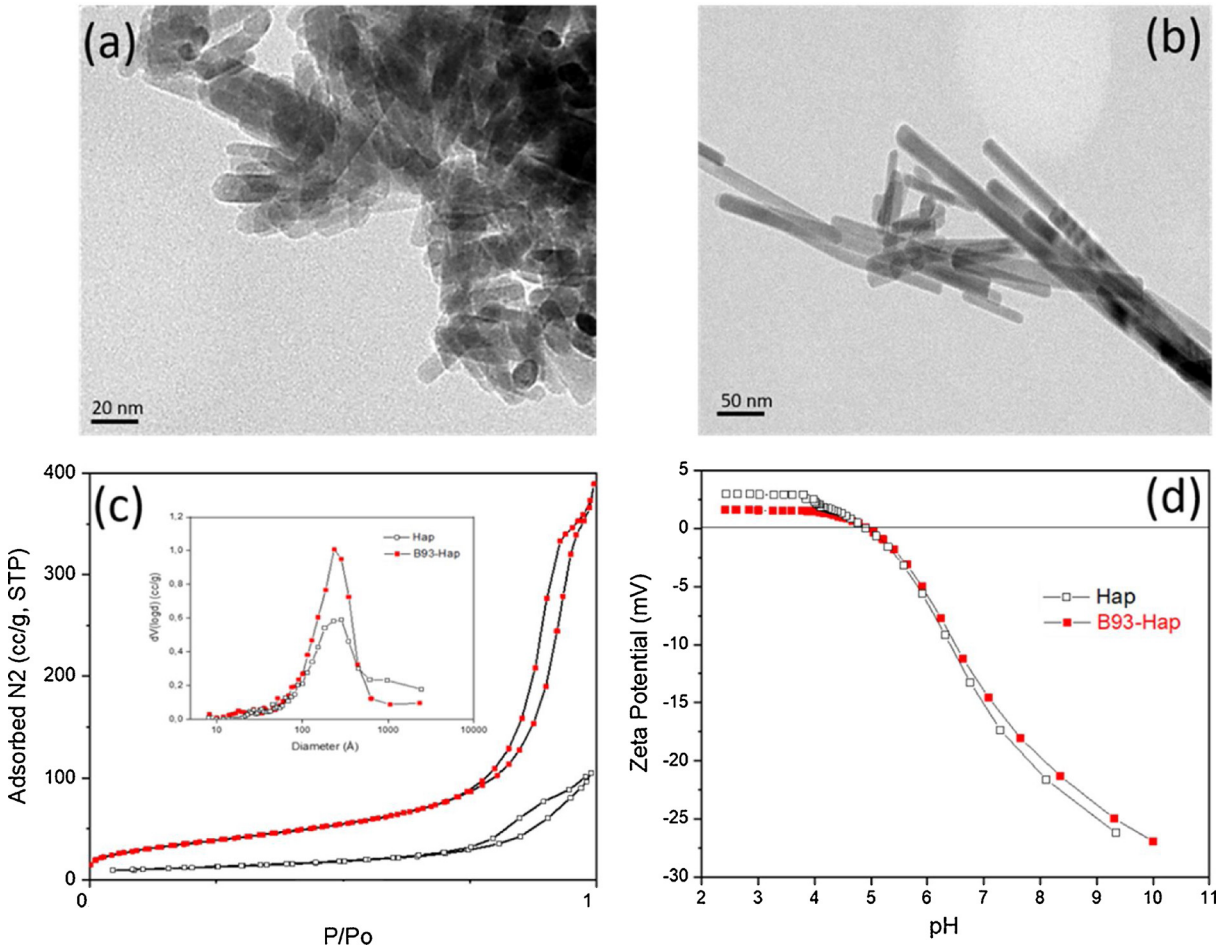


**Fig. 3.** TEM micrographs of (a) unmodified HAp and (b) surfactant modified B93-HAp. (c) $N_2$ adsorption/desorption isotherm of HAp and B93-HAp, inset BJH pore size distribution plot of HAp and B93-HAp. (d) Zeta potential of adsorbents HAp and B93-HAp as function of pH.

synthesized with applying Brij-93 surfactant have diameter and length of 20 and 205 nm, respectively, which are larger than those synthesized without surfactant (i.e. crystal diameter and length are 18 and 63 nm, respectively). These results are in good agreement with our previous report [33].

Fig. 3c shows the $N_2$ adsorption-desorption isotherm of both HAp and B93-HAp adsorbents. Both samples possess a closed adsorption curve that can be classified as a type IV isotherm with a type H3 hysteresis loop, which does not show any limiting adsorption at high p/p° [34]. The type H3 hysteresis loop suggests the presence of irregular and open pores with good connectivity between intra-granular pores with shapes of parallel, slit-like, and open-ended tubes, which is conducive for gas transport and providing space for shale gases. The B93-HAp sample exhibits higher adsorption amount of $N_2$ than that of HAp sample, indicating its higher surface area in comparison with that of HAp sample. The BET specific area of the HAp sample is 86 $m^2$/g, while, the surfactant modified B93-HAp has a $S_{BET}$ of 135 $m^2$/g. This value is higher than most of the HAp materials reported in the literature [29,35]. This high surface area of B93-HAp sample can be explained by the high accessible pore volume resulted from the removal of Brij-93 surfactant during the washing step (inset Fig. 3c).

The $pH_{zpc}$ corresponds to the pH value at which the net surface charge of the adsorbent becomes electrically neutral. At pH < $pH_{zpc}$, the adsorbent surface becomes positively charged, while at pH > $pH_{zpc}$, the adsorbent surface is negatively charged. The pH at which the curve crosses the line corresponds to the $pH_{zpc}$. As shown in Fig. 3d, the surface of both adsorbents has very low positive values below pH 5 due to due to the protonation of the surface phosphate and hydroxyl groups. Both adsorbents exhibit very similar point of zero charge at $pH_{zpc}$ = 5.4 and above this pH value, their surfaces became negatively charged due to the deprotonation of surface groups. The point of zero charge determined for HAp in this work is in good agreement with that reported in the literature [36].

### 3.2. Adsorption studies

#### 3.2.1. Comparison of CR adsorption onto HAp and B93-HAp

The non-modified HAp and the surfactant modified B93-HAp nanoparticles were evaluated as adsorbents for CR removal. Fig. 4 shows the equilibrium adsorption capacity of both HAp and B93-HAp adsorbents for CR with different initial concentrations at pH 5.5 and contact time of 120 min. It can be clearly seen that B93-HAp exhibits much higher adsorption capacity at the same given conditions. The adsorption capacity of both adsorbents for CR increases significantly with increasing the initial dye concentration up to 300 mg/L, and then does not change with further increase in the concentration of the dye. This result can be explained by the availability of several active sites on the surface of HAp and B93-HAp adsorbents those can rapidly adsorb the low concentration of CR dyes. These active sites on the surface of both adsorbents tend to be saturated with the dye at the concentration of 300 mg/L, thus, no further increase in the equilibrium adsorption capacity was observed above this concentration. However, at initial concentration of 300 mg/L, the equilibrium adsorption capacity of B93-HAp adsorbents for CR dyes (145 mg/g) is three times higher than that of the bare HAp (49 mg/g). Accordingly, in the following experiments, surfactant modified B93-HAP nanoparticles was developed as a

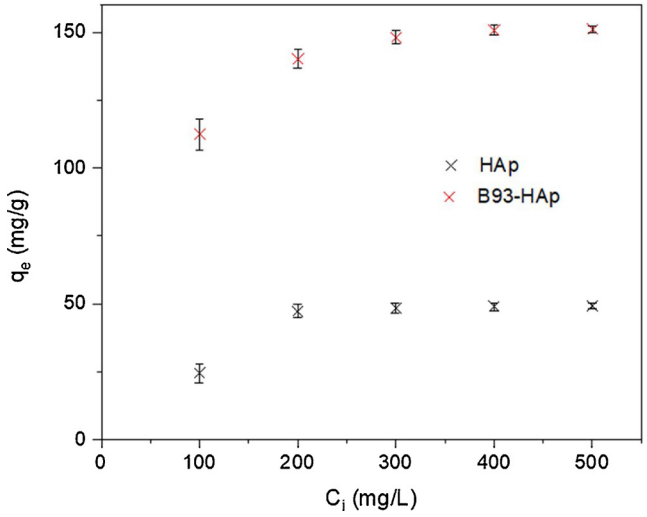


**Fig. 4.** Comparison of CR adsorption onto HAp and B93-HAp nanoparticles (time = 120 min, adsorbent dosage = 2.0 g/L, initial pH: 5.5, and temperature: 298 K).

potential low-cost alternative adsorbent for the removal of CR from contaminated water.

### 3.2.2. Effect of solution pH

The influence of the solution pH on the equilibrium adsorption capacity ($q_e$) of B93-HAp sample was investigated at 300 mg/L initial concentration of CR in the pH range of 2–12 (Fig. 5).

The pH of a solution is a very important factor in the adsorption process, considering the protonation/deprotonation of adsorbates and changes in the surface charges of adsorbents with different pH values. Hence, the B93-HAp adsorbent exhibits higher adsorption capacity in the acidic medium (pH ≤ 5.5) compared to the basic medium (pH ≥ 8). The maximum adsorption capacity (149 mg/g) was found at pH = 5.5, while, the minimum $q_e$ value (114 mg/g) was observed at pH = 12. This effect can be explained by the altering of the surface charge for both adsorbent and adsorbate with the pH of CR solution. As determined in Fig. 2d B93-HAp sample presents a $pH_{pzc}$ value of 5.4, where the surface of the adsorbent is positively charged below this pH value. Moreover, CR is an acid dye containing two sulfonic groups ($-SO_3^-$) which are negatively charged in the acidic conditions [37]. Accordingly, the high adsorption capacity of B93-HAp adsorbent for CR

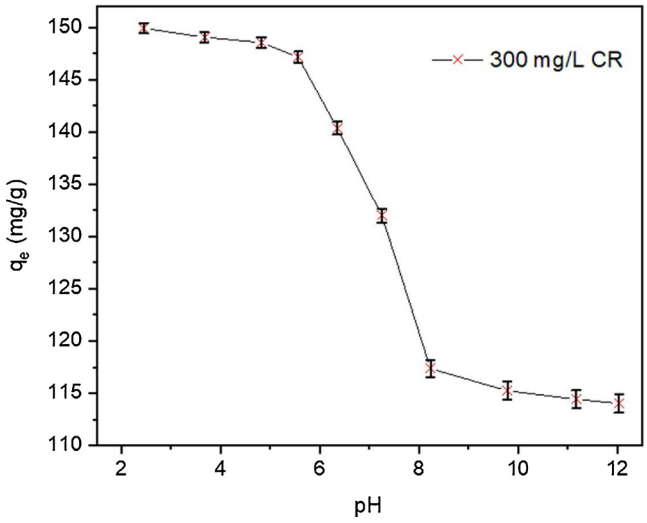


**Fig. 5.** Effect of solution pH on adsorption capacity (time = 120 min, adsorbent dosage = 2.0 g/L, initial concentration: 300 mg/L, and temperature: 298 K).

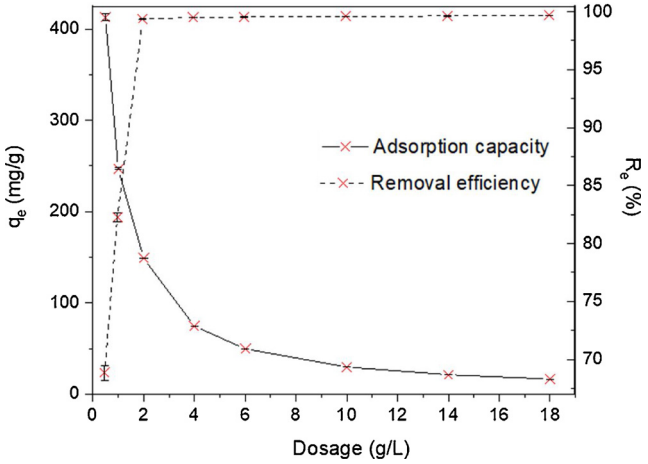


**Fig. 6.** Effect of adsorbent dosage on the adsorption capacity and removal efficiency of CR dye onto B93-HAp (time = 120 min, pH = 5.5, initial concentration: 300 mg/L, and temperature: 298 K).

dye in the acidic conditions (pH < $pH_{pzc}$) can be due to the strong electrostatic attraction between the positively charged surface of the adsorbent and the negatively charged sulfonic groups of the dye. The deprotonation of hydroxyl and phosphate function groups on the surface of B93-HAp becomes more favorable with increasing the solution pH. Thus, the surface of the adsorbent becomes negatively charged, which lead to the electrostatic repulsion between the adsorbent and adsorbent, explaining the lower adsorption capacity obtained at this pH values [38]. Since the maximum $q_e$ was observed at pH 5.5, this value was selected as the optimal one for further adsorption studies.

### 3.2.3. Effect of adsorbent dosage

The effect of B93-HAp dosage on the CR removal (300 mg/L) was evaluated in the range of 0.5–30 g/L at pH = 5.5 and contact time of 120 min. As shown in Fig. 6, the removal efficiency of CR significantly increased from 20 % to 97 % with an increase in the adsorbent dose from 0.5 to 2.0 g/L. This can be assigned to the increase in the number of available active sites required for CR adsorptions with increasing the amount of B93-HAp [39]. Above the dosage of 2 g/L, the CR removal does not change with further increase in the dosage due to the limited availability of CR molecules in the solution. The maximum removal efficiency of CR (99,17 %) was achieved when the dosage increased to 30 g/L. On the other hand, the adsorption capacity remarkably decreased from 149 mg/g to 30 mg/g while increasing the dosage from 2 g/L to 10 g/L. This is due to the saturation of most adsorption sites at high doses of adsorbent [40]. According to these results, 2 g/L was used as the optimum adsorbent dosage for CR in the further experiments.

### 3.2.4. Kinetic studies

The kinetics of adsorption plays an important role in the definition of adsorption rate mechanisms which will drive uptake efficiency and potential application of an adsorbent.

Fig. 7 shows the adsorption capacity of B93-HAp for CR with initial concentration of 300 mg/L as function of contact time at pH = 5.5. The adsorption capacity increased very rapidly with time and the adsorption equilibrium rates were reached after only 20 min with a maximum capacity of 149.36 mg/g. The fast adsorption of CR onto the surface of B93-HAp adsorbent can be explained by the availability of several active sites with functional groups on the adsorbent. The adsorption capacity does not change with further increase in the contact time, which is due to the limited availability of CR molecules in the solution, as 99.4 % has been already removed after 20 min (see Fig. 7a)

Adsorption of CR onto B93-HAp was modeled according to three different models, namely, pseudo-first order, pseudo-second order and

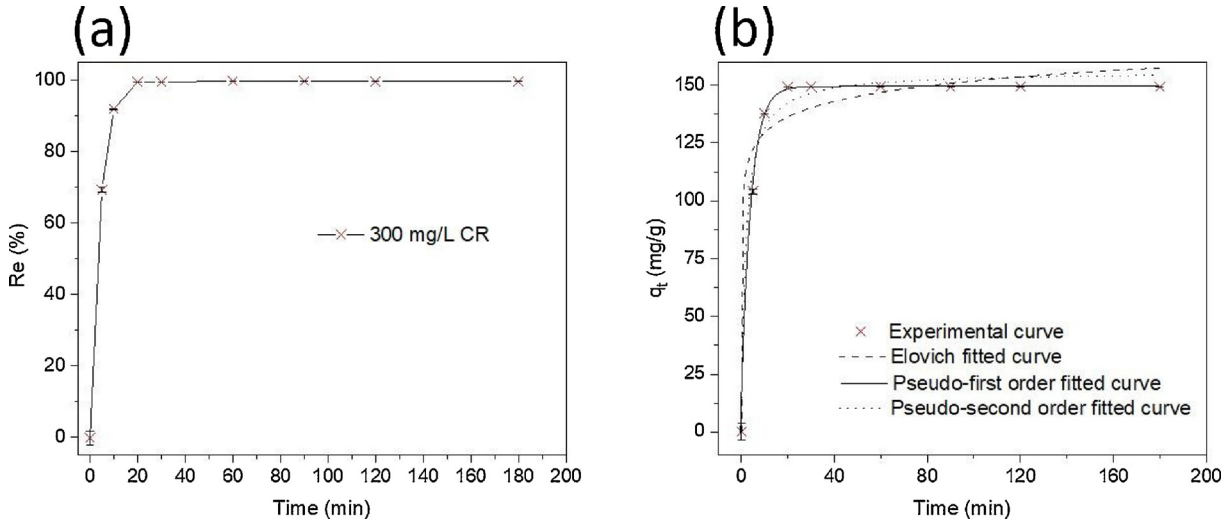


**Fig. 7.** (a) Effect of contact time on the removal efficiency of CR onto B93-HAp, (b) Effect of contact time on the adsorption capacity of CR dye onto B93-HAp and nonlinear fitter curve with kinetic models of pseudo-first order, pseudo-second order and Elovich equation (dosage = 2 g/L, pH = 5.5, initial concentration = 300 mg/L, and temperature: 298 K).

**Table 2**
Kinetic parameters for CR adsorption onto B93HAp with pseudo-first order, pseudo-second order and Elovich models.

| Kinetic Models Parameters | Pseudo-First order $q_{e\ (Cal)}$ $K_1$ $R^2$ (mg/g) (1/min) | Pseudo-Second order $q_{e\ (Cal)}$ $K_2$ $R^2$ (mg/g) (g/(mg.min)) | Elovich α β $R^2$ (mg/g/min) (g/mg) |
|---|---|---|---|
| $q_{e(exp)}$ = 149.36 mg/g | 149.60 24185 0.9998 | 155.15 0.0034 0.9868 | 71.3 0.10425 0.9559 |

Elovich models (see Eqs. (A5)–(A7), respectively) and the related kinetics parameters are listed in Table 2.

According to Fig. 7b and Table 2 the experimental data indicates the satisfactory of pseudo-first order kinetic model for adsorption rate of CR dye ($R^2 > 0.9998$), in comparison with the pseudo-second order ($R^2 > 0.9868$) and Elovich ($R^2 > 0.9559$). In addition, the calculated value of adsorption capacity $q_e$ from pseudo-first order model was 149.6 mg/g, which is in a perfect agreement with the experimental value 149.4 mg/g. It is worth noting that, the same kinetic model was reported previously for the adsorption of reactive yellow 4 dye onto biowaste-derived hydroxyapatite [41].

### 3.2.5. Adsorption isotherms

The adsorption isotherms studies provide useful insight into the adsorption mechanism as well as the surface properties and affinity of the adsorbents. Therefore, the experimental adsorption data CR onto B93-HAp at equilibrium were analyzed using three common isotherm models Langmuir, Freundlich and Temkin isotherm models (see (Eqs. (A1)–(A3), respectively). In order to avoid the errors which are inherent to the commonly used linearized models, nonlinear regression was used in the analyses. The parameters resulted from the fitting of the three models are listed in Table 3. As shown in Fig. 8 and Table 3, Freundlich model gave a better fit ($R^2 > 0.9961$) in comparison with Langmuir

**Table 3**
Isotherms parameters for CR adsorption onto B93-HAp with Langmuir, Freundlich and Tempkin models.

| Isotherm Models | Langmuir | Freundlich | Tempkin | |
|---|---|---|---|---|
| Parameters | $q_m$ $k_L$ $R^2$ (mg/g) (L/mg) | $1/n$ $k_f$ $R^2$ ((mg/g)(L/mg)$^{1/n}$) | $k_T$ b (L/mg) | $R^2$ |
| | 122.42 0.09 0.9249 | 0.27 30.34 0.9961 | 410.98 0.26 0.8536 | |

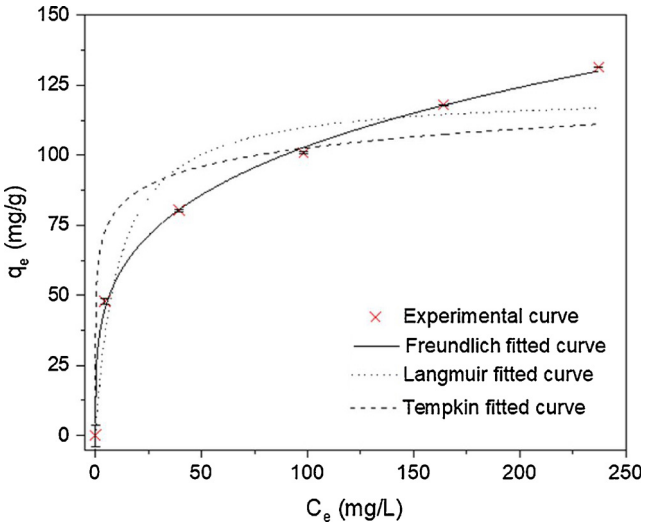


**Fig. 8.** Effect of CR concentration on the adsorption capacity onto B93-HAp and nonlinear fitted curve with isotherm models of Langmuir, Freundlich and Temkin (dosage = 2 g/L, pH = 5.5, time = 120 min, and temperature: 298 K).

($R^2 > 0.9249$) and Tempkin ($R^2 > 0.8536$). The obtained Freundlich coefficient $1/n$ as an indicator for the degree of the surface heterogeneity was found to be 0.27, suggesting favorable adsorption conditions, while $1/n > 1$ indicates unfavorable adsorption [42]. These results are in consistence with previous work showed that the Freundlich isotherm is better representing the adsorption of serval textile dyes such as the blue hydron (HB), blue solophenyl (SB) and turquoise solophenyl (ST) onto synthetic hydroxyapatite [43]. Freundlich model assumes a multilayer adsorption process on heterogeneous surface of the B93-HAp adsorbent [44]. Pantuso et al. assumed that in case of a multilayer sorption, the dye surface can be divided in two regions: A region that

**Table 4**
Comparison of maximum adsorption capacity of different adsorbents for CR removal.

| Adsorbents | $q_m$(mg/g) | CR concentration (mg/L) | Reference |
|---|---|---|---|
| Activated carbon (IPAC) | 101.9 | 50 – 450 | [47] |
| Commercial silica gel (CSG) | 66.5 | 5 – 80 | [46] |
| Ca-bentonite | 107.41 | 50 – 200 | [51] |
| Tea Waste | 43.48 | 50 – 250 | [52] |
| Alginate/bentonite | 95.55 | 25 – 300 | [53] |
| $Ni_{0.6}Fe_{2.4}O_4$ | 72.73 | 5 – 60 | [54] |
| Natural phosphate | 19.81 | 50 – 250 | [55] |
| C. Procera leaf | 25.77 | 25 – 150 | [56] |
| Wheat bran | 22.73 | 20 – 200 | [57] |
| B93-HAp | 138.59 | 5 – 250 | Our work |

supports only a limited number of adsorbed layers due to geometric restrictions, and another region that can adsorb an unlimited number of layers [45]. The obtained maximum adsorption capacity of synthesized B93-HAp for CR was found to be 139 mg/g, which is much higher than those previously reported for low-cost adsorbents (see Table 4). Despite low-cost adsorbents usually display lower maximum adsorption capacities in comparison to commercial ones, B93-Hap sample displayed higher adsorption capacity compared to commercial silica gel (CSG) [46] and indigenously prepared activated carbons (IPAC) [47]. Thus, this work shows that the waste transformed adsorbent could compete with available commercial adsorbents for the removal of CR.

### 3.2.6. FTIR and XPS studies of the adsorption mechanism

To understand the adsorption mechanism of CR onto B93-HAp, the adsorbent was characterized by FT-IR and XPS analysis before and after the adsorption process. As shown in Fig. 9a, the B93-HAp sample before adsorption exhibits vibrational bands of hydroxyapatite [33]. The absorption bands at 560 and 602 $cm^{-1}$ can be attributed to $\nu_4$ mode of phosphate group ($PO_4^{3-}$), while the band at 960 $cm^{-1}$ is due to its $\nu_1$ mode. The peaks corresponding to $\nu_3$ mode of phosphate group are observed at 1012 and 1095 $cm^{-1}$. The broad absorption bands at 3539 $cm^{-1}$ is due to the stretching vibration of $OH^-$ group in the HAp lattice. On the other hand, the FT-IR spectrum of CR dye reveals absorption bands corresponding to its main functional groups such as N−H at about 3466 $cm^{-1}$, the $-SO_3$- stretching vibrations at 1121 and 1223 $cm^{-1}$, C=N vibrations at 1405 $cm^{-1}$, aromatic-nitrogen bond (Ar−N) at 1217 $cm^{-1}$ and C−H (aromatic) stretching at 668 $cm^{-1}$. It can be noticed that the characteristic absorption bands of CR dye were observed in the IR spectrum of B93-HAp after CR adsorption. Moreover, some of absorption peaks such as those corresponding to OH- and $PO_4^{3-}$ of hydroxyapatite and $-NH_2$ group of CR dye are shifted to higher wavenumber, which suggests the hydrogen bonding between CR and the hydroxyapatite adsorbent. This finding is also confirmed by XPS analysis. Fig. 9b–d displays the X-ray Photoelectron P 2p, Ca 2p and O 1s spectra of B93-HAp before and after adsorption of CR. It can be clearly observed that the peaks of P 2p, O 1s and Ca 2p observed at 132.2, 530.3 and 346.3 eV, respectively, in the XPS spectrum of B93-HAp before adsorption are shifted to 132.5, 530.7 and 346.8 eV after the CR adsorption. The shifts of these XPS peaks to higher binding energies confirm the chemical interaction between $Ca^{2+}$, $PO_4^{3-}$ and OH- sites of B93-HAp and CR. Moreover, the atomic ratio Ca/P ratios on the surface of the adsorbent increased from 1.45 to 1.49 after adsorption, suggesting the ion exchange between $PO_4^{3-}$ of HAp and $SO_3$- of CR dye [30,48]. In summary, the adsorption of CR onto the surface of HAp can be likely explained by the following mechanisms: (i) the hydrogen bonding of the azo or amino groups of CR with OH- and $PO_4^{3-}$ of HAp, (ii) chelation of $Ca^{2+}$ ions on the HAp surface by the azo, amino or sulfonate groups of CR, and (iii) anion exchange between $PO_4^{3-}$ of HAp and $SO_3$- of CR, resulting in attachment of the dye through these groups. These findings are in the line with a recently proposed mechanisms for the adsorption of azo dyes onto the surface of HAp adsorbent [30,48].

### 3.2.7. Desorption and regeneration of B93-HAp

Regeneration is the most significant aspect of the adsorption study. In order to make the adsorption process more economical, it is crucial to reuse the adsorbent [49]. For this purpose, it is preferable to desorb the adsorbed CR dye first, then apply consecutive adsorption-desorption cycles repeated for six cycles, in our case, using the B93-HAp adsorbent. Batch desorption experiments were carried out using 0.1 M solution of different diluents HCl, NaOH, $H_2SO_4$, Ethanol and $H_2O$, in the same conditions. Fig. 10a shows the comparison between the different desorption capacities. HCl showed the highest desorption capacity of 98.21 mg/g (64 %), while the use of $H_2O$ and NaOH resulted in very low desorption capacity, 33.03 mg/g (21.53 %) and 54.17 mg/g (35.31 %) respectively. Accordingly, HCl (0.1 M) was used as the most suitable desorbing agent. It is noteworthy that an increase in HCl concentration leads to a decrease in desorption percentage, due to the deterioration of active sites on the B93-HAp surface [50].

The recovery test was repeated for six cycles and the results are illustrated in Fig. 10b. As shown, the adsorption capacities of B93-HAp decrease for every new cycle. The maximum adsorption capacity of B93-HAp for CR was found to be 139 mg/g. After six cycles, the adsorption capacity dropped to 98.56 mg/g, which corresponds to 64.23 % of removal efficiency. These promising results demonstrated that B93-HAp could be regenerated and repeatedly used in dye removal.

## 4. Conclusion

In this study, hydroxyapatite nanorods adsorbents with high surface area are successfully synthesized from phosphogypsum waste by surfactant-assistant hydrothermal method at pH = 11, at 200 °C after 15 h. HAp nanorods with 205 nm length, 20 nm diameter and high specific area of 135 $m^2/g$ was obtained by using 0.01 mol of Brij-93 surfactant during the synthesis. Due to its higher surface area, the adsorption capacity of CR dye on B93-HAp adsorbent, which obtained with applying surfactant in the synthesis, is superior compared to HAp adsorbent synthesized without Brij-93 surfactant. At initial concentration of 300 mg/L, the equilibrium adsorption capacity of B93-HAp adsorbents for CR dyes (145 mg/g) is three times higher than that of the bare HAp (49 mg/g). The adsorption process was found to be represented best by the Freundlich isotherm model, i.e. multilayer adsorption process. The calculated maximum adsorption capacity of B93-HAp adsorbent for CR was found to be 139 mg/g, which is much higher than those previously reported for most of low-cost adsorbents as well as commercial silica gel (CSG) [46] and indigenously prepared activated carbons (IPAC) [47]. Desorption studies demonstrated that the adsorbent B93-HAp could be regenerated after six cycles with a removal efficiency of 64.23 %. Therefore, this study demonstrates that our waste-transformed adsorbent could conciliate between cost effectiveness, high adsorption efficiency and can compete with available commercial adsorbents.

## CRediT authorship contribution statement

**Hiba Bensalah:** Writing - original draft, Writing - review & editing, Conceptualization, Visualization, Methodology, Formal analysis, Investigation. **Saad Alami Younssi:** Resources, Validation. **Mohamed Ouammou:** Resources, Funding acquisition. **Aleksander Gurlo:** Supervision, Validation, Resources. **Maged F. Bekheet:** Supervision, Writing - review & editing, Validation.

## Declaration of Competing Interest

The authors declare that they have no known competing financial interests or personal relationships that could have appeared to influence the work reported in this paper.

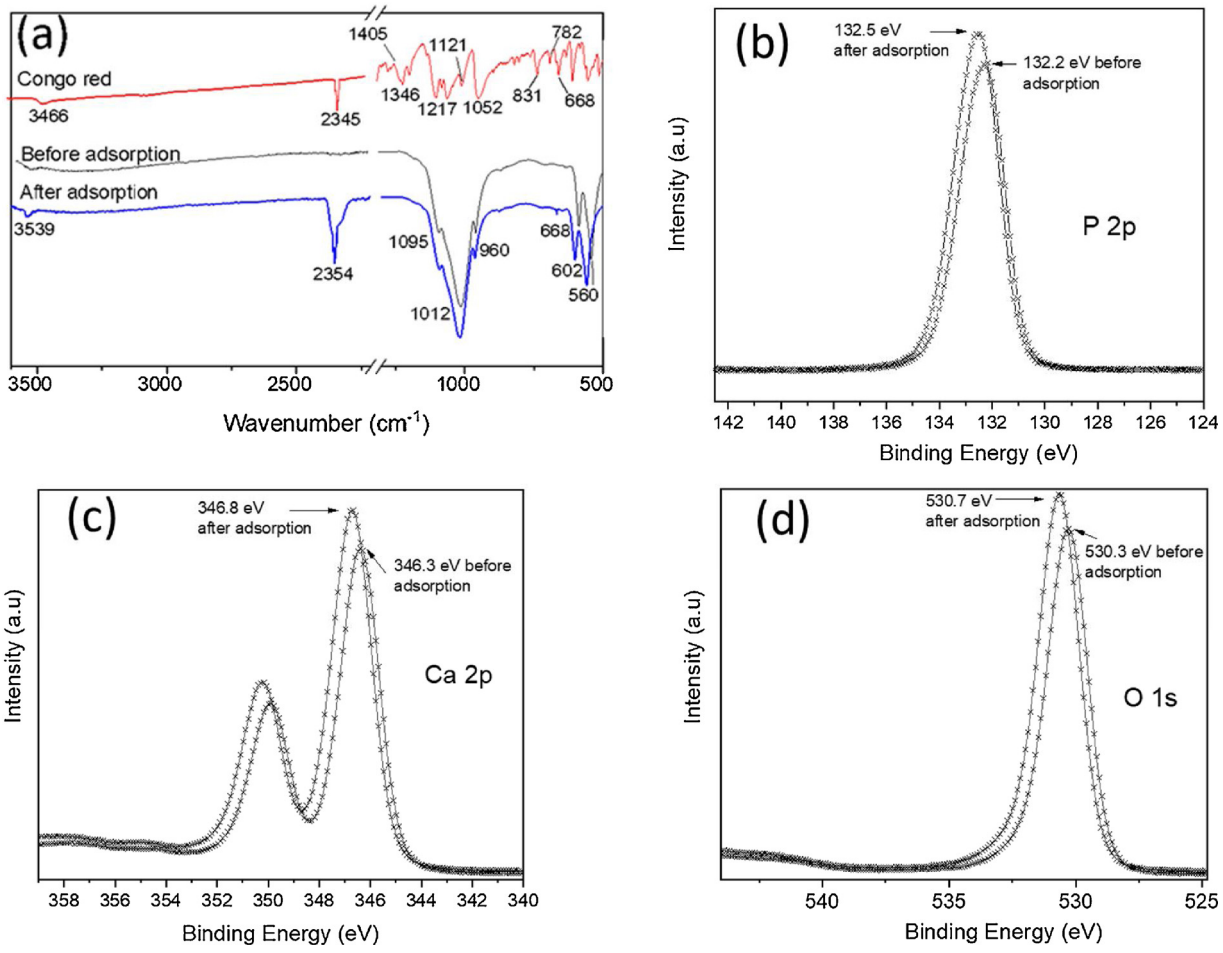


**Fig. 9.** (a) FT-IR spectra of CR (red), B93-HAp before (black) and after (blue) adsorption and X-ray photoelectron spectra of (b) P 2p, (c) Ca 2p and (d) O 1s for B93-HAp.

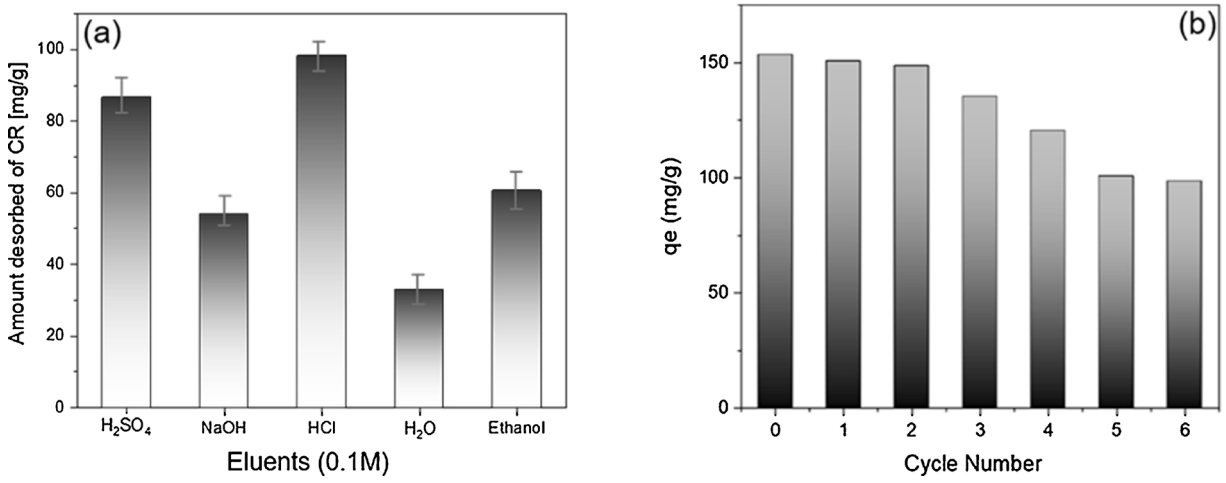


**Fig. 10.** (a) Desorption of CR dye from loaded B93-HAp using various eluents (0.1 M) and (b) effect of recovery cycles on the adsorption capacities of CR onto B93-HAp.

**Acknowledgments**

The financial support by the Bayer Foundation Fellowship Program 2017/2018, application F-2017-BS-0121 is greatly acknowledged. We would like to kindly thank Dr. Patrick Höhne for Zeta potential measurements, Dr. Xifan Wang for XPS measurements and Christina Eischenauer for nitrogen sorption measurements.

## Appendix A

*Adsorption isotherm and kinetics equations*

The non-linear form of Langmuir isotherm model is calculated by [58]:

$$qe = qm\,kL\frac{Ce}{(1 + kLCe)} \tag{A1}$$

where $q_m$ (mg/g) is the Langmuir maximum adsorption of the dyes per unit weight of the adsorbent and $k_L$ (L/mg) is the Langmuir isotherm constant related to the rate of adsorption.

The non-linear form of Freundlich model is represented by [42]:

$$qe = kf\,Ce^{1/n} \tag{A2}$$

where $k_f$ and $n$ are the Freundlich isotherm coefficients in $(mg/g)(L/mg)^{1/n}$ and (mg/g), respectively.

The non-linear expression of Tempkin is described as [59]:

$$qe = \left(\frac{RT}{b}\right) kT\,Ce \tag{A3}$$

Where $q_e$ is expressed in terms of the adsorption heat $b$ (equal to -$\Delta H$, kJ/mol) and the Tempkin isotherm constant $k_T$ (L/mg).

The adsorption quantity $q_t$ (mg/g) of the dye onto the phosphate at time $t$ was calculated according to:

$$q_t = \frac{(C_i - C_t)V}{m} \tag{A4}$$

where $C_t$ (mg/L) is the concentration of the dye solution at time $t$.

The expressions of the three kinetic models rearranged in a non-linear form:

**Pseudo-first-order model** [60]:

$$qt = qe\,(1 - e^{-K1t}) \tag{A5}$$

**Pseudo-second-order model** [61]:

$$qt = \frac{K2qe2t}{1 + K2qe} \tag{A6}$$

where $K_1$ (1/min) and $K_2$ (g/(mg.min) represent the kinetic rate constant of pseudo-first-order adsorption and pseudo-second-order adsorption.

**Elovich kinetic model** [62]:

$$q_t = \frac{1}{\beta}\ln(\alpha\beta) + \frac{1}{\beta}\ln t \tag{A7}$$

α (mg/g/min) and β (g/mg) refers to initial adsorption rate and the Elovich desorption constant in Elovich kinetic model.

## References

[1] K. Grabas, A. Pawełczyk, W. Stręk, E. Szełęg, S. Stręk, Study on the properties of waste apatite phosphogypsum as a raw material of prospective applications, Waste Biomass Valorization 10 (2019) 3143–3155.
[2] Y. Ennaciri, I. Zdah, H. El Alaoui-Belghiti, M. Bettach, Characterization and purification of waste phosphogypsum to make it suitable for use in the plaster and the cement industry, Chem. Eng. Commun. (2019) 1–11.
[3] S. Folek, B. Walawska, B. Wilczek, J. Miśkiewicz, Use of Phosphogypsum in Road Construction 13 (2011), p. 18.
[4] J. Zhou, H. Gao, Z. Shu, Y. Wang, C. Yan, Utilization of waste phosphogypsum to prepare non-fired bricks by a novel hydration–recrystallization process, Constr. Build. Mater. 34 (2012) 114–119.
[5] M. Singh, M. Garg, S.S. Rehsi, Purifying phosphogypsum for cement manufacture, Constr. Build. Mater. 7 (1993) 3–7.
[6] F.J. Heiligtag, M. Niederberger, The fascinating world of nanoparticle research, Mater. Today 16 (2013) 262–271.
[7] W.J. Stark, P.R. Stoessel, W. Wohlleben, A. Hafner, Industrial applications of nanoparticles, Chem. Soc. Rev. 44 (2015) 5793–5805.
[8] M. Koch, A. Yediler, D. Lienert, G. Insel, A. Kettrup, Ozonation of hydrolyzed azo dye reactive yellow 84 (CI), Chemosphere 46 (2002) 109–113.
[9] P.K. Malik, S.K. Saha, Oxidation of direct dyes with hydrogen peroxide using ferrous ion as catalyst, Sep. Purif. Technol. 31 (2003) 241–250.
[10] S. Benkhaya, B. Achiou, M. Ouammou, J. Bennazha, S. Alami Younssi, S. M'rabet, A. El Harfi, Preparation of low-cost composite membrane made of polysulfone/polyetherimide ultrafiltration layer and ceramic pozzolan support for dyes removal, Mater. Today Commun. 19 (2019) 212–219.
[11] A. Ozer, G. Akkaya, M. Turabik, Biosorption of Acid Blue 290 (AB 290) and Acid Blue 324 (AB 324) dyes on Spirogyra rhizopus, J. Hazard. Mater. 135 (2006) 355–364.
[12] M. Breida, S. Alami Younssi, A. Bouazizi, B. Achiou, M. Ouammou, M. El Rhazi, Nitrate removal from aqueous solutions by γ-Al2O3 ultrafiltration membranes, Heliyon 4 (2018) e00498.
[13] C. Jung, A. Son, N. Her, K.-D. Zoh, J. Cho, Y. Yoon, Removal of endocrine disrupting compounds, pharmaceuticals, and personal care products in water using carbon nanotubes: a review, J. Ind. Eng. Chem. 27 (2015) 1–11.
[14] W.A. Cabrera-Lafaurie, F.R. Román, A.J. Hernández-Maldonado, Removal of salicylic acid and carbamazepine from aqueous solution with Y-zeolites modified with extraframework transition metal and surfactant cations: equilibrium and fixed-bed adsorption, J. Environ. Chem. Eng. 2 (2014) 899–906.
[15] N.R. de Mattos, C.R. de Oliveira, L.G.B. Camargo, R.S.R. da Silva, R.L. Lavall, Azo dye adsorption on anthracite: a view of thermodynamics, kinetics and cosmotropic effects, Sep. Purif. Technol. 209 (2019) 806–814.
[16] B. Silva, M. Martins, M. Rosca, V. Rocha, A. Lago, I.C. Neves, T. Tavares, Waste-based biosorbents as cost-effective alternatives to commercial adsorbents for the retention of fluoxetine from water, Sep. Purif. Technol. 235 (2020) 116139.
[17] S. De Gisi, G. Lofrano, M. Grassi, M. Notarnicola, Characteristics and adsorption capacities of low-cost sorbents for wastewater treatment: a review, Sustain. Mater. Technol. 9 (2016) 10–40.
[18] B.R. Müller, S. Majoni, D. Meissner, R. Memming, Photocatalytic oxidation of ethanol on micrometer- and nanometer-sized semiconductor particles, J. Photochem. Photobiol. A: Chem. 151 (2002) 253–265.
[19] B.R. Müller, Effect of particle size and surface area on the adsorption of albumin-bonded bilirubin on activated carbon, Carbon 48 (2010) 3607–3615.
[20] R.D. Welham, The early history of the synthetic dye industry*, J. Soc. Dye. Colour. 79 (1963) 98–105.
[21] W.S. Wan Ngah, M.A. Hanafiah, Removal of heavy metal ions from wastewater by chemically modified plant wastes as adsorbents: a review, Bioresour. Technol. 99 (2008) 3935–3948.
[22] J.C. Elliott, Chapter 3 - Hydroxyapatite and nonstoichiometric apatites, Studies in Inorganic Chemistry, Elsevier, 1994, pp. 111–189.
[23] Chapter 3 - Hydroxyapatite and nonstoichiometric apatites, in: J.C. Elliott (Ed.), Studies in Inorganic Chemistry, Elsevier, 1994, pp. 111–189.
[24] I. Mobasherpour, M.S. Heshajin, A. Kazemzadeh, M. Zakeri, Synthesis of nanocrystalline hydroxyapatite by using precipitation method, J. Alloys. Compd. 430 (2007) 330–333.
[25] H. El Boujaady, A. El Rhilassi, M. Bennani-Ziatni, R. El Hamri, A. Taitai, J.L. Lacout,

Removal of a textile dye by adsorption on synthetic calcium phosphates, Desalination 275 (2011) 10–16.
[26] N. Barka, S. Qourzal, A. Assabbane, A. Nounah, Y. Ait-Ichou, Removal of Reactive Yellow 84 from aqueous solutions by adsorption onto hydroxyapatite, J. Saudi Chem. Soc. 15 (2011) 263–267.
[27] K. Allam, A. El Bouari, B. Belhorma, L. Bih, Removal of methylene blue from water using hydroxyapatite submitted to microwave irradiation, J. Water Resource Prot. 08 (2016) 358–371.
[28] M. Chahkandi, Mechanism of Congo red adsorption on new sol-gel-derived hydroxyapatite nano-particle, Mater. Chem. Phys. 202 (2017) 340–351.
[29] Y. Guan, W. Cao, X. Wang, A. Marchetti, Y. Tu, Hydroxyapatite nano-rods for the fast removal of Congo red dye from aqueous solution, Mater. Res. Express 5 (2018) 065053.
[30] H. Hou, R. Zhou, P. Wu, L. Wu, Removal of Congo red dye from aqueous solution with hydroxyapatite/chitosan composite, Chem. Eng. J. 211–212 (2012) 336–342.
[31] S.M. Mousa, N.S. Ammar, H.A. Ibrahim, Removal of lead ions using hydroxyapatite nano-material prepared from phosphogypsum waste, J. Saudi Chem. Soc. 20 (2016) 357–365.
[32] D. Zhang, H. Luo, L. Zheng, K. Wang, H. Li, Y. Wang, H. Feng, Utilization of waste phosphogypsum to prepare hydroxyapatite nanoparticles and its application towards removal of fluoride from aqueous solution, J. Hazard. Mater. 241–242 (2012) 418–426.
[33] H. Bensalah, M.F. Bekheet, S. Alami Younssi, M. Ouammou, A. Gurlo, Hydrothermal synthesis of nanocrystalline hydroxyapatite from phosphogypsum waste, J. Environ. Chem. Eng. 6 (2018) 1347–1352.
[34] K.S.W. Sing, Reporting physisorption data for gas/solid systems with special reference to the determination of surface area and porosity (Provisional), Pure Appl. Chem. 54 (1982) 2201–2218.
[35] M. Sharma, A. Mishra, A. Mehta, D. Choudhury, S. Basu, Effect of Surfactants on the Structure and Adsorption Efficiency of Hydroxyapatite Nanorods, (2018).
[36] L.C. Bell, A.M. Posner, J.P. Quirk, Surface charge characteristics of hydroxyapatite and fluorapatite, Nature 239 (1972) 515–517.
[37] S. Liu, Y. Ding, P. Li, K. Diao, X. Tan, F. Lei, Y. Zhan, Q. Li, B. Huang, Z. Huang, Adsorption of the anionic dye Congo red from aqueous solution onto natural zeolites modified with N,N-dimethyl dehydroabietylamine oxide, Chem. Eng. J. 248 (2014) 135–144.
[38] R. Zhang, J. Zhang, X. Zhang, C. Dou, R. Han, Adsorption of Congo red from aqueous solutions using cationic surfactant modified wheat straw in batch mode: kinetic and equilibrium study, J. Taiwan Inst. Chem. Eng. 45 (2014) 2578–2583.
[39] R.R. Mohammed, M.R. Ketabchi, G. McKay, Combined magnetic field and adsorption process for treatment of biologically treated palm oil mill effluent (POME), Chem. Eng. J. 243 (2014) 31–42.
[40] Q. Du, J. Sun, Y. Li, X. Yang, X. Wang, Z. Wang, L. Xia, Highly enhanced adsorption of Congo red onto graphene oxide/chitosan fibers by wet-chemical etching off silica nanoparticles, Chem. Eng. J. 245 (2014) 99–106.
[41] A. Bhatnagar, E. Kumar, A. Minocha, B.-H. Jeon, H. Song, Y.C. Seo, Removal of Anionic Dyes from Water Using Citrus limonum (Lemon) Peel: Equilibrium Studies and Kinetic Modeling, (2009).
[42] H. Freundlich, Ueber Kolloidfällung und Adsorption, Zeitschrift für Chemie und Industrie der Kolloide 1 (1907) 321–331.
[43] W.C. Wanyonyi, J.M. Onyari, P.M. Shiundu, Adsorption of Congo red dye from aqueous solutions using roots of Eichhornia Crassipes: kinetic and equilibrium studies, Energy Procedia 50 (2014) 862–869.
[44] Y.L. Kang, S.K.S. Toh, P. Monash, S. Ibrahim, P. Saravanan, Adsorption isotherm, kinetic and thermodynamic studies of activated carbon prepared from Garcinia mangostana shell, Asia-Pacific J. Chem. Eng. 8 (2013) 811–818.
[45] F.S. Pantuso, M.P. Tolaba, R.J. Aguerre, A BET approach to multilayer adsorption in swelling products, J. Food Eng. 122 (2014) 68–71.
[46] R.Sd. Farias, H.Ld.B. Buarque, M.Rd. Cruz, L.M.F. Cardoso, Td.A. Gondim, V.Rd. Paulo, Adsorption of congo red dye from aqueous solution onto amino-functionalized silica gel, Eng. Sanit. E Ambient. 23 (2018) 1053–1060.
[47] N. Kannan, M. Meenakshisundaram, Adsorption of Congo red on various activated carbons. A comparative study, Water, Air, Soil Pollut. 138 (2002) 289–305.
[48] R.L. Speirs, The reaction between some dyes and synthetic hydroxyapatite I. The uptake of dyes in relation to their structures, Histochem. J. 2 (1970) 45–66.
[49] T. Singh, R. Singhal, Methyl Orange adsorption by reuse of a waste adsorbent poly (AAc/AM/SH)-MB superabsorbent hydrogel: matrix effects, adsorption thermodynamic and kinetics studies, Desalin. Water Treat. 53 (2013) 1942–1956.
[50] M.R. Malekbala, M.A. Khan, S. Hosseini, L.C. Abdullah, T.S.Y. Choong, Adsorption/desorption of cationic dye on surfactant modified mesoporous carbon coated monolith: equilibrium, kinetic and thermodynamic studies, J. Ind. Eng. Chem. 21 (2015) 369–377.
[51] L. Lian, L. Guo, C. Guo, Adsorption of Congo red from aqueous solutions onto Ca-bentonite, J. Hazard. Mater. 161 (2009) 126–131.
[52] M. Foroughi-Dahr, H. Abolghasemi, M. Esmaili, A. Shojamoradi, H. Fatoorehchi, Adsorption characteristics of Congo red from aqueous solution onto tea waste, Chem. Eng. Commun. 202 (2014) 181–193.
[53] A. Oussalah, A. Boukerroui, A. Aichour, B. Djellouli, Cationic and anionic dyes removal by low-cost hybrid alginate/natural bentonite composite beads: adsorption and reusability studies, Int. J. Biol. Macromol. 124 (2019) 854–862.
[54] S. Zeng, S. Duan, R. Tang, L. Li, C. Liu, D. Sun, Magnetically separable Ni0.6Fe2.4O4 nanoparticles as an effective adsorbent for dye removal: synthesis and study on the kinetic and thermodynamic behaviors for dye adsorption, Chem. Eng. J. 258 (2014) 218–228.
[55] H. Bensalah, M.F. Bekheet, S.A. Younssi, M. Ouammou, A. Gurlo, Removal of cationic and anionic textile dyes with Moroccan natural phosphate, J. Environ. Chem. Eng. 5 (2017) 2189–2199.
[56] R. Kaur, H. Kaur, Calotropis procera an effective adsorbent for removal of Congo red dye: isotherm and kinetics modelling, Model. Earth Syst. Environ. 3 (2017).
[57] J.P. Chen, Biosorption of Congo red from aqueous solution using wheat bran and rice bran: batch studies AU - Wang, Xue Song, Sep. Sci. Technol. 44 (2009) 1452–1466.
[58] I. Langmuir, The adsorption of gases on plane surfaces of glass, mica and platinum, J. Am. Chem. Soc. 40 (1918) 1361–1403.
[59] M.I. Temkin, The kinetics of some industrial heterogeneous catalytic reactions, in: D.D. Eley, H. Pines, P.B. Weez (Eds.), Advances in Catalysis, Academic Press, 1979, pp. 173–291.
[60] S. Lagergren, Ueber die Dämpfung electrischer Resonatoren, Annalen der Physik 300 (1898) 290–314.
[61] Y.-S. Ho, Review of second-order models for adsorption systems, J. Hazard. Mater. 136 (2006) 681–689.
[62] I.S. McLintock, The Elovich equation in chemisorption kinetics, Nature 216 (1967) 1204–1205.

# 5.Conclusions and outlook

The ***first goal*** of this thesis has been achieved since natural phosphate was found to be an effective low-cost adsorbent for the removal of two azo dyes: cationic dye rhodamine 6G (Rh6G) as well as anionic dye congo red (CR) from contaminated water. The Rietveld refinement of the XRD data showed that the sample contains fluoroapatite $Ca_5(PO_4)_3F$ with minor amount of $SiO_2$ and $CaCO_3$. The adsorption efficiency of the anionic dye CR decreased with an increasing pH, in the opposite of the cationic dye Rh6G. The Langmuir model demonstrated that a monolayer adsorption process occurs on the homogeneous surface of the natural phosphate without considering the interaction between adsorbate molecules. The calculated maximum adsorbed quantity $q_{max}$ of CR and Rh6G were found 19.81 and 6.84 mg/g, respectively, which was superior to other conventional adsorbents such as activated carbon. The pseudo-second-order equation was followed for the adsorption of CR and Rh6G on natural phosphate. The elution of CR and Rh6G from natural phosphate was the highest at 0.1M HCl. This work proved that Moroccan natural phosphate is a promising low-cost adsorbent for both cationic and anionic dyes.

Many theoretical and empirical models have been proposed for describing mechanisms of dyes adsorption from aqueous solution. In fact, it is necessary to establish equilibrium correlation of sorbent to predict behaviour of sorbent under different experimental conditions. This equilibrium correlation is developed by using equilibrium isotherms. These isotherms express way of sorbent interaction with the surface of adsorbent, that is, whether it is monolayer or multilayer sorption. However, this thesis provides practical guidance for choosing an appropriate method by comparing three or four models only. Therefore, we suggest that the interpretation of adsorption isotherms can be reviewed for the applications of the one-parameter isotherm of Henry's model, two-parameter isotherms such as Hill-Deboer, Fowler-Guggenheim, Flory-Huggins, Hill, Hasley, Harkin-Jura, Jovanovic, or Kiselev models, three-parameter isotherms of Redlich-Peterson, Sips, Toth, Kahn, Radke-Prausnits or Jossens models, four-parameter isotherms of Fritz-Schlunder, Baudu, Weber-Van Vliet and Marczewski-Jaroniec models. Some of those suggested models are detailed in section 2.2.1.

Similarly, thermodynamic studies are of prime importance to predict whether the adsorption is spontaneous or not. Furthermore, it provides information about suitable temperature range for sorption and nature of sorbent and sorbate at equilibrium. Consequently, adsorption

experiments can be carried out at different temperature conditions and then calculate parameters included enthalpy ΔH, entropy ΔS, and Gibbs free energy ΔG. For instance, negative values of free energy (ΔG) would indicate that adsorption of dyes is spontaneous, and positive values for change in enthalpy may be due to endothermic nature of adsorption.

In addition, the use of apatite as an adsorbent can be further extended to the removal of heavy metals from aqueous solutions. Also, among common non-metals, fluoride is one of the most ubiquitous inorganic contaminants in drinking water. Natural apatite can be used for the removal of fluoride from contaminated solutions. For instance, because of similarity of the charge and sizes of fluoride ion with that of hydroxyl ion, easy exchange between these two is facilitated in the natural environment, enabling fluoride ion to enter the aqueous solution readily.

Recently, membrane technology has known a rapid evolution and especially the need of membranes made of low-cost materials. Accordingly, we already succeeded in elaborating a new graphene oxide (GO) composite membrane using a silane modified ceramic support made of Moroccan natural phosphate. The physical and chemical properties, and the morphology of both ceramic support and GO/ceramic membrane were investigated. This manuscript "*Graphene oxide used as a coating for a new composite membrane made of natural phosphate via silane-graft modification*" is under preparation and is going to be submitted soon.

The ***second goal*** of this dissertation has been achieved by successfully synthesizing nanocrystalline hydroxyapatite (HAp) from industrial waste phosphogypsum (PG) and potassium dihydrogen phosphate $KH_2PO_4$ by hydrothermal method. The purity and morphology of prepared HAp strongly depends on the conditions of hydrothermal synthesis. XRD data reveal that phase-pure HAp is hydrothermally obtainable in strong alkaline medium (i.e. pH=11) at 200 °C after sufficient long time (15 h). SEM and TEM characterizations showed that the prepared HAp consists of uniform rod-like nanoparticles with different aspect ratios depending on the concentration of the Brij-93 surfactant used in the synthesis. The Brij-93 surfactant capped at the surface of the HAp crystals leads to the preferential growth in one direction preventing simultaneously the agglomeration of nano-rods.

The performed recycling of PG can be extended to the fabrication of other useful materials. It is of prime importance to find an efficient way to minimize the negative environmental impacts of this waste. In fact, PG can be used as an environmental-friendly source for the production of sodium sulfate and calcium silicate. Calcium silicate compounds are highly demanded mainly

in building materials as a basis material for Portland cements, for instance. Another procedure to convert PG waste into valuable products, is converting it into calcite and lithium sulfate monohydrate. The last one is recommended in lithium batteries studies, while the calcite can be useful in several industrial fields, such as plastics, paper, automotive… Some studies can be undertaken in order to examine the potential recovery of metals, with a great economic interest, in PG wastes. Besides, environmentally friendly applications are worth being investigated. One of them is based on the use of PG as a calcium source for $CO_2$ mineral sequestration in the framework of the mitigation of greenhouse gases emission.

The ***third goal*** of this thesis has been achieved since surfactant-modified nano B93-HAp well performed the CR adsorption compared to unmodified nano-HAp. The BET specific area (SBET) of the prepared HAp was 85.88 $m^2/g$, while, the surfactant modified B93-Hap had SBET of 135.25 $m^2/g$. The adsorption of CR on B93-HAp was more favoured at lower pH solution, during 120 min, with an adsorbent dosage of 2.0 g/L at an initial concentration of CR 300 mg/L. The maximum adsorption capacity was determined 139.0 mg/g that could be well fitted by Freundlich model with $R^2 > 0.9961$. Following the kinetic studies, the experimental data fitted with the pseudo-first order model. FTIR and XPS results showed the existence of an electrostatic interactions of anionic CR dye and $Ca^{2+}$ site and hydrogen bonding of amine group and phosphate of B93-HAp surface. Desorption studies demonstrated that the adsorbent B93-HAp can be regenerated after six cycles with a removal efficiency of 64.23%. Finally, it can be concluded that this new synthesized B93-Hap from an industrial waste can be used as an effective low-cost adsorbent for removing of dyes from industrial wastewater.

For applications in several areas, control of several parameters, including particle size, surface area, pore size and morphology, is important as they dictate the properties of the HAp products. Consequently, many techniques aimed at producing HAp that meets these properties have been explored. In order to control the morphology of HAp, surfactants are generally used as directing agents and templates. In our work, we suggested a surfactant-assistant hydrothermal method to produce very pure nano-crystalline HAp with needle-like shape, using a non-ionic. It would be interesting to study the effect of cationic and anionic surfactants on the morphology of HAp. For instance, the use of cationic and anionic surfactants may inhibit the growth of the fibres, leading to the coexistence of spherical aggregates. And in this context, spherical hydroxyapatite may be clinically applied towards orthopaedic or maxillofacial surgery as fillers and as biological chromatography supports.

# Symbols and abbreviations

(*in order of appearance*)

| Abbreviations | |
|---|---|
| FAp | Fluoarapatite |
| HAp | Hydroxyapatite |
| PG | Phosphogypsum |
| PR | Phosphate Rock |
| CR | Congo Red |
| Rh6G | Rhodamine 6G |
| B93-HAp | Surfactant modified hydroxyapatite |
| DNA | Deoxyribonucleic acid |
| AC | Activated carbon |
| LCA | Low-cost adsorbent |
| REE | Rare earth elements |
| P | Phosphorus |
| OCP | Office Cherifien de Phosphate |
| GDP | Gross Domestic Product |
| MRI | Magnetic resonance imaging |
| SBF | Simulated Body Fluid |
| PEG | Polyethylene glycol |
| CaP | Calcium phosphate |
| DH | Dihydrate |
| HH | Hemihydrate |
| AH | Anhydrite |

| | |
|---|---|
| CMC | Critical micelle concentration |
| CTAB | Cetyl-trimethylammonium bromid |
| SDS | Sodium dodecyl sulfate |
| Triton X-100 | Octyl phenol ethoxylate |
| Brij 93 | Polyethylene glycol oleyl ether |
| XRD | X-ray diffraction |
| SEM | Scanning electron microscopy |
| EDX | Energy-dispersive X-ray spectroscopy |
| TEM | Transmission electron microscopy |
| FT-IR | Fourier-transform infrared spectroscopy |
| UV-VIS | Ultraviolet-visible spectroscopy |
| XPS | X-Ray photoelectron spectroscopy |

## Symbols

| Symbol | Quantity | Units |
|---|---|---|
| $q_e$ | Adsorption capacity | $mg.g^{-1}$ |
| Re | Removal efficiency | % |
| Ce | Equilibrium mass concentration | mg/L |
| a | Lattice parameter | Å |
| $K_1$ | Kinetic rate constant | 1/min |
| $K_L$ | Langmuir isotherm constant | L/mg |
| $K_f$ | Freundlich isotherm coefficient | - |
| B | Adsorption heat | kJ/mol |
| $K_T$ | Temkin isotherm constant | L/mg |
| $K_D$ | D-R isotherm constant | $mol^2/kJ^2$ |

## Greek Letters

| | | |
|---|---|---|
| α | Initial adsorption rate | mg/g/min |
| β | Elovich desorption constant | g/mg |
| λ | Wavelength | μm |
| θ | Glancing angle for XRD analysis | - |

# Acknowledgments

This PhD thesis represents a group effort of the collaboration between University Hassan II of Casablanca and Technische Universität Berlin. This work has been accomplished under the supervision of Prof. Saad Alami Younssi, head of "*Materials, Membranes and Environment*" laboratory at the faculty of Sciences and Techniques - Mohammedia, and Prof. Dr. Aleksander Gurlo, head of "Advanced Ceramic Materials" chair at Fakultät III Prozesswissenschaften.

I would like to express my gratitude to my joint PhD supervisors, Prof. Alami Younssi and Prof. Mohamed Ouammou. Prof. Alami Younssi has been a great support during this PhD journey. He believed in me and always provided me references in order to obtain research funding. Also, special thanks to my co-supervisor Prof. Mohamed Ouammou for his precious help and academic guidance. Besides, I am specifically indebted to Prof. Dr. Aleksander Gurlo for welcoming me among his group and giving me the opportunity and the meanings to carry out my research in the best conditions. I truly enjoyed working in such a research environment that stimulates original thinking and initiative. I would like to extend my gratitude to my PhD degree supervisor and my mentor, Dr. Maged F. Bekheet, who greatly contributed to shape this project and patiently assisted me with his valuable skills in analysing data, structuring and writing papers.

This thesis might have probably never seen light without the financial support of the Erasmus Mundus EU-Metalic program, Erasmus Mundus International+ at the Aristotle University of Thessaloniki in Greece and the Bayer Foundation Fellowship Program.

Making a PhD thesis is definitely not an individual experience; it is a journey that includes several persons, whom I would like to thank sincerely. First of all, my dear colleagues and friends from office 312: Dr. Xifan Wang, Mathias Czasny, Anthony Wang and David Karl. This office was a great space for peer support, very long scientific discussions but also a lot of fun. Then, I would like to thank my amazing colleagues, who made my work so much easier and more enjoyable; Franz Kamuzki, Albert Gili, Dorian Hanaor, Lukas Schlicker, Onur Kaba, Fabian Zemke, Kai Weisser, Maria Colmenares, Laura Marie Henning, Jun Wang, Amanmyrat Abdullayev and Mehvish Zahoor. Special thanks go to Dr. Ulla Simon and Dr. Franziska Schmidt for their valuable time and effort. I wish to acknowledge the support received from all the staff, the technicians, the students and my PhD colleagues in both groups. I have been lucky enough to have a chance to spend a part of my life working surrounded by such inspiring colleagues.

Nobody has been more important for me in the fulfilment of this project than my parents Samira Hilmi & Mohamed Bensalah. You are a great inspiration for me and I owe you a huge debt of gratitude for your unconditional support, sacrifice, love, and patience. Marou and Ihab, thank you for being such great supportive brothers. Love you! Last but not least, I would like to thank the family we don't chose, my great friends: Yasmin, Fati, Zou, Zineb, Basma, Kim, Lucile, Mimi, and Emeline. Those are the rare people who always showed up at the tight time, helped me through the hard ones and stayed into the best ones. You are the best and I'm lucky to have all of you in my life!